DEVELOPMENT OF A HIGH FIDELITY FINITE ELEMENT MODEL OF A WIND TURBINE BLADE VIA MODAL TESTING

A THESIS SUBMITTED TO
THE GRADUATE SCHOOL OF NATURAL AND APPLIED SCIENCES
OF
MIDDLE EAST TECHNICAL UNIVERSITY

BY
CHADI AMER

IN PARTIAL FULFILLMENT OF THE REQUIREMENTS
FOR
THE DEGREE OF MASTER OF SCIENCE
IN
AEROSPACE ENGINEERING

APRIL 2015

Approval of the thesis:

DEVELOPMENT OF A HIGH FIDELITY FINITE ELEMENT MODEL OF A WIND TURBINE BLADE VIA MODAL TESTING

Submitted by **CHADI AMER** in partial fulfilment of the requirements for the degree of **Masters of Science in Aerospace Engineering Department, Middle East Technical University** by,

Prof. Dr. M. Gülbin Dural Unver
Dean, Graduate School of **Natural and Applied Sciences** _____

Prof. Dr. Ozan Tekinalp
Head of Department, **Aerospace Engineering** _____

Assoc. Prof. Dr. Melin Şahin
Supervisor, **Aerospace Engineering Dept., METU** _____

Examining Committee Members:

Prof. Dr. Yavuz Yaman
Aerospace Engineering Dept., METU _____

Assoc. Prof. Dr. Melin Şahin
Aerospace Engineering Dept., METU _____

Prof. Dr. Serkan Özgen
Aerospace Engineering Dept., METU _____

Assist. Prof. Dr. Ercan Gürses
Aerospace Engineering Dept., METU _____

Assoc. Prof. Dr. Ender Ciğeroğlu
Mechanical Engineering Dept., METU _____

Date: 17.04.2015

I hereby declare that all information in this document has been obtained and presented in accordance with academic rules and ethical conduct. I also declare that, as required by these rules and conduct, I have fully cited and referenced all material and results that are not original to this work.

Name, Last name: Chadi Amer

Signature:

ABSTRACT

DEVELOPMENT OF A HIGH FIDELITY FINITE ELEMENT MODEL OF A WIND TURBINE BLADE VIA MODAL TESTING

Amer, Chadi

M.S., Department of Aerospace Engineering

Supervisor: Assoc. Prof. Dr. Melin Şahin

April 2015, 125 pages

The design of an optimised horizontal axis 5-meter-long wind turbine rotor blade, is a research and development project, in order to fulfil the requirements of high efficiency torque-from-wind production. For this purpose, a research study is presented here, by investigating the structural characteristics of a composite wind turbine blade via finite element modelling and experimental modal analysis. At first, modal tests are performed by using various sensor-actuator pair combinations. After that the geometry was drawn via CATIA software. The materials are assigned as; two different types of glass fabrics, polymeric foam core material and steel-balsa wood combination and the finite element model of the blade was generated via MSC© PATRAN software with various meshes created on each structural part of the blade. MSC© NASTRAN was used as a solver for the dynamic analyses in order to obtain the natural frequencies and the corresponding mode shapes, namely; the first three out-of-plane bending, the first in-plane bending and the first torsional ones. Mesh independency check is also made before the analyses. In all analyses, the blade's

boundary conditions are set as free-free and fixed-free. Finally, the experimental modal analysis results are used to update the low fidelity model via FEMTools software in order to obtain a high fidelity finite element model of the wind turbine blade.

Keywords: Horizontal Axis Wind Turbine Rotor Blade, Fiber Reinforced Composites, Finite Element Modelling and Analysis, Modal Test Verifications, High Fidelity Models.

ÖZ

BİR RÜZGAR TÜRBİNİ KANADININ YÜKSEK SADAKATLİ SONLU ELEMANLAR MODELİNİN MODAL TESTLER YARDIMIYLA GELİŞTİRİLMESİ

Amer, Chadi

Yüksek Lisans, Havacılık ve Uzay Mühendisliği Bölümü

Tez Yöneticisi: Doç. Dr. Melin Şahin

Nisan 2015, 125 sayfa

Yatay eksenli, 5 metre uzunluğunda, optimize bir rüzgar türbini kanadının tasarımı; rüzgardan yüksek verimlilikte tork elde etme gereksinimleri sağlamak amacına yönelik bir araştırma ve geliştirme projesidir. Bu bağlamda burada, bir kompozit rüzgar türbini kanadının yapısal karakteristiklerinin incelenmesine sonlu elemanlar modelleme ve deneysel modal analizler ile odaklanan bir araştırma çalışması sunulmaktadır. Öncelikle, kanat üzerinde çeşitli algılayıcı ve uyarıcı kombinasyonları kullanılarak modal testler icra edilmiştir. Kanat geometrik özelliklerinin CATIA yazılımı yardımıyla çizilmesini takiben, malzeme olarak iki farklı cam elyaf kumaş, polimerik köpük çekirdek malzemesi ve çelik-balsa ahşap birleşimi kullanılmış ve kanadın yapısal parçalarının sonlu elemanlar modellemeleri MSC© PATRAN yazılımında çeşitli ağlar yaratılmak suretiyle tamamlanmıştır. Ayrıca, sonlu elemanlar ağından bağımsızlık kriteri de dikkate alınarak, MSC© NASTRAN yazılımı tüm dinamik analizlerde çözücü olarak kullanılmış ve yapının doğal

frekansları ve bu frekanslara karşılık gelen biçim şekilleri ilk üç düzlem dışı eğilme, ilk düzlem içi eğilme ve ilk burulma şekillerine odaklanarak elde edilmiştir. Tüm bu analizlerde, serbest-serbest ve ankastre durumlar kanat sınır koşulu olarak alınmıştır. Son olarak, daha önce elde edilmiş olan deneysel modal analiz sonuçları FEMTools yazılımı ile birlikte rüzgar türbini kanadının yüksek sadakatli sonlu elemanlar modelini elde etmek için düşük sadakatli modelin güncellenmesinde kullanılmıştır.

Anahtar Kelimeler: Yatay Eksen Rüzgar Türbini Rotor Kanadi, Fiber Takviyeli Kompozitler, Sonlu Eleman Modelleme ve Analizlari, Modal Test Doğrulamaları, Yüksek Sadakatli Modeller.

To My family, and my friends.

ACKNOWLEDGMENTS

The author wishes to express his deepest gratitude to his supervisor Assoc. Prof. Dr. Melin Şahin for his guidance, advice, criticism, encouragements and insight throughout the research, especially at the modal testing chapter of this thesis.

The author also thanks his friends, in the structure laboratory of the aerospace engineering department, especially Mr. Nima Pedramasl for his suggestions, comments and unconditional support.

Author also, highly appreciates the support provided by METU – Center For Wind Energy (METUWIND).

Finally, this Master's degree study, as well as the undergraduate level of the author, was supported financially mostly by the Republic of Turkey, specifically, the Turkish Abroad and Related Communities Association that is gratefully acknowledged.

TABLE OF CONTENTS

LIST OF TABLES

LIST OF FIGURES

CHAPTER 1

INTRODUCTION

1.1. Motivation of the Study

Nowadays, in Turkey, similar to other developed countries, the energy demand and the green energy production are being set into consideration especially in the last ten years. Aiming to reduce the dependency on imported gas and laying on outside resources, Turkey has set a goal to increase its wind energy output to 20,000 MW by 2023 [1]. For this reason, the government decision of investing on the wind energy research and development is set into action by creating the METUWIND (Center for Wind Energy) [2], which is one of the leading research and development centre in wind energy in Turkey and it is located in the campus of METU in Ankara.

The wind energy which is well known to be driven by wind turbines has the blades as the most critical part. This part must be well engineered in order to access the greatest amount of energy from air and transport it to the turbines creating the electrical energy. Thus, the blades, aerodynamically and structurally speaking, are the basic parts of this technology that must be studied and improved to the best way possible.

Structural analysis, being one of the primary aims of this study, comprises the modal analysis which is generally defined as the field of detecting the natural frequencies and the corresponding mode shape of a given structure. When under some particular excitation frequencies, a structure shows an excessive response and drastically high vibration amplitudes. Such vibrations will eventually lead to catastrophic failures and complete destruction of the structures and this phenomena is called as resonance. Especially for a machines having huge scales and performing

under continuously varying conditions such as wind turbines, investigating the dynamic characteristics of them has an extreme importance.

Therefore, in this thesis, the modal analysis and testing of a 5-meter-long horizontal axis, composite material, wind turbine blade is performed. By using advanced software in finite element modelling and analysis, i.e. MSC Patran/Nastran®, the numerical solutions are acquired. Then, these finite element models are updated via previously obtained benchmark experimental modal analysis results in order to obtain a high fidelity model that could be used for further studies regarding dynamic analyses.

1.2. Objectives of the Study

The objectives of this research study can be listed as follows:

- Performing an experimental modal analysis in order to extract the dynamic characteristics of the blade.

- Generating a low fidelity finite element model for a previously designed wind turbine blade through its design blue prints [3] by using the finite element modelling software MSC Patran® [4].

- Performing structural dynamic analysis via normal mode dynamic analysis solution types of MSC Nastran® [4] and checking the mesh independency of the finite element model in the calculation of various natural frequencies and the corresponding mode shapes, and comparing them with the ones obtained from the experimental modal analysis.

- Updating the former low fidelity finite element model to reach a high fidelity one.

1.3. Limitations of the Study

The limitation of this research study can be listed as follows:

- In the finite element analyses of the blade, the modes of the blade in the first three out-of-plane bending, the first torsional and a coupled one (first in-plane bending and second out-of-plane) are of interest.

- Although finite element analyses are performed for both fixed-free and free-free boundary conditions, experimental modal analyses are performed for only free-free condition due to the unavailability of the fixture to clamp the blade.

1.4. Outline of the Study

The organization of this thesis can be given as follows:

In Chapter 2, a brief literature survey about wind turbines and composite materials is provided. The focus is given more on the studies of modal analysis performed on wind turbine blades. The general procedure of constructing finite element models in order to perform the analysis and to setup the experimental measurements are also presented in this particular chapter.

In Chapter 3, the modal tests of the blade is presented in order to obtain the dynamic characteristics it by also providing the details on the experimental setup, instrumentation and the test procedure.

In Chapter 4, the details of the finite element modelling of the blade structure and the performed dynamic analyses for various boundary conditions are presented.

In Chapter 5, model updating is performed based on the data obtained from experimental modal analyses in order to obtain a high fidelity finite element model for the blade via FEMTools software [5].

Chapter 6 comprises the general conclusions drawn from this research study and provides recommendations for the future work.

CHAPTER 2

LITERATURE SURVEY

2.1. Introduction

As a part of the study, a survey has been performed in order to provide the necessary information and answer various questions about the wind turbine blades. The main topics are then summarized as; the locations of the wind turbines, their way of functioning, their advantages and disadvantages and the reasons of their preference. Additionally, a design of a blade is introduced by providing the properties of the material used in their production. Finally, vibration causing phenomena and the detection methods are presented with various modal analyses and experimental verification studies.

2.2. Wind Turbines

2.2.1. World Use of Wind Energy

Mariah Energy website [6] has presented a research on the top ten countries where wind turbines are mostly used. The power generation using wind turbines is being a global choice among many countries around the world. Although wind energy is mainly a clean and environmentally friendly source with almost zero greenhouse gas emissions, the localization of the wind turbines is still a crucial issue in order to harness the largest amount of energy available without affecting the Earth's nature.

The United States have plenty of wind turbine fields located all over its land which reduces the foreign oil dependency of the US and the local environmental

pollution. India produces 5% of its total energy from wind where this percentage increases year after year by aiming to take the lead over the developed nations using this technology. Germany and Spain are in the top countries in the green energy domain having 10% of their energy production from wind power. The United Kingdom, although possessing a significant number of wind turbines with a consistently high level of wind all year, only 2% of the country's energy is provided through wind. China has also started working to provide a clean energy to its huge population. Italy has also used this technology to keep the country's beauty and environment by providing the wind turbines for homes and business offices. Portugal, being relatively a smaller country, is also providing 11% of the nation's total energy by wind. Finally, Denmark, having 20% of its energy by wind, is the country on the top of the list of the most energy efficient countries [6].

Turkey, on the other hand, as the majority of the countries in the last decade, is also considering the renewable energy by aiming to implement it to a daily utilization. Turkey is obtaining its total installed power capacity from hydraulic, thermal and wind resources which was 49,524 MW at the end of year 2010. Although 37% of Turkey's land has a capacity to locate wind turbines, the percentage of the wind energy is only 3% of the total. The biggest wind energy power plant in the country is a 140.1 MW capacity one which was constructed in Soma-Manisa in 2012 [7].

2.2.2. Wind Turbines' Properties

Darvill website [8] provides much information about wind Turbines' history where long time ago the wind energy was being in use. Starting from the Babylonians, Chinese pumped water in the Middle Ages and in Europe, the grinding of corn was another way of using the wind where the term "windmill" comes from.

Referring to Figure 2.1, the following can be expressed about how the wind turbines function:

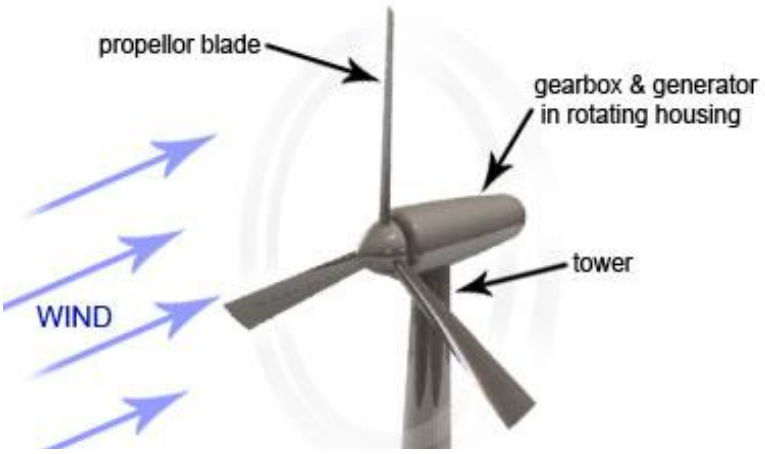

Figure 2.1. Wind Turbine [8]

Because of the uneven sun heating in the atmosphere, some areas become warmer than others. Hot air rises because of its low density and cold air replaces it creating a flow, so-called wind. The wind turbines are made by locating a large propeller on top of a tall tower as the air at a certain level up is usually faster than the one near ground level. Blowing wind makes the propeller turn which by itself turns a generator to produce electricity. Building many turbines near each other creates the well-known “wind farm” which produce more electricity, nonetheless, the steady state manner of the wind is an important parameter to consider by also avoiding some turbulences. In addition to these, the wind turbines with a relatively smaller blades and generators sizes are also placed on sailing vehicles like boats and caravans to charge batteries (Figure 2.2). Some blades can change their pitching angle in order to deal with the varying wind speeds in order to get the optimum energy.

Figure 2.2. Wind Turbine on Top of a Boat [8]

2.2.3. Wind Turbines' Locations

Coastal areas, top of rounded hills, open areas and gaps in mountains are known to be best locations to place the wind turbines (Figure 2.3) where wind is strong and reliable by providing the required average wind speeds [8].

Figure 2.3. Wind Farms [8]

2.2.4. Advantages and Disadvantages of Wind Turbines

The advantages of the wind turbines can be listed as follows [8];

- Since wind is abundant, the energy produced from it is relatively cheap.
- Since wind produces neither waste nor any greenhouse gases, thus there is no direct pollution effect.
- Since the turbines' towers are high, there is no total waste of the ground areas and the land below the turbines which can easily be used for farming purposes.
- In contrary to oil based electricity stations requiring tubing and long cable networks, the energy can be supplied locally and independently to far areas.

On the other hand, some disadvantages of the wind turbines seem to be unavoidable as follows [8];

- The inconsistency of the speed of the wind and its direction lead a discontinuity and a possible drop at the levels of the energy production.
- The coasts, being a good location for turbines, are generally more expensive than other lands by making wind turbine installation expensive.
- Covering landscapes by wind turbines disturbs the view and creates a scenery pollution to viewers.
- Since birds accidents are likely to happen, the migratory routes should be considered prior to place wind turbines.
- Since electromagnetic emissions of the turbines can affect radio-television reception, keeping them at a safe distance from residential areas is also important.
- Noise can be considered as the worst effect of the wind turbines (Figure 2.4).

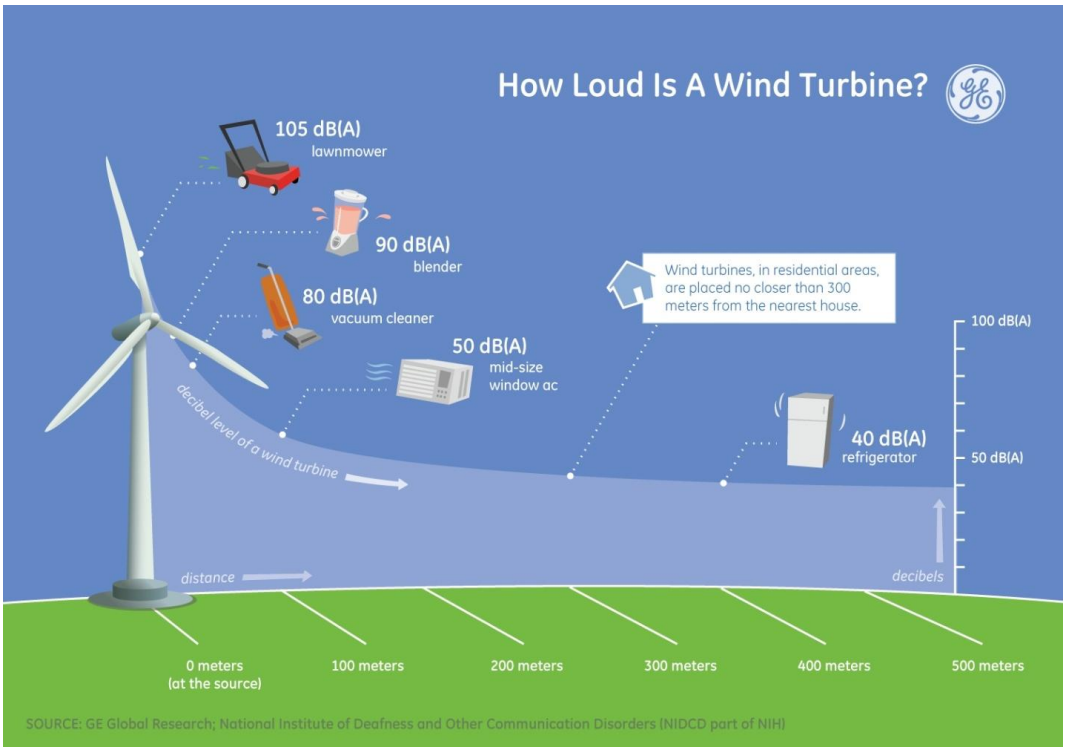

Figure 2.4. Wind Turbine Noise Comparing to Daily Used Machines [8]

2.2.5. World Production and Energy Price

All over the world, the wind power energy has shown a great growth, especially from 1995 to 2009 at a rate of 30%. At the end of 2008, the world's wind generating capacity was around 120,800 megawatts and produced about 260 terawatt-hours. This quantity is able to cover energy needs of approximately 26 million North American homes. The expected capacity by the industry is around 186,499 megawatts by 2010 and 332,100 megawatts by 2013. The cost of this generation in the United States is mentioned as $0.05 US per kilowatt-hour. Hydro-Quebec purchases 2,000 megawatts of wind energy for an average cost of $0.87 Canadian dollar per kilowatt-hour. While the Ontario Power Authority pays $0.1108 per kilowatt-hour. Nevertheless, these prices are expected to get much lower in the coming 100 years. In Canada, Texas, and the Great Britain, the wind power prices today competes with that of natural gas-fired and coal-fired electricity [9].

2.3. Wind Turbine Blades Manufacturing

The blades of the wind turbines are the most basic part of the system yet their design and engineering is one of the most complicated one. The important aspects of wind turbine technology require these blades to be durable, quiet, light and affordable. Balsa Wood and Plastic cardboard are some kind of materials used in its production referring the KidWind Blade Design [10].

Although two-bladed rotors exist, nowadays, most rotors have three blades and a horizontal axis with a diameter between 40 m to 90 m. However, three bladed ones are seen to be more efficient, allowing better distribution of mass and making the rotation smoother with a calmer appearance. The materials used mainly are synthetics reinforced with fibreglass and carbon fibre glued generally together by epoxy-resin. Wood, wood epoxy, and wood-fibre-epoxy compounds also exist and its advantages lay in their recycling capability. Aluminium and steel alloys are heavier and they usually suffer from material fatigue and therefore are only used over small scales [11].

Providing information about the blades, one should mention the World's biggest blade which is designed and produced by Siemens, namely; B75 (Figure 2.5). Its 75-meter-long (246 ft) blade component is made from epoxy resin and balsa reinforced with glass fibre. It is aimed to be located in a prototype 6-MW offshore turbine at Denmark's' national test centre at Osterild. Its sweep will cover 18,600 m^2 (200,200 ft^2) and the tip of the blades will move at 290 km/h (180 mph) at full lick. At a wind speed of 10 m/s (19.4 knots), the turbine will be hit by 200 tons (181 metric tonnes) of air every second. The blade length of 75 m is actually way too larger than an Airbus A380 [12].

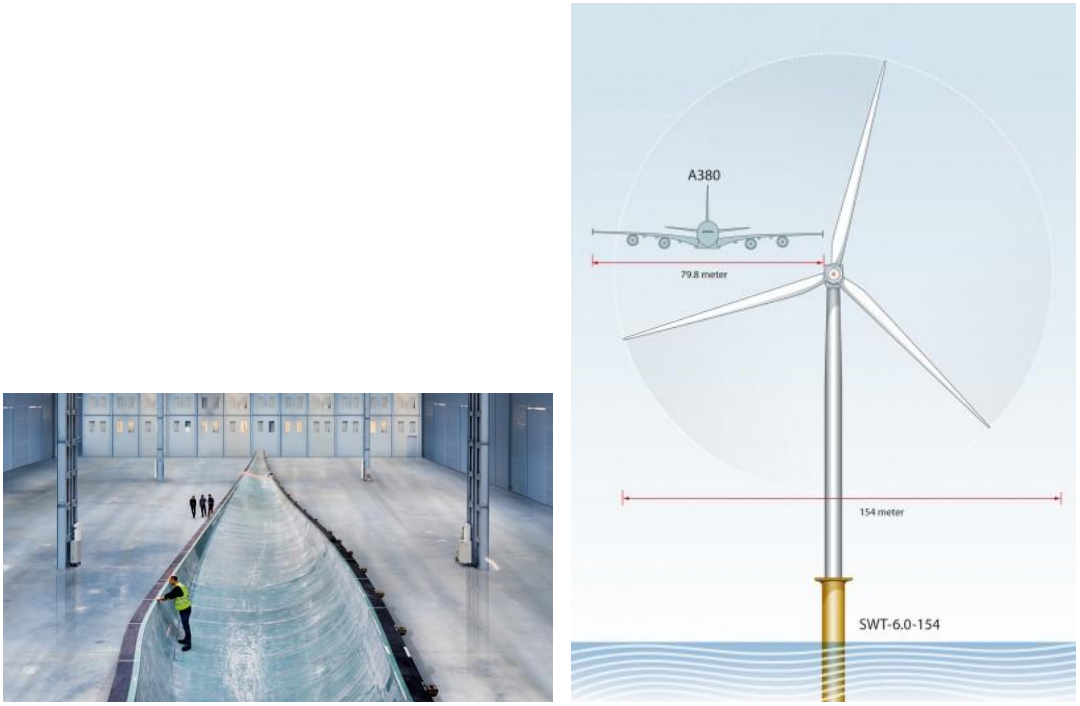

(a) **(b)**

Figure 2.5. The B75 Wind Turbine Blade Made By Siemens (a) In Production (b) A Scale Comparative Schema [12]

Since the modelling and the production of the wind turbine is one of the essential part of the research, a study about composite wind blade engineering and manufacturing done by TPI Company is presented [13]. First of all, the anatomy of a wind turbine blade can been seen in Figure 2.6. The blade made by TPI are composites, multiple of non-homogenous materials, mainly strings and glues which are put up together. Many method of production might be used and mainly infusion is the most frequently used one (Figure 2.7). The aforementioned company has produced multiple size wind turbines from 1980 to 2014 and are planning to continue manufacturing till 2020 with increase in sizes as it can be seen in Figure 2.8.

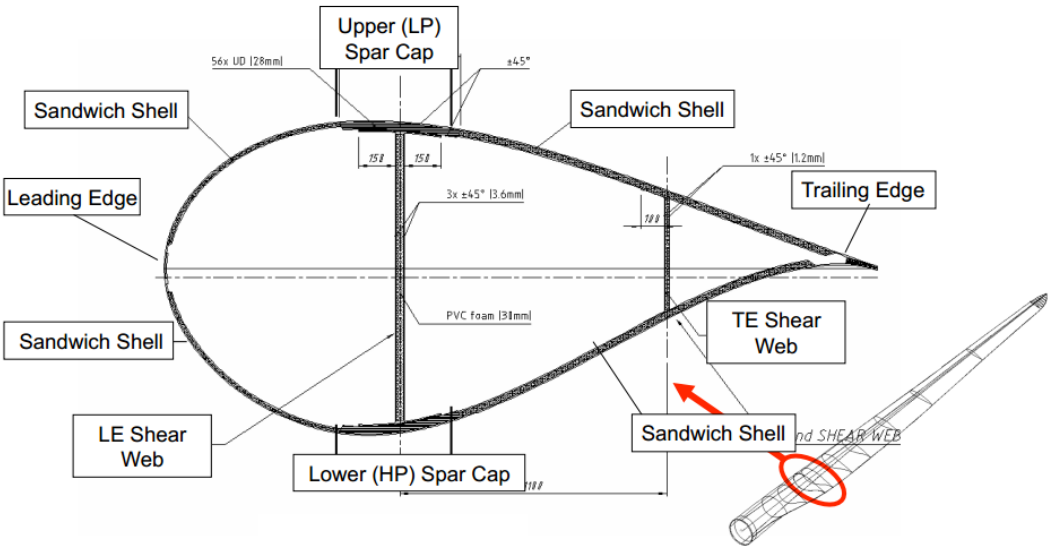

Figure 2.6. A Wind Turbine Blade Anatomy by TPI [13]

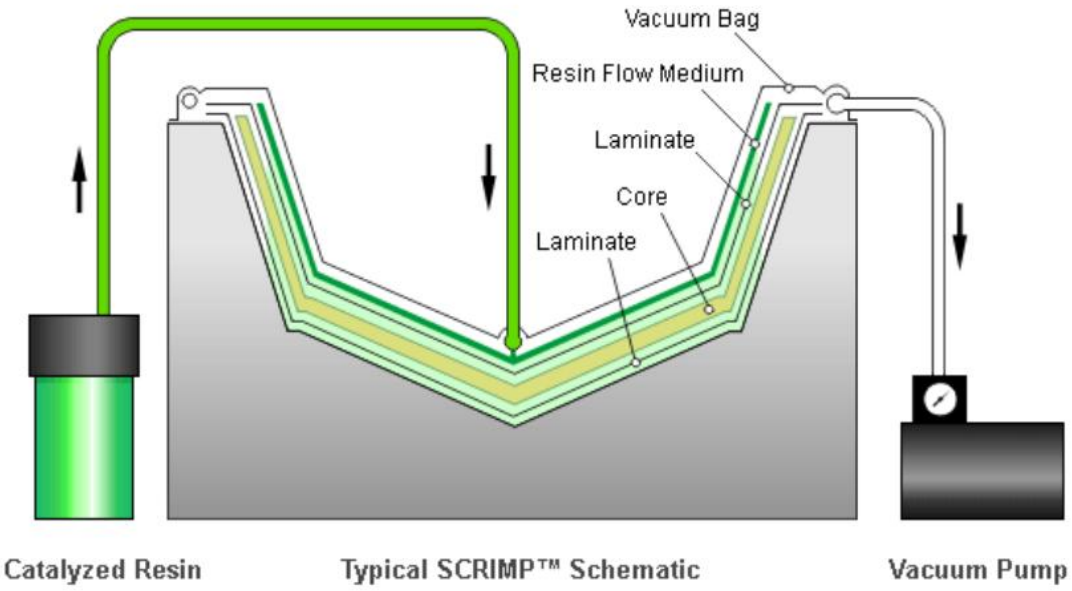

Figure 2.7. Seemann Composite Resin Infusion Molding Process (SCRIMP), by TPI [13].

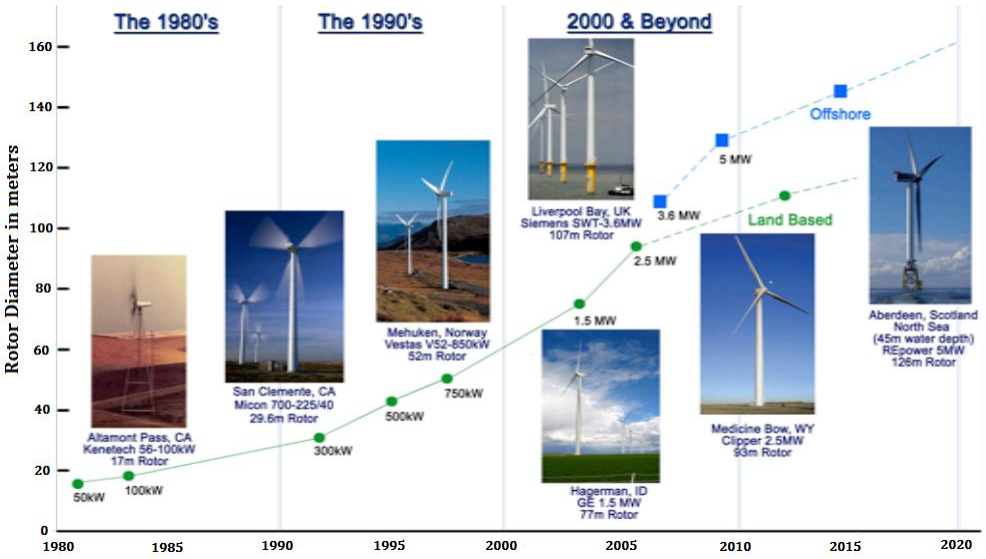

Figure 2.8. Historical Review and Future Plans of Wind Turbines by TPI [13].

When it comes to the materials used in wind turbine blades engineering, new designed composite materials have their own properties with a privilege over wrought materials. As the wind turbines are made up of these materials, it is important to understand their advantages and disadvantages [13].

Their advantages can be listed as;

- Possession of higher specific strength and specific modulus characteristics, where they are lighter and stronger than wrought materials such as wood, aluminium, etc.
- Mechanical properties can be regulated as requested by changing the layer number and orientation, thus providing an optimized structure.
- Manufacturing operation is easier in the terms of generating smooth surfaces.
- Because of its easiness of shape deformation in production, replacing many parts are easier.
- Composites are less affected by corrosion, chemical integration and weather conditions.

On the other hand, they come with some disadvantages;

- Composite materials are more brittle than wrought materials.
- Repairing them needs extra time and special equipment since the materials require hot curing in general and refrigerated transportation and storage.
- Rivets, in case of repetitive implementation, can easily damage them.
- Drying is required before repairing, since it includes in general moisture-absorbing materials.

The diverse material used in engineering can be shown and compared in the figure below and wrought materials shown here have lower Specific Ultimate Tension and Specific Modulus values compared to the composites, especially T and M-type ones (Figure 2.9) [14].

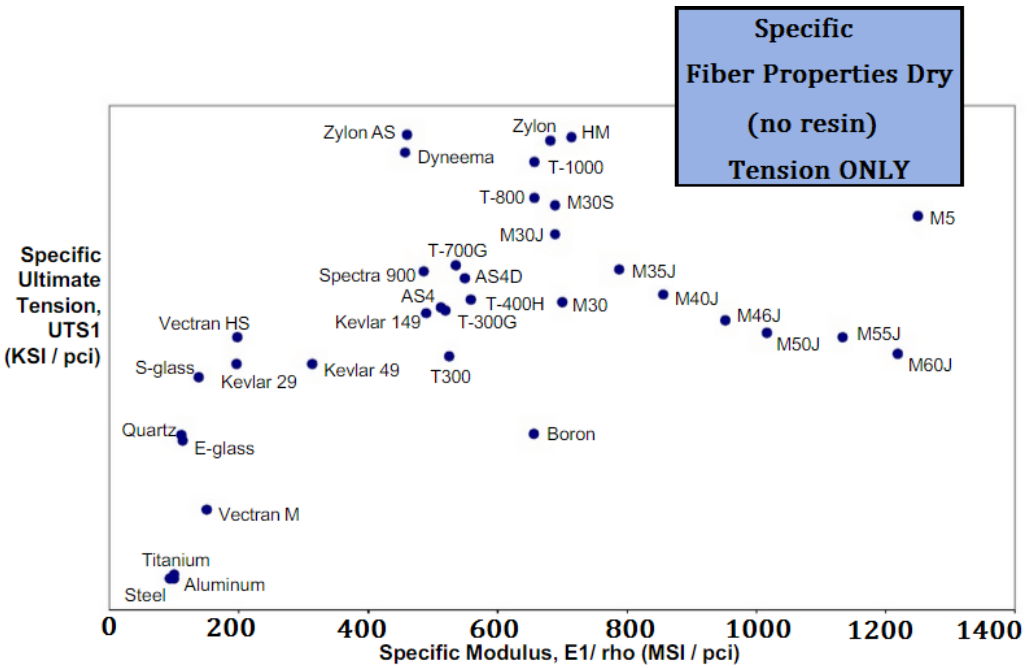

Figure 2.9. Composite and Wrought Materials Comparison [14]

Figure 2.10 represents the increase of use of composites by Boeing Company over time. One of the very examples of the development at the Boeing Company is its lastly developed B787 Dreamliner which is shown in the Figure 2.11 by specifically presenting the location of materials used all over the aircraft's structure [14].

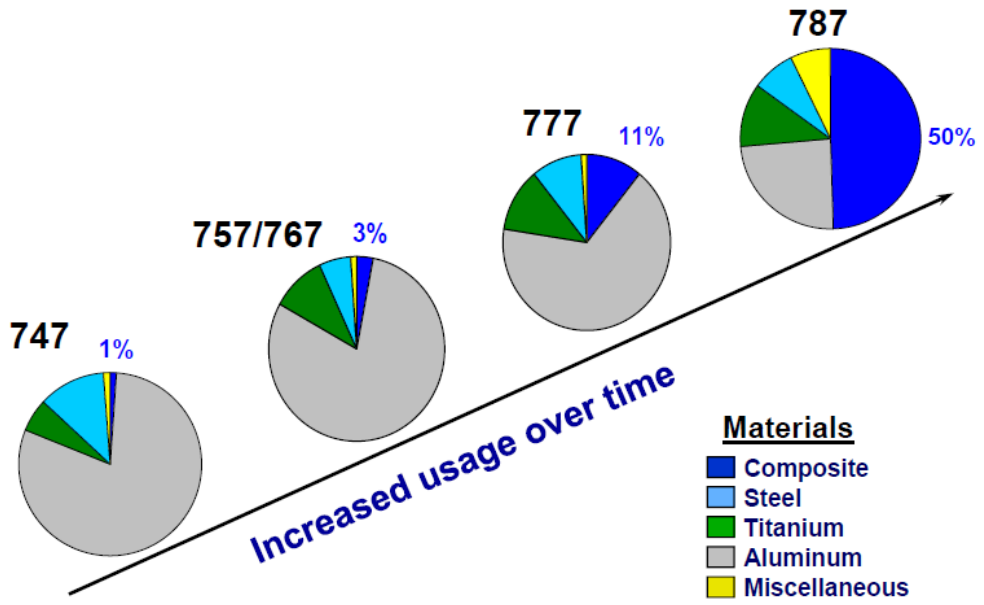

Figure 2.10. Boeing Companies Materials Usage Percentage over Time [14]

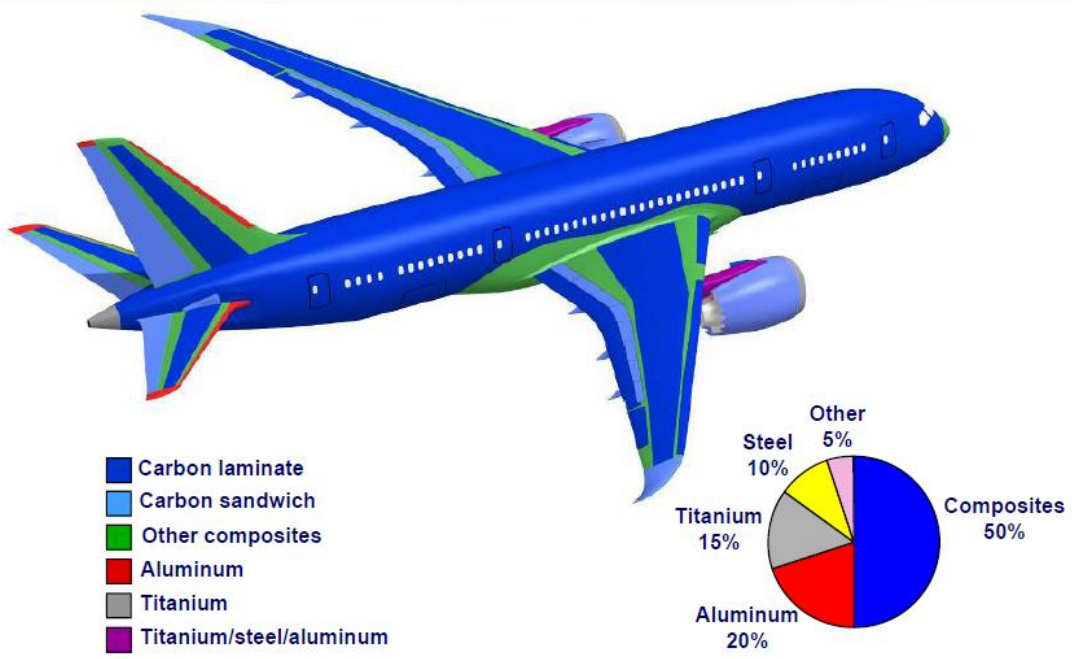

Figure 2.11. Boeing Companies B787 Material Usage [14]

The use of composites became so wide among almost all industries such as; aircraft industry, boats, underwater, sport equipment, medical prosthetic devices, electronic circuit boards and automotive. Aside the requirements of each of the applications, all these have the generation of reliable, strong and well-shaped light designs in common.

As main ingredient of the composite materials, so-called matrices can be classified as follows: The epoxies remain a primary resin used in European based blade designs. Additionally, vinyl-esters are attracting much interest by blade designers as well. On the other hand, polyester resin is still prominent in the industry while the thermoplastics and other "toughened" matrices might also be used. Figure 2.12 shows a production setup of an example of one section of a blade. Two-part epoxy paste adhesives specifically formulated for their thixotropic properties are the mainstay for bonding and assembly. Figure 2.13 shows a scene of adhesive pasting. Core materials are also essential in blade manufacturing as they are used primarily at large areas to provide stability in leading/trailing edge panels and shear webs. They are, in general, End Grain Balsa (low cost with high shear strength properties), Foam Cores (such as PVC, SAN, Urethane, PET) or Engineered Core Materials (such as Webcore TYCOR, and NexCore) [13].

The basic materials in a primary design can be set as follows [13]:

- For Reinforcements: Glass (with low-cost, high specific strength, modest specific stiffness) or Carbon (with high cost, high specific strength and stiffness) are used. The Aramids and Basalt might also be used.
- For Resins: Epoxies, Vinyl/Poly-ester, "Toughened" Resins (such as ETBN/CTBN Reactive liquid polymers), Core Shell Rubber and Thermoplastics are used.

Figure 2.12. A Blade Production Setup [13]

Figure 2.13. Adhesive Pasting [13]

The reinforcement forms for wind turbine blade manufacturing can be listed as follows [13]:

Pre-impregnated and/or dry reinforcement forms:

- Consolidation of Prepregs
- Vacuum Resin Infusion (VARTM – Vacuum Assisted Resin Transfer Molding, SCRIMP - Seeman Composite Resin Infusion Molding Prosses)
- Hand Layup/Vacuum Assisted Hand Layup
- Automation (Prepreg tape and "Tow-pregs")

Woven Fabrics forms and properties of the materails:

- Used in tooling applications and pre-impregnated forms
- Higher costs and less applicable as structural components for blades
- Used in areas of high stress fields

Non-woven Multiaxials forms and properties of the materails:

- Used in VARTM processes
- Lower costs and Non-crimp form results in superior performance
- Available in the form of "Uni-directional", Biaxial, Double Bias, Triaxial and Quadraxial as well as Glass/Carbon/Aramid Hybrids.

Centraltrykkeri [17] expresses the rotor blades as mixture of fiberglass mats which are impregnated with a material such as polyester glass reinforced plastics. The polyester is hardened after it is impregnated to the fibre-glass and in some cases epoxy is also used instead of a polyester. Likewise, the reinforcements are sometimes made wholly or partly of carbon fibres forming a lighter but more expensive material with a high strength. Wood epoxy laminates are also preferred in large rotor blades.

2.4. Finite Element Modelling of Wind Turbine Blades

In the development of wind turbine blades, finite element method (FEM) has been used among many researchers, to detect the general behaviour, in terms of eigenvalues, tip deflections and main stress/strain levels, of the structure. Adding to that, the finite element simulation predicts global stiffness and stresses with a reasonably good accuracy. Jensen et al. stated that, to have a good accuracy in the simulation of such geometries, modelling may be performed by using two different approaches. Either by using the two-dimensional shell models to generally represent the global behaviour or via the three-dimensional solid models which are more accurate yet requires longer computation time and advanced computers. Additionally, the solid model may not be hundred percent accurate without updating the FE model as a certain tolerance and it is inevitable to have difference between the manufactured and the designed models [15].

In the work of Branner and Blasque [16], in the analysis of 8 meter long wind turbine blade, the model was created using MSC Patran/Nastran finite element analysis using 20-noded solid elements (Hex20) and 8-noded shell elements (Quad8). The solid elements were applied to model the core (foam) and/or adhesive bonds (glue) while the sandwich face layers and caps were modelled with layered shell elements. Mckittrick et al. [18], in their modelling of composite wind turbine blade in ANSYS, developed the FEM using shell elements capable of showing layer options through thickness of the shell. Furthermore, Nicholas S. Asseff [19] made a selective decision of his finite elements for modelling an ocean current turbine blade by using ANSYS code where shell elements were used. Yanbin et al. [20] created a model of a wind turbine blade in CATIA and they imported this three-dimensional generated model into ANSYS where shell elements were used as linear and multi-layered elements. In addition to this research, Zhu and Rustamov [21] performed a structural design and finite element analyses of 24 m-long composite wind turbine blade using ANSYS software via 3-D linear layered structural shell elements. They achieved a high accuracy both in static analyses (i.e. in the calculation of the tip deflection, total mass and the centre of mass of the blade) and in dynamic ones (i.e. in the calculation of the natural frequencies).

2.5. Modal Analysis and Testing Methods for Wind Turbine Blades

In the same study of Mckittrick et al. [18] mentioned above, they also calculated the characteristics values corresponding to fixed and static case of the blade. Yanbin et al. [20] also performed modal analysis via finite element where they expressed the modal analysis theories prior to their tests. They mentioned that the essence of modal analysis is to solve the motion vector of the modal equations with a finite number of degree of freedom under no-damping and no-external load condition.

The instrumentation and measurements techniques were introduced by Chauhan et al. [22], when they performed the analysis over a three bladed turbine of 3MW power output and rotor diameter of 100.8 m namely; the ECO 100. The frequencies of interest were under 50 Hz, based on that, Bruel&Kjaer (B&K) DC accelerometers Type 4575 where chosen and an optical tachoprobe B&K Type MM-0360 measured the RPM. The data acquisition software used was also B&K PULSE Data Recorder type 7780 and the data were analysed via PULSE OMA Type 7760 to estimate modal parameters for dynamic characterization of the turbine. In order to cover possible vibrations with a wide dynamic range four B&K PULSE IDA frontends Type 3560 were used.

In addition to aforementioned modal tests, Larsen et al. [23] explained the theory behind modal analysis by representing the wind turbine (Figure 2.14) where they assumed the degrees of freedom (i.e. the direction of vibration) as translational in two perpendicular directions x and y and also adding the rotational one (i.e. theta).

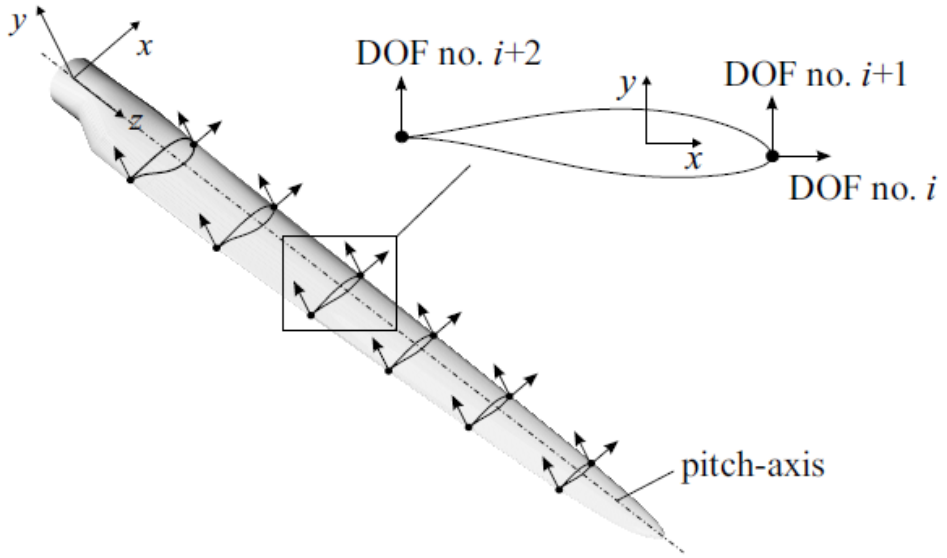

Figure 2.14. The Degrees of Freedom Measured For a Wind Turbine Blade [23]

Experimental methods for modal analysis techniques were then presented by explaining how to excite the wind turbine blade and how to ensure acceleration responses. For the excitation techniques, two categories were defined as the basic transient for free vibration (instantaneous release from an initial deflection) and continued excitation for forced vibration (with electromagnetic or hydraulic based exciters inducing many kinds of excitations like: swept-sine, white noise, pseudo-random and periodic-random excitation). Response at other side, consists of accelerations measured in various number of sections along the pitch axis. Uniaxial, bi- or triaxial-accelerometers might be used taking into consideration in every direction of vibration to be covered. One setup based on the experiences gained during the experimental campaign is introduced for the test of LM 19 m blade in Figure 2.15.

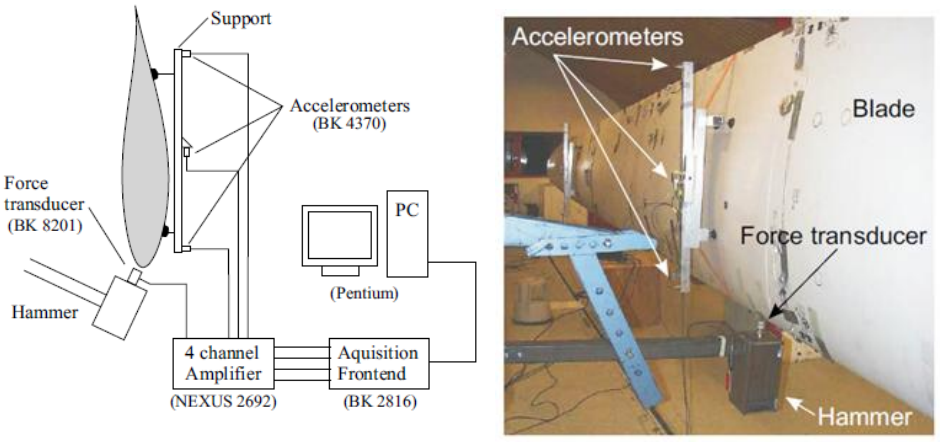

(a) **(b)**

Figure 2.15. Recommendation for Experimental Setup (a) Schematic View (b) Real View [23]

In their modal testing of the TX-100, Griffith et al. [24] used bungee cords in order to simulate a free-free boundary condition. The two hanging configuration they used are presented in Figure 2.16 as two point hanging pre and post the Centre of Gravity (CG) of the blade (Figure 2.16a) and the CG point hanging (Figure 2.16b). These two configurations showed a bouncing/rolling rigid body motions under around 3 Hz and a 25 Hz one for the 1st flexible body mode. 34 accelerometers were used in biaxial configuration and nine data sets were acquired. Using an impact hammer, six flap wise and three edge wise excitations were created and in all these cases periphery locations were chosen to have better effect of the hits.

In the study of model validation and structural analysis of a small wind turbine blade of Pabut et al. [25], the experimental modal analysis was performed in the form of calibrated impulse hammer (Model AU01) test where soft restraint was applied to the test specimen. FRFs were acquired after exciting the structure at predefined points by using SigLab Model 20-22A and the experimental modal analysis setup was done as presented in Figure 2.17.

(a)

(b)

Figure 2.16 Bungee hanging setup (a) at Two Points (b) at One Point [24]

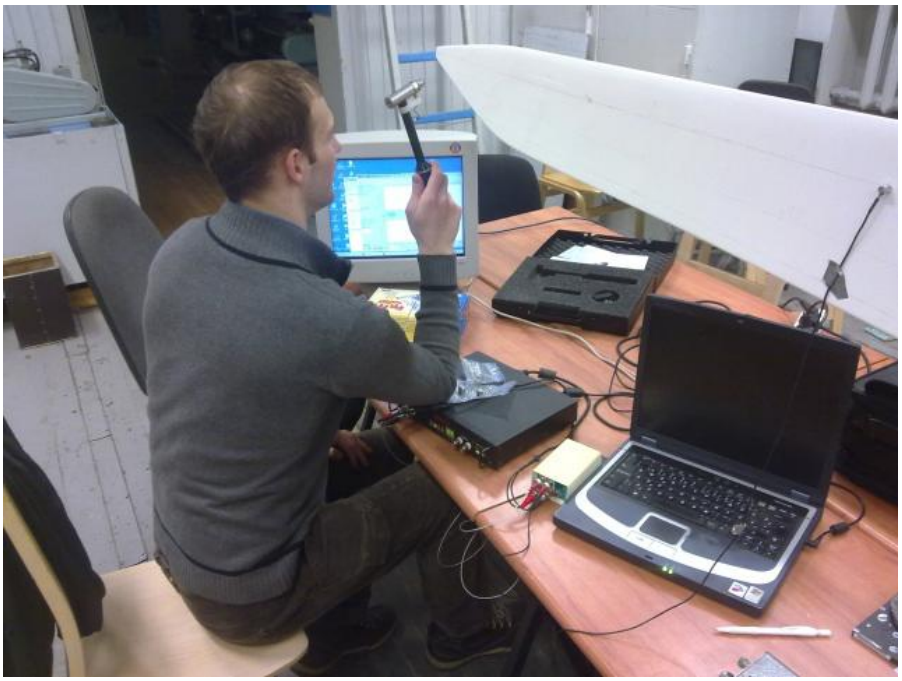

Figure 2.17. An Experimental Modal Analysis Setup Example [25]

In this study both free-free and fixed-free boundary conditions were made. As they mentioned, the free-free boundary conditions allow to discard the stiffness of the restraints and therefore exhibits fewer degrees of uncertainty while the second configuration (i.e. fixed-free) simulates the actual working condition of the blade better. As a result, correlations were done between FEA and experimental analyses with around 7% errors for low frequencies and higher errors for high frequencies which were out of concern since they were away from the range of the real working condition.

2.6. Conclusion

With this literature review, the World use of wind energy, locations and properties of the wind turbines, their advantages and disadvantages were summarised by also outlining the World production and stressing the corresponding energy prices. The review also provided the basis for the wind turbine blade manufacturing and focused on the finite element modelling/analysis and modal testing methods of wind turbine blades.

CHAPTER 3

MODAL TESTS OF THE WIND TURBINE BLADE

3.1. Introduction

The manufacturing process of the blade of interest has been done in CompBlades company, in Athens, Greece [26]. This company is the main manufacturer and supplier of the blueprints of the manufacturing for this project. Having received the actual blade from the company, the Classical Modal Analysis and testing of the blade at Free-Free boundary condition is performed by using different techniques in the laboratories of METU, Department of Aerospace Engineering. First, the Impact Hammer is used as an excitation and the accelerometers are for the vibration response recording for a quick diagnostic dynamic test. As a second test, on the other hand, the modal shaker is used for the excitation with the previously used response transducers. The third test is performed via modal shaker and the Laser Vibrometer combination.

3.2. Tools and Instruments

The main instruments and tools used in the tests can be listed as follows:

- Accelerometers
- Force Transducers
- Impact Hammer
- Modal Shaker
- Scanning Laser Vibrometer
- Data Acquisition System

The accelerometers used are the Brüel & Kjaer (B&K) of two types, the uniaxial of type (4508B) Piezoelectric CCLD accelerometer [27] and the triaxial of the type (4506) to measure the output as acceleration [27]. While the force transducers are of two types; one of is that measures the amplitude of the applied force by the Impact Hammer of the type (8206/53678) [27], and the other is of the type (8230-002 /54760) [27] DeltaTron® located on the top of the stringer connected to the Shaker of the type B&K 4825 [27]. In addition, to the signal generator of the type Agilent - 33120A Function (Arbitrary Waveform Generator, 15 MHz) [34], an amplifier [35], a High Performance Scanning Laser Vibrometer [PSV-400-B Polytec] [36], and the 6-Channel Pulse Data Acquisition System were used [37]. All these instruments can be seen figures below.

Figure 3.1. Uniaxial Accelerometer [27]

Figure 3.2. Triaxial Accelerometer [27]

Figure 3.3. Impact Hammer [27]

Figure 3.4. Force Transducer [27]

Figure 3.5. Modal Exciter (Shaker) [27]

Figure 3.6. Signal Generator [27]

Figure 3.7. B&K Power Amplifier [28]

Figure 3.8. Scanning Laser Vibrometer [29]

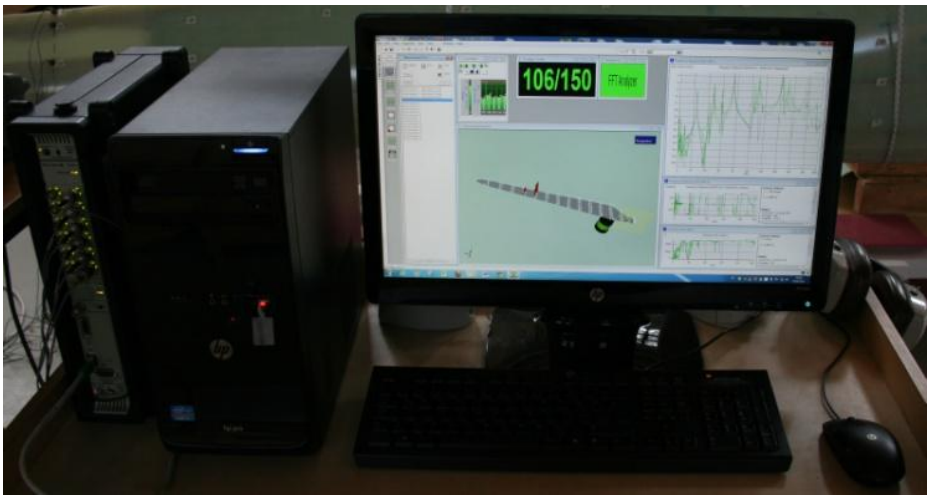

Figure 3.9. Data Acquisition System [27]

3.3. Test Software

B&K 3560-C PULSE^{TM} platform is used for data acquisition [27]. It is a 6-channel system and works compatible with the software PULSE^{TM} Labshop 13.5.0 [27]. In PULSE^{TM} Labshop, first the accelerometers and force transducer are introduced to the system. Then the measurements locations and the test geometry are defined in Modal Test Consultant (MTC) part of the software Labshop. Before starting test, Fast Fourier Transform (FFT) analysis settings were set regarding the number of FFT lines, frequency span and each measurement length. A sample screen for the PULSE^{TM} Labshop software given in Figure 3.10.

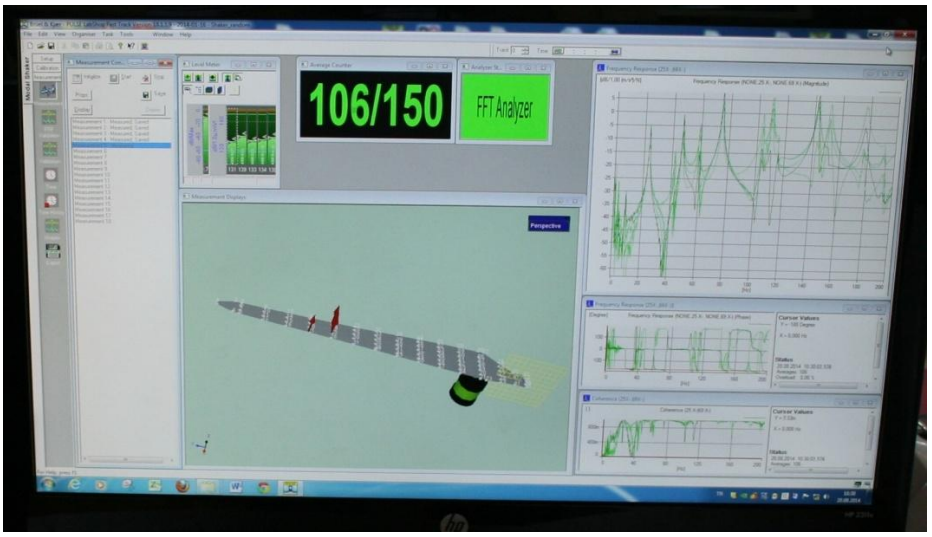

Figure 3.10. Sample Screen for the PULSE^{TM} Labshop Software

3.4. Test Preparation

The test setup of the examined blade and the equipment enrolled in the tests are presented in this section. The Free-Free boundary condition is set for the tests and it is presented in Figure 3.11.

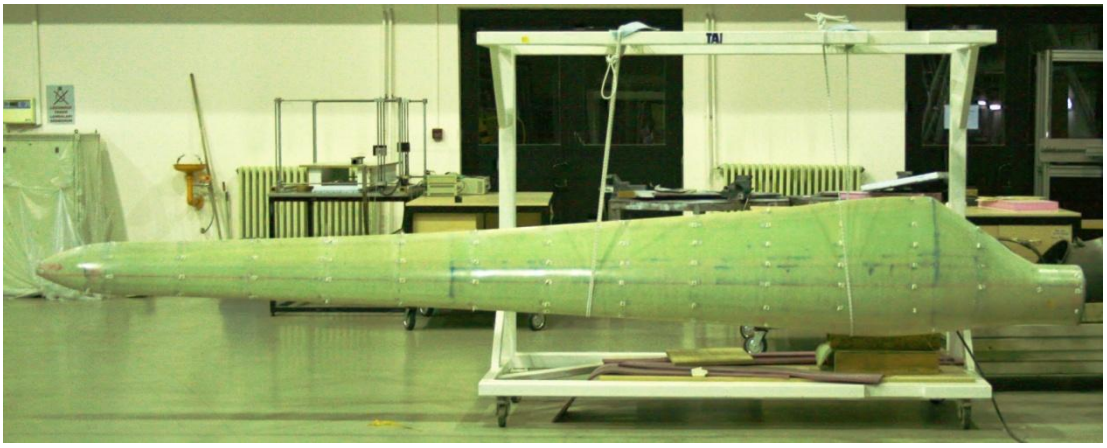

Figure 3.11. Free-Free Hanged Blade with Measurement Points

As it can be seen from the above figure that the blade is hanged from two different positions around the centre of gravity by an elastic yet strong wires connected to a steel truss-like structure. The blade was divided into sections each of which having measurement points, 87 in total. The suspension of the blade has been equilibrated horizontally and the zoom view of the blade is shown in Figure 3.12.

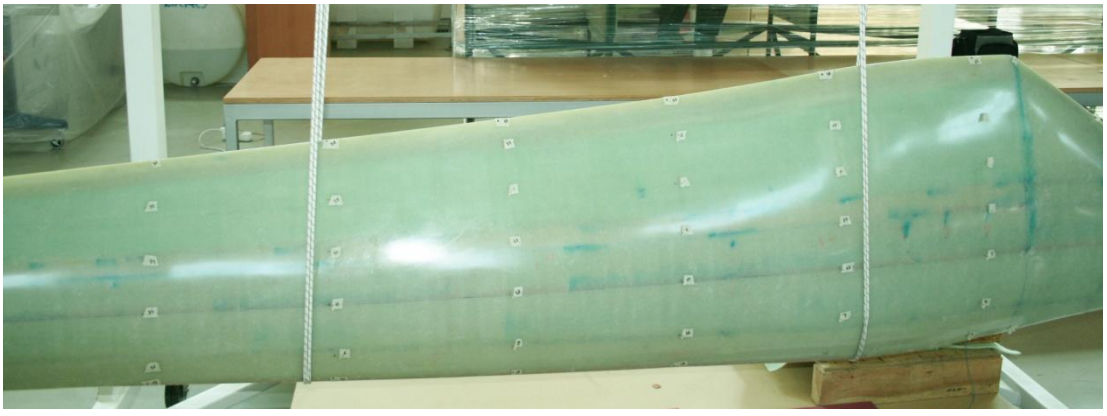

Figure 3.12. Free-Free Hanged Blade – Zoomed View

3.5. Classical Modal Analysis

At the experimental part of this study, the Classical Modal Analysis techniques are used for modal testing of the composite blade. Rowing impact hammer testing is first one to be conducted aiming to excite the blade both in out-of-plane and in-plane directions. Then, modal shaker tests are performed by using both distributed accelerometers and a Scanning Laser Vibrometer. These modal tests are detailed in the following sections.

3.5.1. Rowing Impact Hammer Tests

Impact Hammer testing is one of the most practical ways for modal testing requiring less equipment and relatively short measurement time. It is done by hitting the object studied by a sudden gentle impact in a very short time with no physical attachment, in contrary to the stringer of modal shaker method. The tip of the hammer is one critical issue to be chosen relatively to the desired frequencies. Three types of tips exist, namely; the rubber, plastic and the aluminium. The following Figure 3.13 shows the force spectrums and the frequency range covered by each different tip. For each signal in time domain (at the left), can be presented in the frequency domain (at the right), by using the Fourier Transform methods.

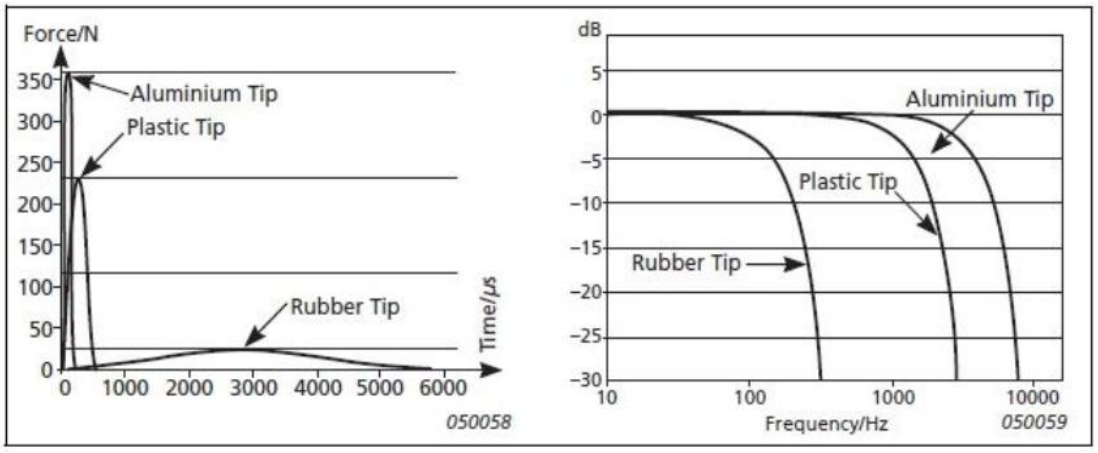

Figure 3.13. Impulse Shapes (Left) and Force Spectrums (Right) For Different Impact Hammer Tips [32]

Comparing to the desired coverage by the FEM (Table 4.8), a frequency range of approximately 11-70 Hz is required to be covered in an adequate modal analysis. By also considering the stiffness of the fibreglass surface of the blade, plastic tip was found convenient to be used. For the (Fast Fourier Transform) FFT analysis, the analysis parameters are set up regarding the interested frequency range. These parameters are given in Table 3.1.

Table 3.1. FFT Analysis Settings

Parameter	Value
FFT Lines	400
Span [Hz]	0-100
Measurements	4
Time [s]	4

Here the FFT lines are the number of discrete points where the FFT calculations are taken into account. The results of FFT, mainly the power spectral density as cross-spectral analysis, for both input and output, forms the FRFs, known as the frequency response functions. The Span is the interval where these calculations are made. Measurements are made for 4 hits per points. The time is selected considering the decay of the acceleration output of the test structure. The second step, is to draw the studied blade in the analysis software. Figure 3.14 represents the measurement mesh created in the Modal Test Consultant (MTC) software where each point of it, depending on the measurement type, corresponds to either the locations of the accelerometers or that of impact hammer over the real blade. Therefore, this particular geometry was used for impact hammer as well as shaker tests.

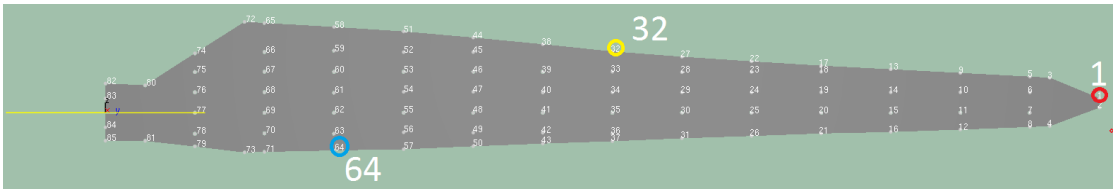

Figure 3.14. MTC Geometry with the Measurement Points

3.5.1.1. Out-of-Plane Excitation

For this particular test, two uniaxial miniature accelerometers were put over the blade at the points numbered (1) (red circle) and (64) (blue circle) and one triaxial accelerometer was located at the point (32) (yellow circle, in Figure 3.14). The locations of these accelerometers were chosen as such in order to cover both bending and torsional mode shapes. In Figure 3.15, the impact hammer head is resembled in black pointed heads, while uniaxial accelerometers are resembled by the red arrows, the measurement sensitivity directions of the triaxial one are presented by red, blue and black arrows.

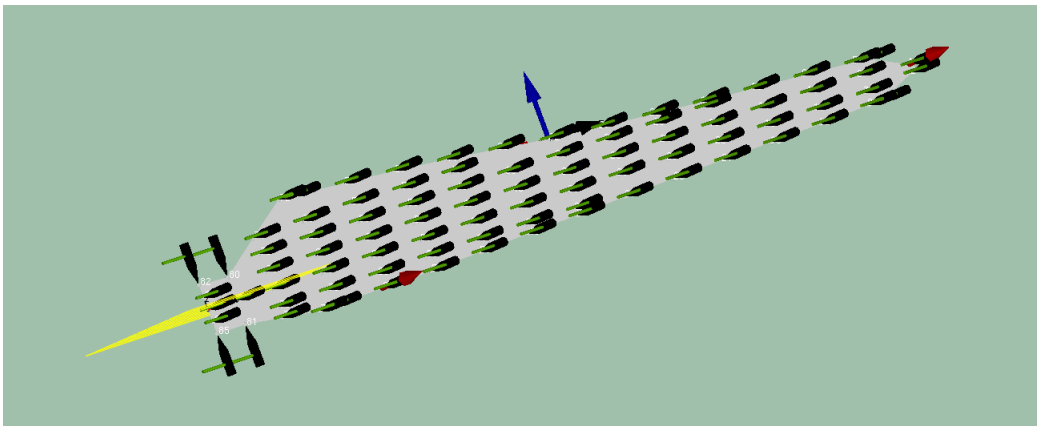

(a)

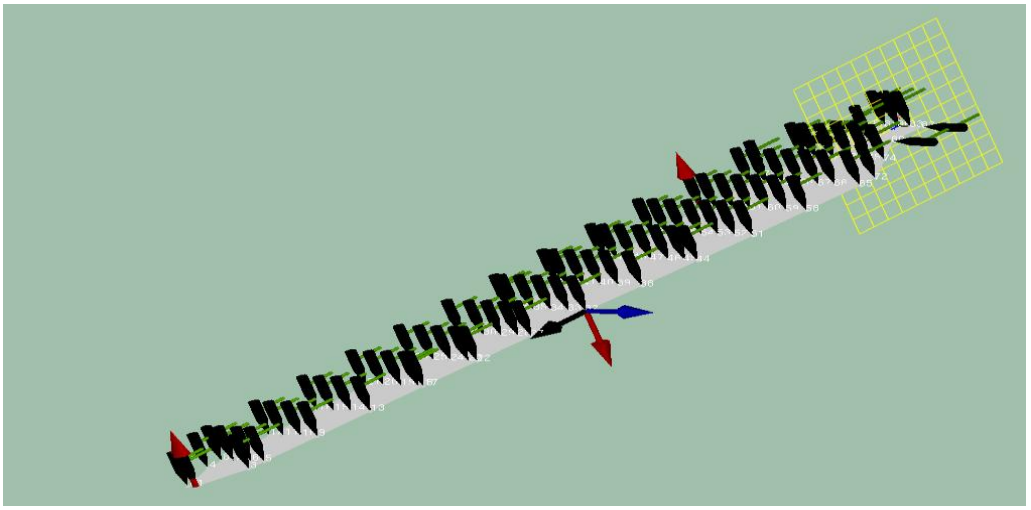

(b)

Figure 3.15. MTC Geometry for the Out-of-Plane Excitation Setup (a) Front view (b) Isometric view

By looking up to the real setup, an accelerometer's sample location is perpendicular to the surface which is bonded with bee wax and roller sticky band for safety as it can be seen in Figure 3.16.

Figure 3.16. Sample Location of the Uniaxial Accelerometer

This particular test was performed by hitting some selected points by the impact hammer, by ensuring that the excitation is parallel to the main sensitivity axis of the accelerometers, i.e. satisfying the condition for the out-of-plane excitation, and the corresponding responses were detected via three aforementioned accelerometers. The Frequency Response Function (FRF) curves of Accelerance for this test, are shown in Figures 3.17, 3.18 and 3.19 for the measurements taken from the accelerometers at Point (1), Point (64) and Point (32) respectively.

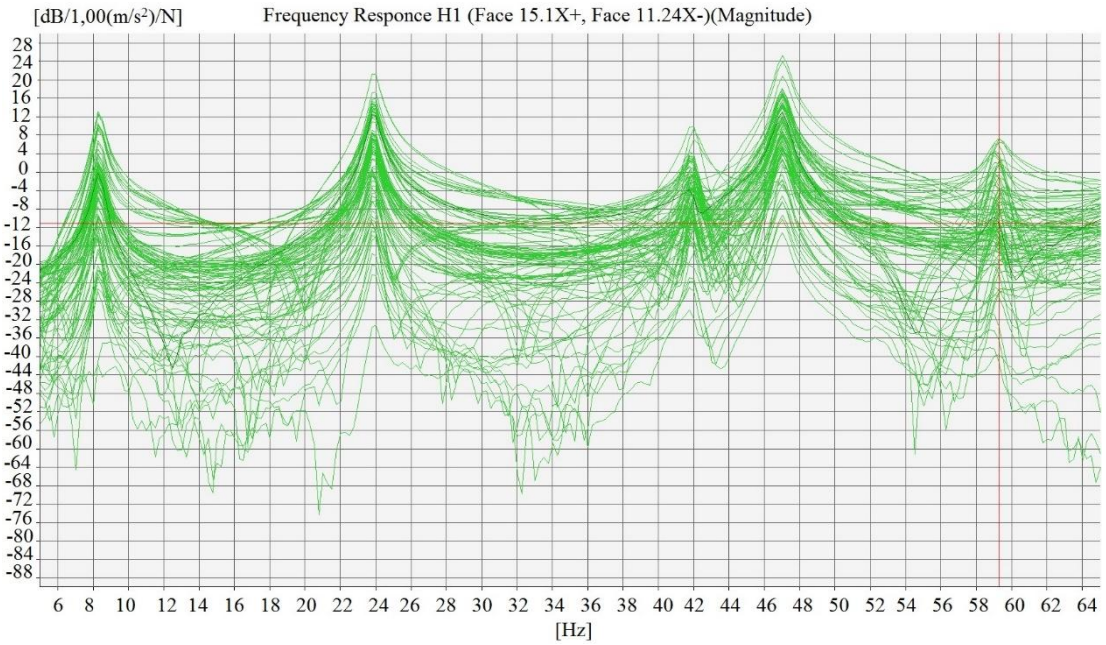

Figure 3.17. Accelerance FRFs of Force Transducer (Impact Hammer) and Uniaxial Accelerometer (4508 B) at Point 1

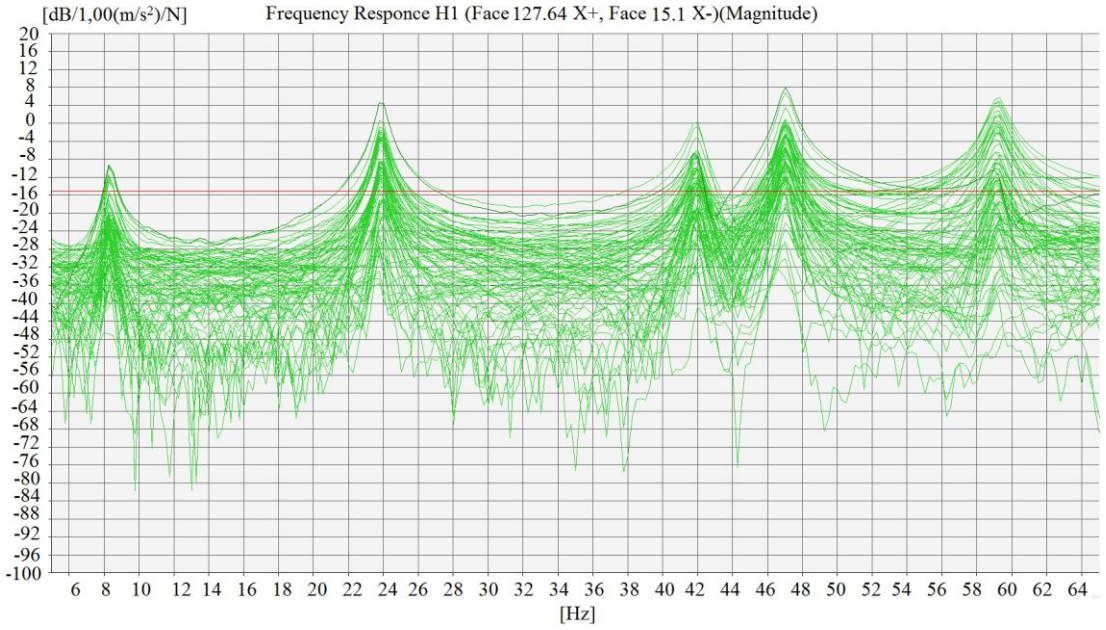

Figure 3.18. Accelerance FRFs of Force Transducer (Impact Hammer) and Uniaxial Accelerometer (4508 B) at Point 64

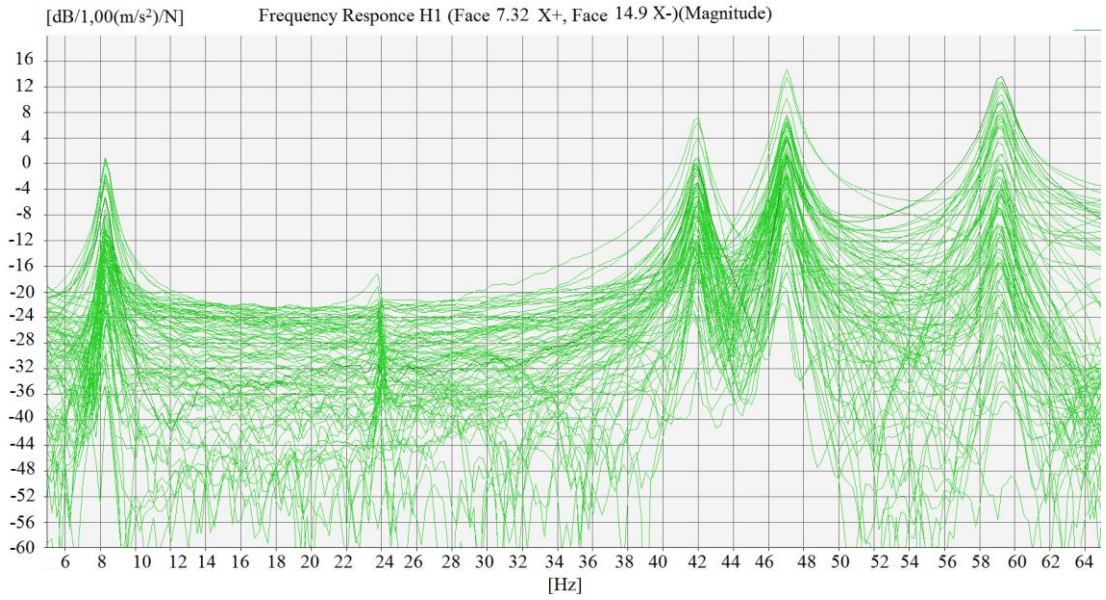

Figure 3.19. Accelerance FRFs of Force Transducer (Impact Hammer) and Triaxial Accelerometer (4506 B) at Point 32

By detecting the peak points of these FRF's the resonance frequencies are found and presented in Table 3.2. The corresponding mode shapes are also given in Figure 3.20-3.24.

Table 3.2. Resonance Frequencies obtained via Impact Hammer Through the Out-of-Plane Excitation

Mode Shapes	Resonance Frequencies [Hz]
1st Out-of-plane Bending	8.25
2nd Out-of-plane Bending	23.75
2nd Out-of-plane Bending with 1st In-Plane Bending coupling	41.50
3rd Out-of-plane Bending	47.00
1st Torsion Coupling	59.00

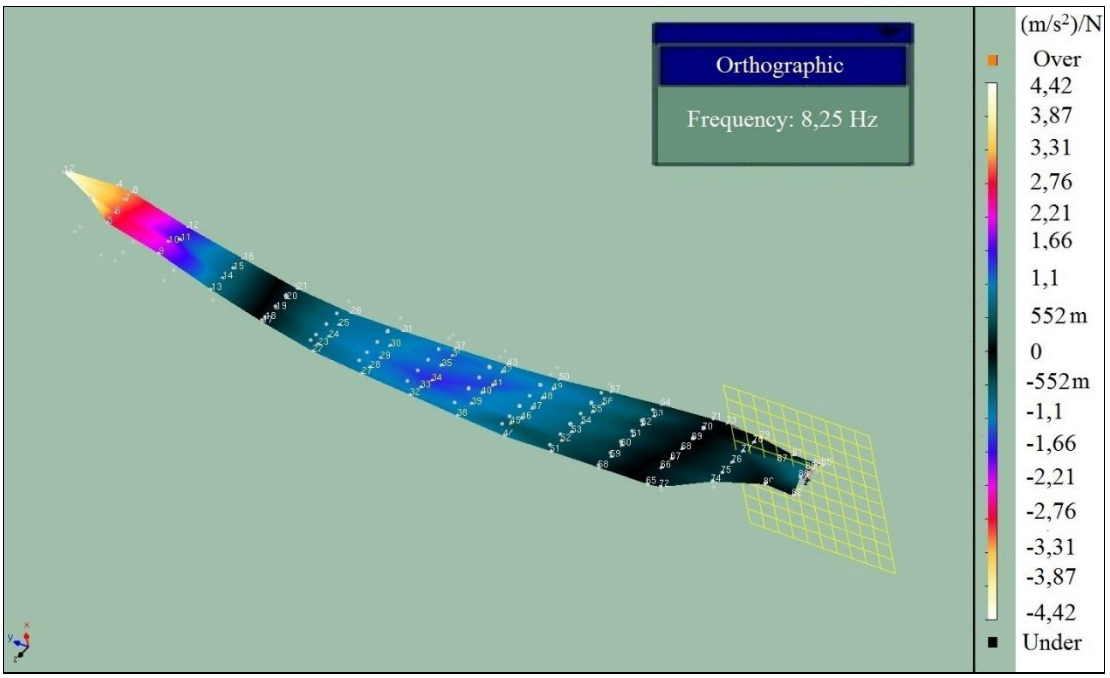

Figure 3.20. 1st Out-of-Plane Bending [8.25 Hz] – Rowing Impact Hammer

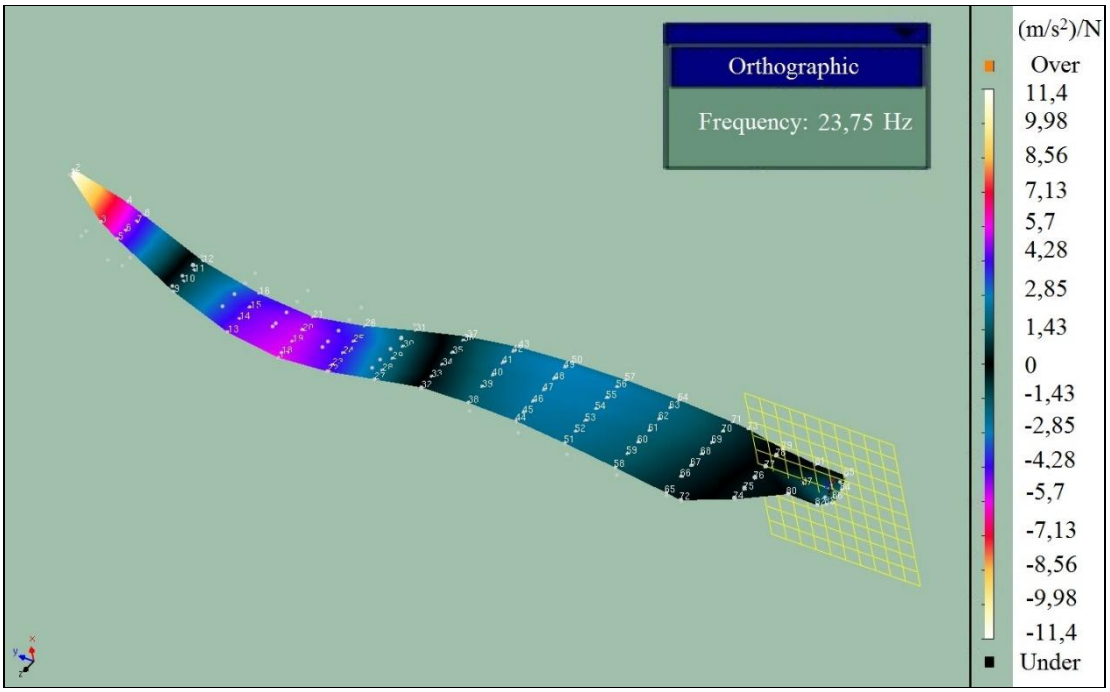

Figure 3.21. 2nd Out-of-Plane Bending [23.75 Hz] – Rowing Impact Hammer

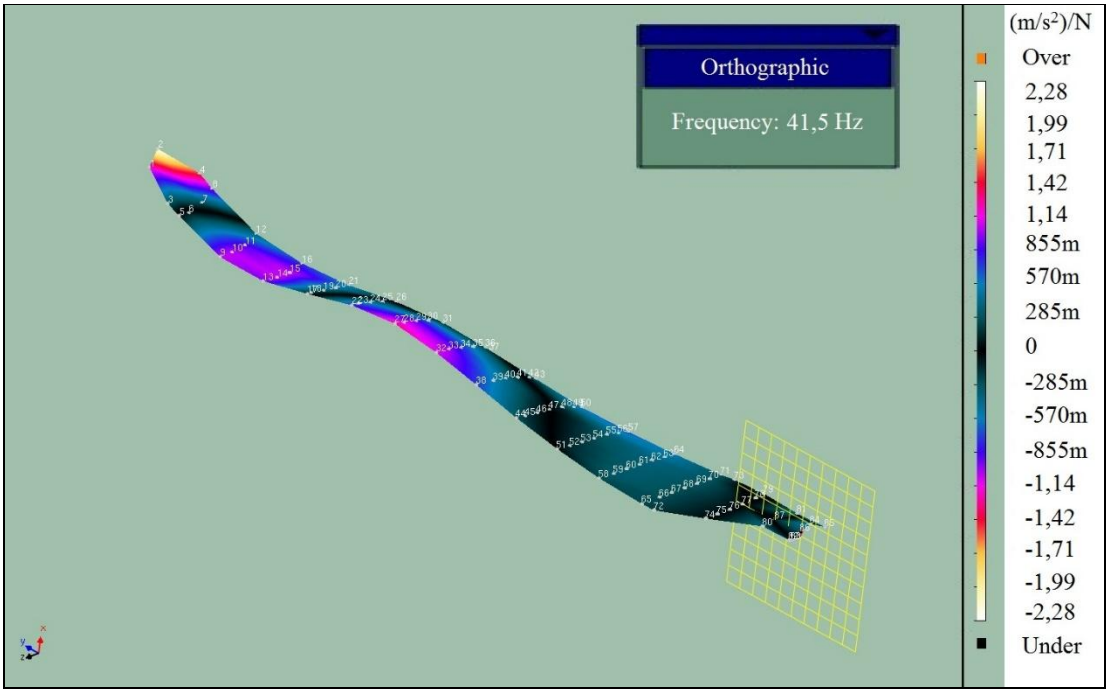

Figure 3.22. 2nd Out-of-Plane Bending with 1st In-Plane Coupling [41.50 Hz] – Rowing Impact Hammer

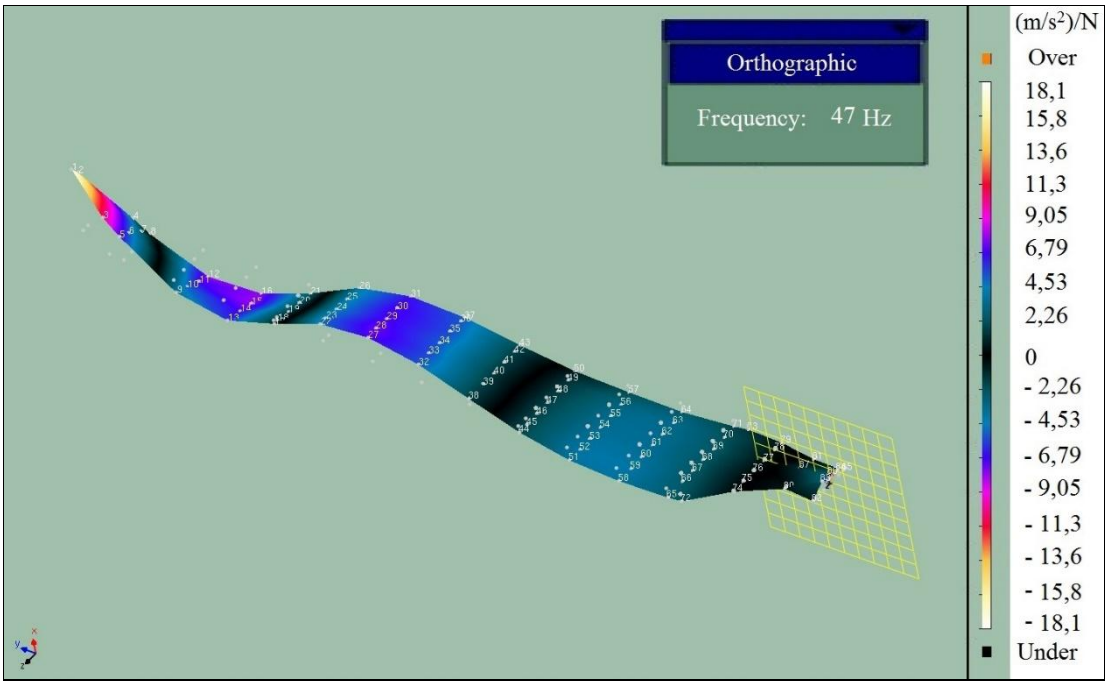

Figure 3.23. 3rd Out-of-Plane Bending [47.00 Hz] – Rowing Impact Hammer

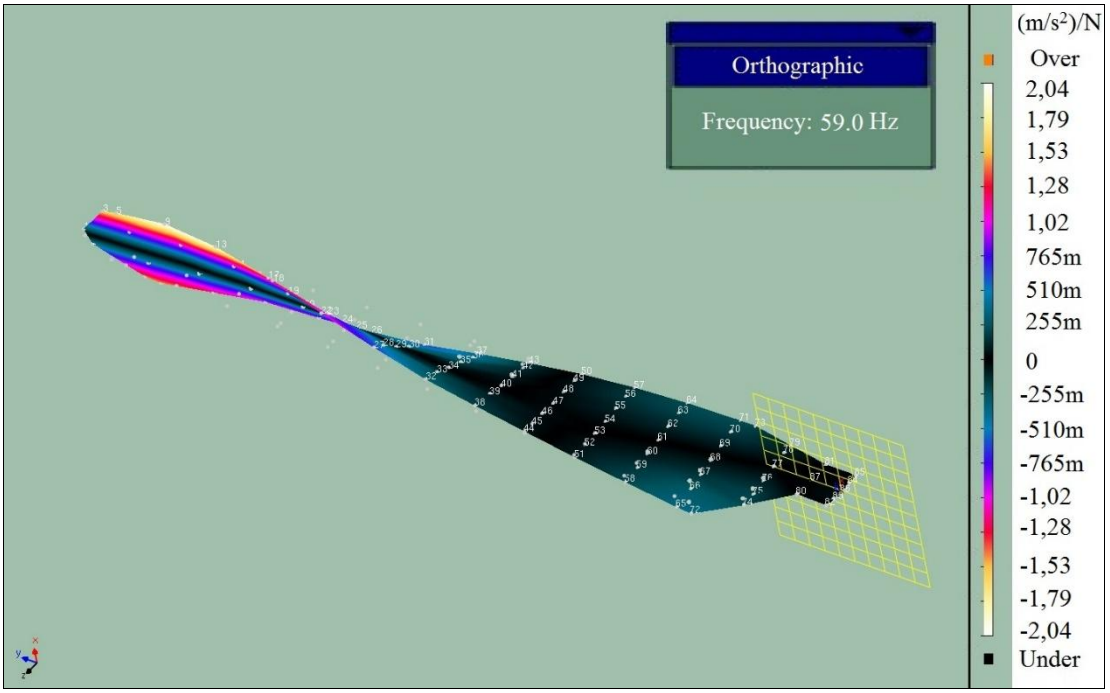

Figure 3.24. 1st Torsion [59.00 Hz] – Rowing Impact Hammer

3.5.1.2. In-Plane Excitation

For the In-Plane hammer test, no further modification was made in the software regarding the geometry and the measurement points. However, in order to have an excitation in the required plane, the blade was hit via impact hammer in its edge-wise direction (Figure 3.25).

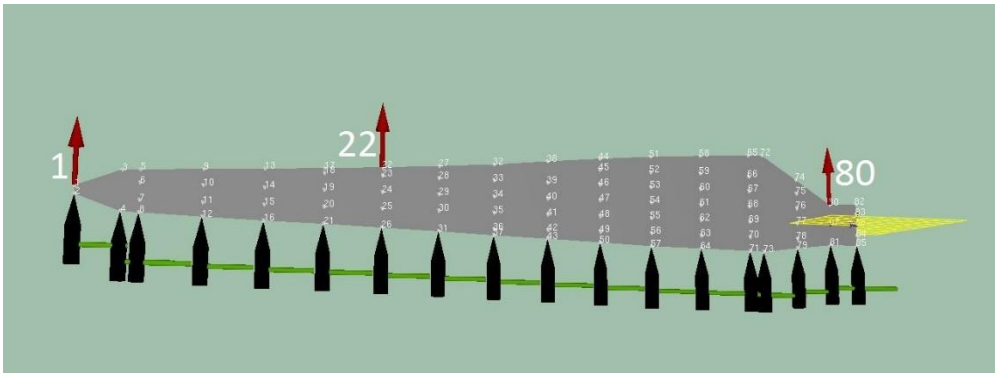

Figure 3.25. MTC Geometry for the In-Plane Excitation Setup – Front

As the leading edge of the blade is thicker then it's trailing edge, the hammer hits were performed along and in this part of the blade (Figure 3.26). The points numbered as (1), (22) and (80) were locations of the three uniaxial accelerometers of type (4508 B). The main aim of performing such a test is to obtain the in-plane mode shape(s) more clearly. A sample positioning of the miniature uniaxial accelerometer at Point (1) in the in-plane direction is shown in Figure 3.27.

FRF curves for the in-plane excitation are shown in Figures 3.28, 3.29 and 3.30 for the measurements taken from the accelerometers at Point (1), Point (22) and Point (80), respectively. By detecting the peak point of these FRF's, the resonance frequency at the first in-plane mode (41.75 [Hz]) is found and the corresponding mode shape is presented in Figure 3.31.

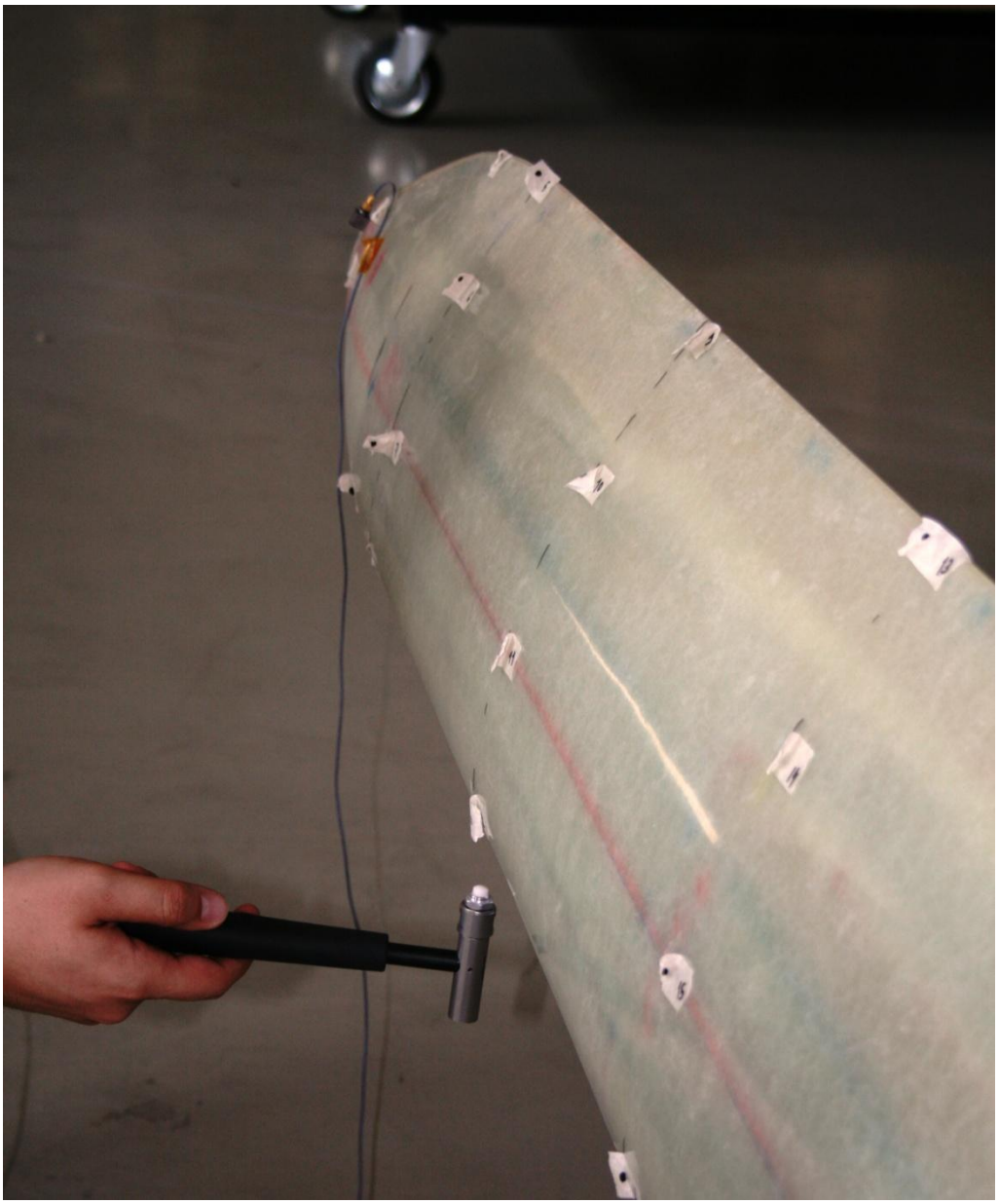

Figure 3.26. Hammer Hit at the Leading Edge of the Blade

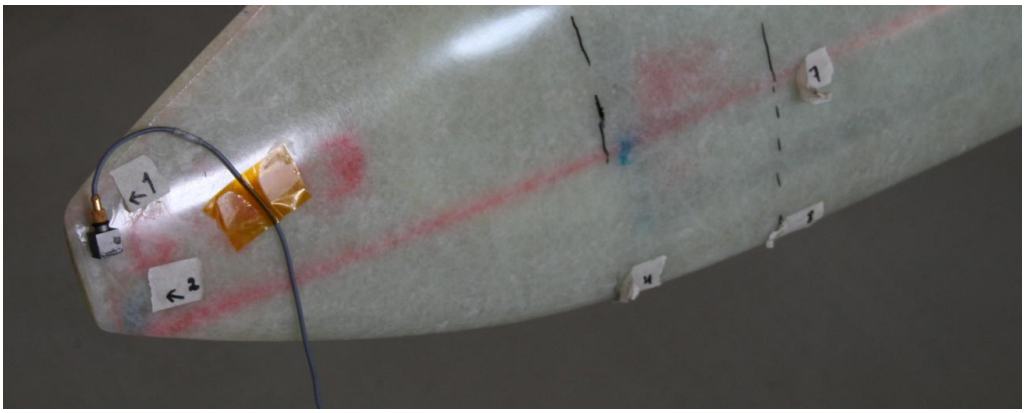

Figure 3.27. Uniaxial Accelerometer Positioned at Point 1

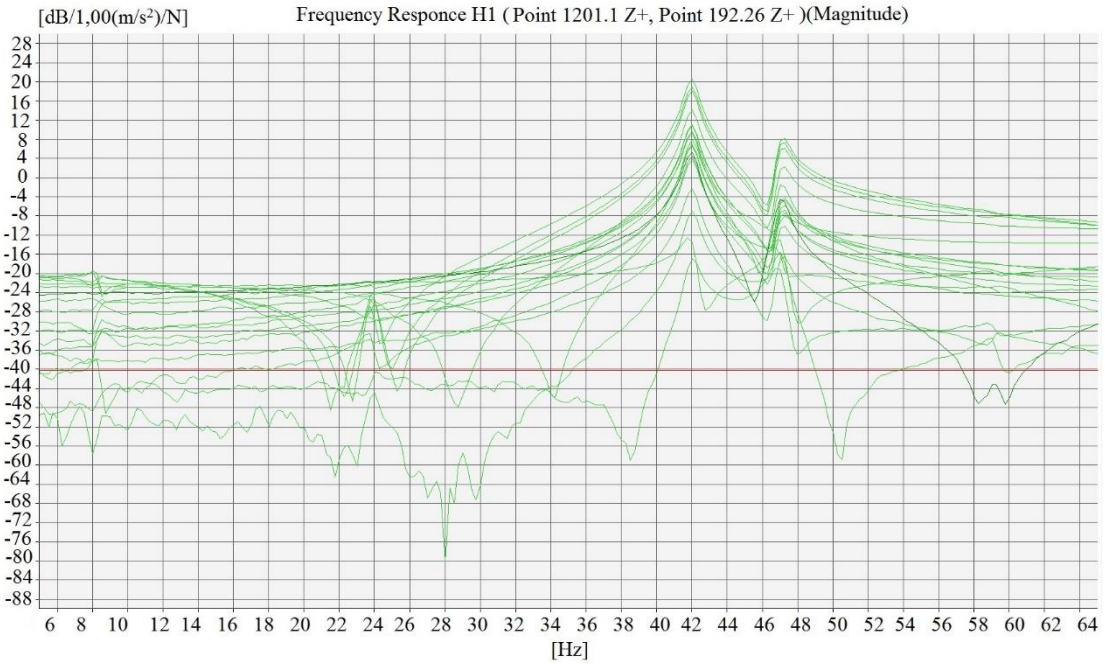

Figure 3.28. Accelerance FRFs of Force Transducer (Impact Hammer) and Uniaxial Accelerometer (4508 B) at Point 1

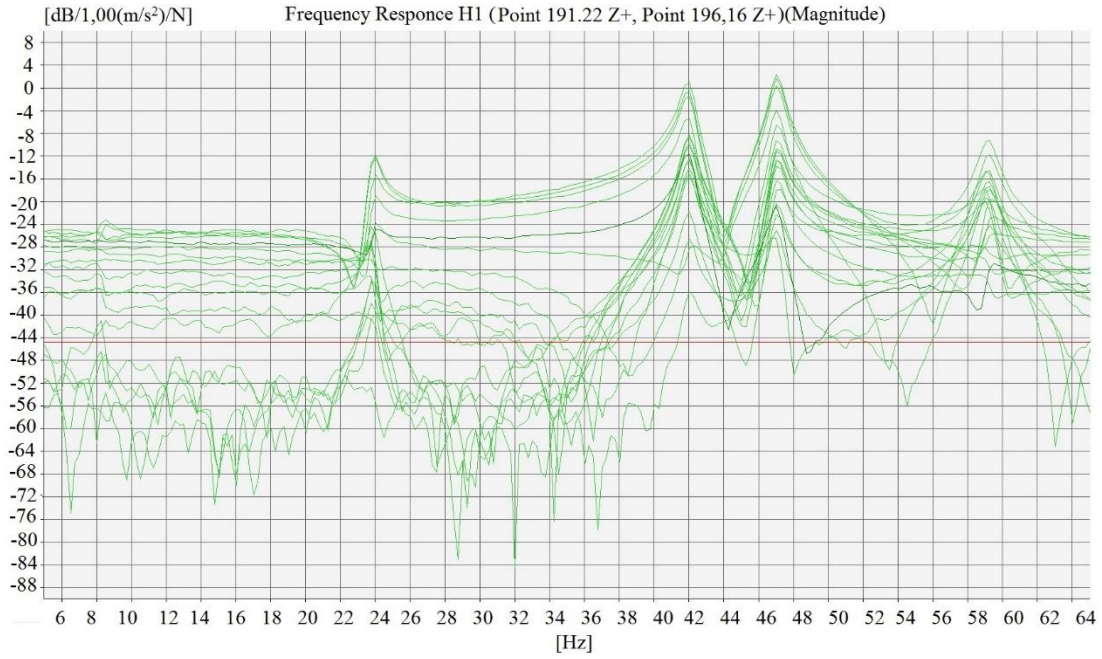

Figure 3.29. Accelerance FRFs of Force Transducer (Impact Hammer) and Uniaxial Accelerometer (4508 B) at Point 22

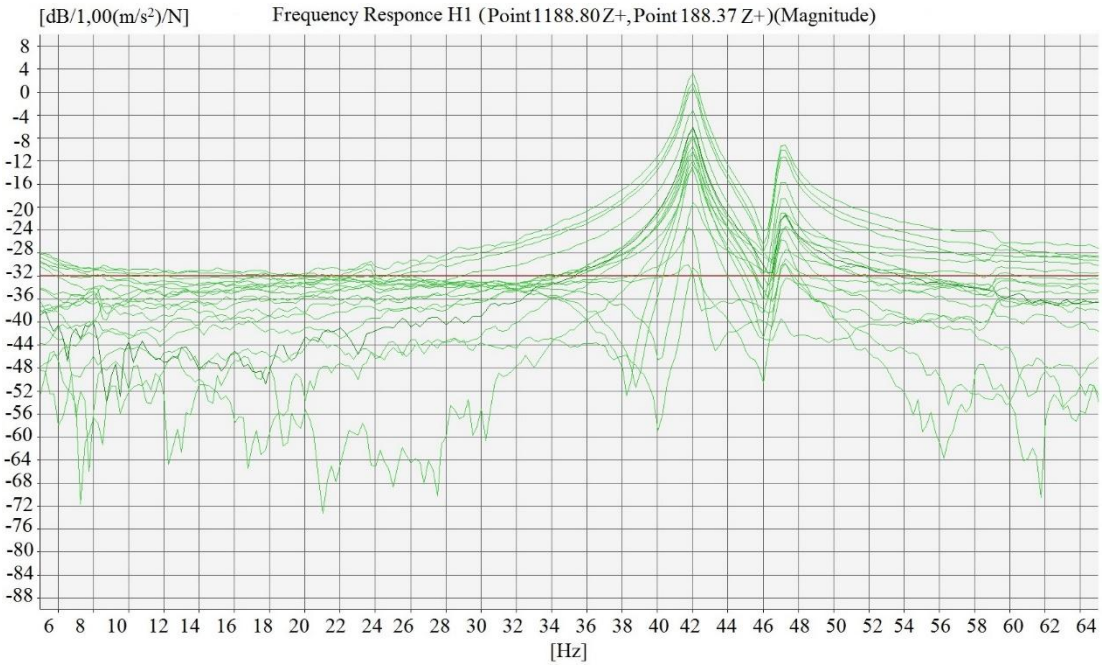

Figure 3.30. Accelerance FRFs of Force Transducer (Impact Hammer) and Uniaxial Accelerometer (4508 B) at Point 80

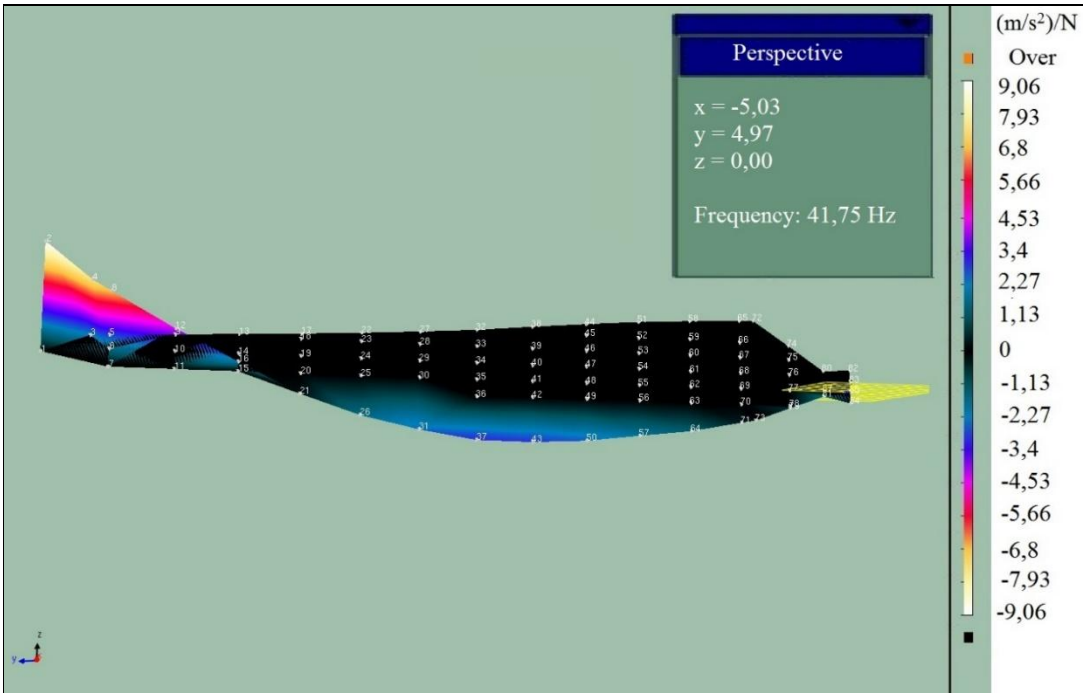

Figure 3.31. First In-Plane Bending [41.75 Hz]

3.5.2. Modal Shaker Tests

3.5.2.1. Shaker with Accelerometer Tests

Modal shakers are widely used equipment for modal analysis as they can provide different type of excitations by using different signals from a signal generator. In this shaker tests, a random signal is given by the signal generator and applied to the structure via stringer attached to the force transducer. After defining the geometry and measurement points in the software (see Section 3.2.2), the FFT analysis setup is completed. The main parameters used in the analysis are given in Table 3.3.

Table 3.3. FFT Analysis Setup Parameters for Shaker Test

Parameter	Value
FFT Lines	800
Span	200 [Hz]
Number of Averages	150
Time for one Measurement	202.7 [s]
Overlap	66.67%

The FFT lines and the span parameters are already defined in the impact hammer test (See Section 3.2.5). On the other hand, number of averages is the parameter for the number of spectra or time records and the time for one measurement is either given manually by the user or calculated by using the number of averages and overlap parameters. The overlap is the parameter which decides the percentage of the overlaps of time record segments. It supplies better amplitude accuracy and prevents the loss of measurement data. For the measurement process, the accelerometers are rowed to 87 different points shown in Figure 3.16. As five accelerometers of type 4508 were set, 18 measurements were taken. The modal test consultant configuration is presented in Figure 3.32.

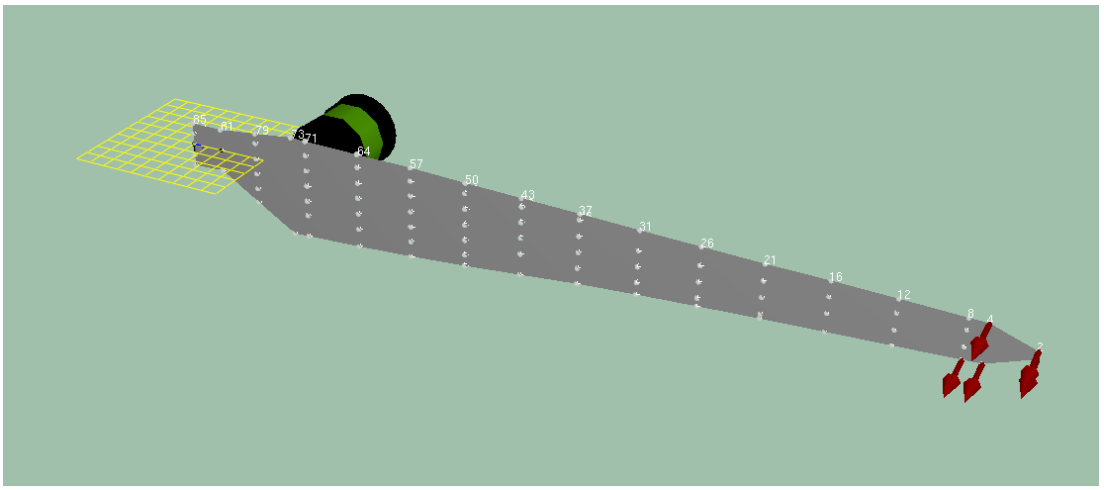

(a)

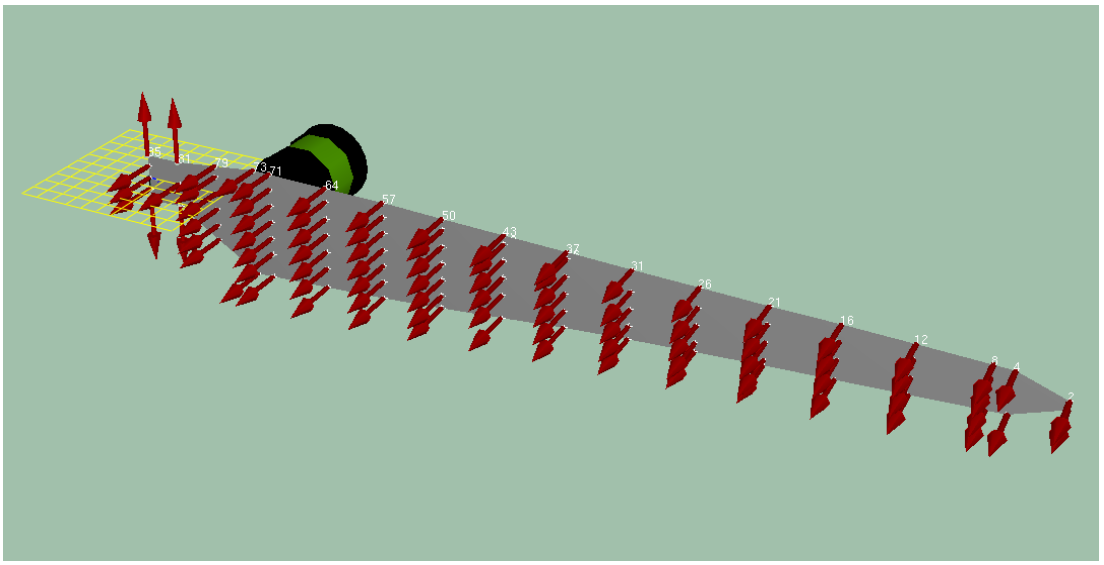

(b)

Figure 3.32. Modal Test Consultant Geometry for Shaker Test setup with Accelerometers (a) At the First Five Points (b) All Points

In test setup, Figure 3.33 shows the position of the shaker near the root at the measurement point numbered (70). For the shakers, as mentioned above, a row of five accelerometer was positioned for each group of measurements and a sample measurement for one of these configurations is shown in Figure 3.34. The accelerance FRF curves for the shaker test with accelerometers are shown in Figures 3.35 to 3.40 for the measurements taken from the five accelerometers at Points (1) to (87).

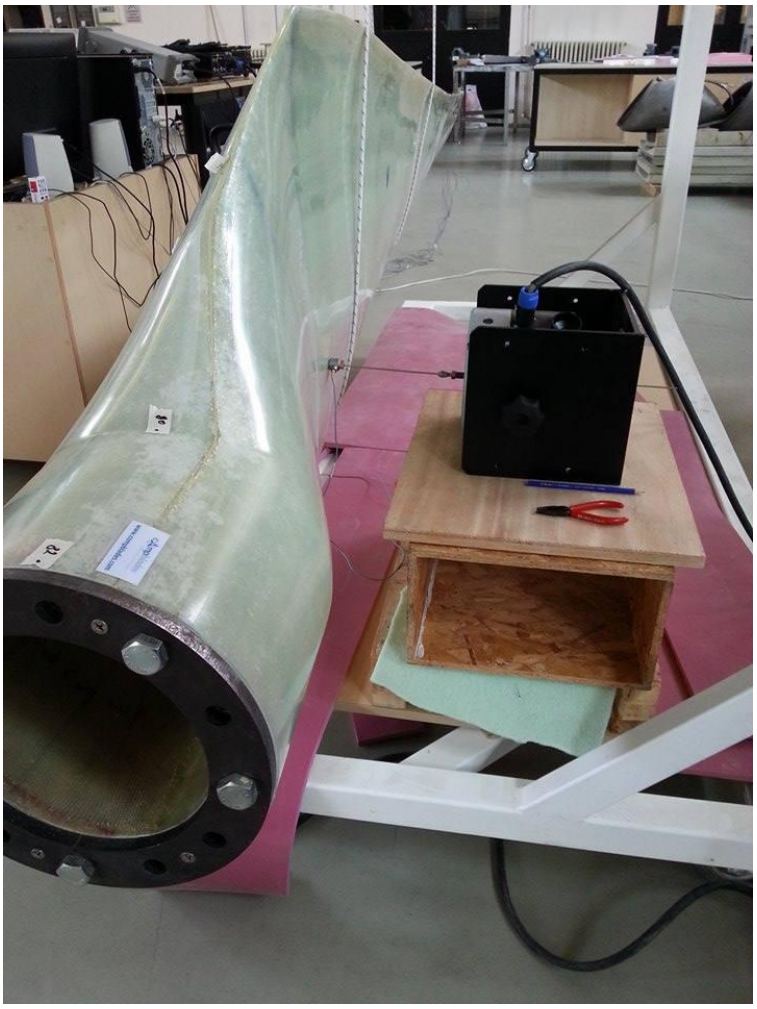

(a)

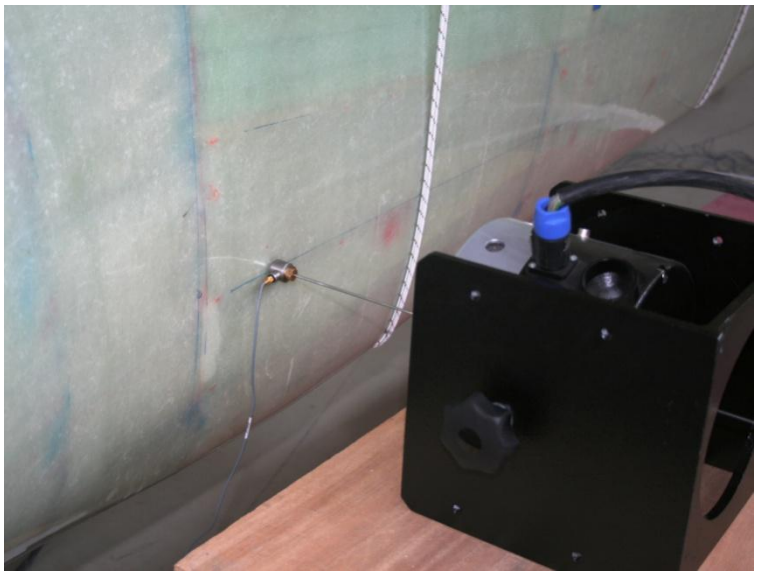

(b)

Figure 3.33. Shaker Position in Test Setup (a) Side View (b) Zoomed View

(a)

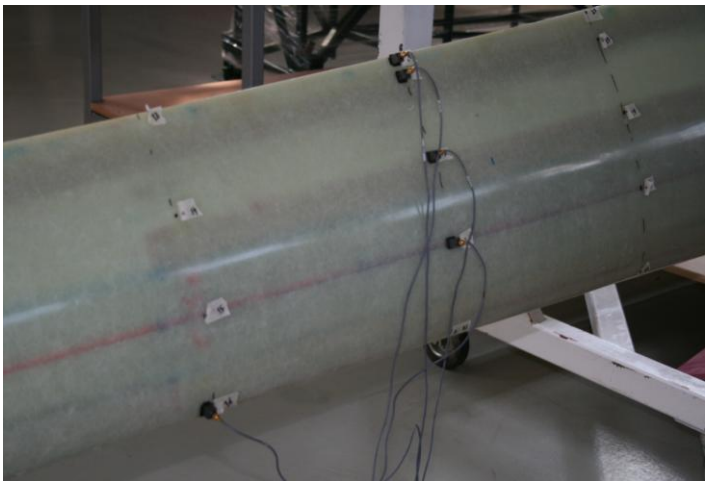

(b)

Figure 3.34. Accelerometer Positions in Test Setup (a) Isometric View (b) Zoomed View

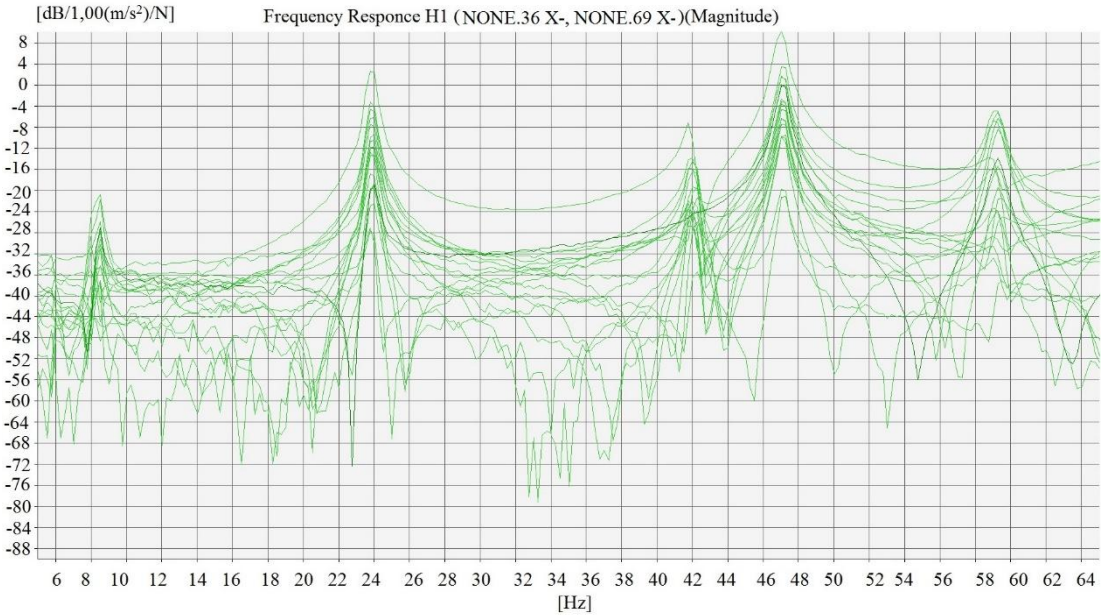

Figure 3.35. Accelerance FRFs of Force Transducer (Modal Shaker) and the Uniaxial Accelerometer #1 (4508 B)

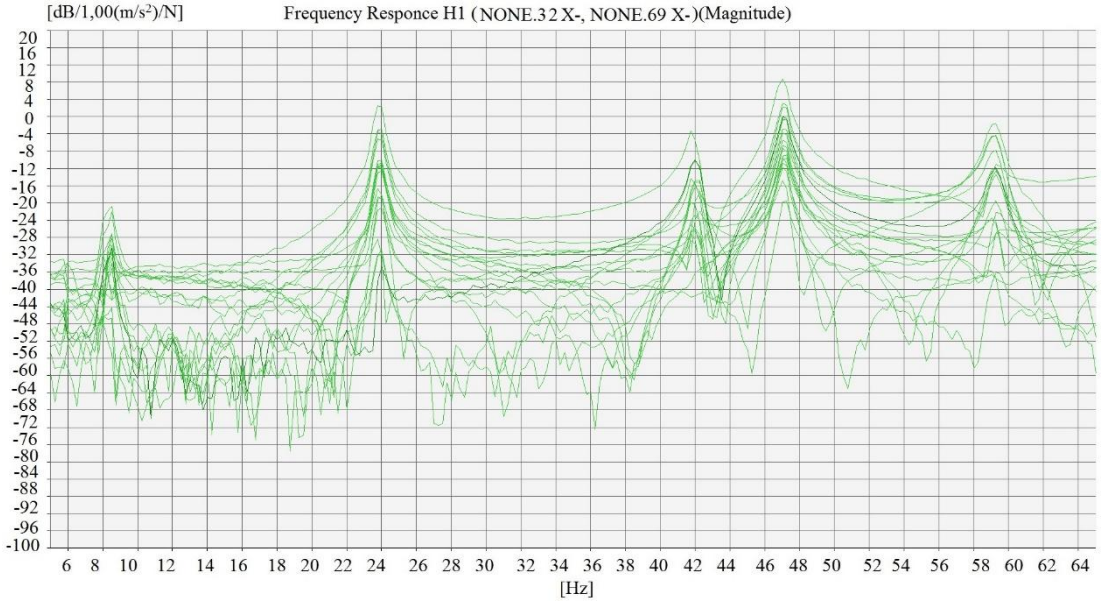

Figure 3.36. Accelerance FRFs of Force Transducer (Modal Shaker) and the Uniaxial Accelerometer #2 (4508 B)

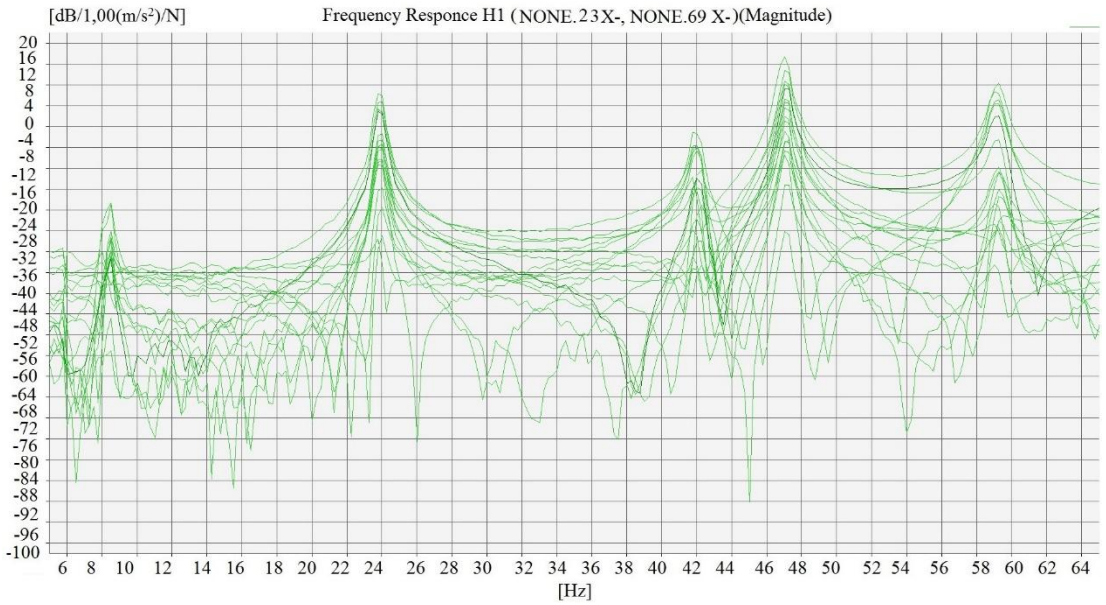

Figure 3.37. Accelerance FRFs of Force Transducer (Modal Shaker) and the Uniaxial Accelerometer #3 (4508 B)

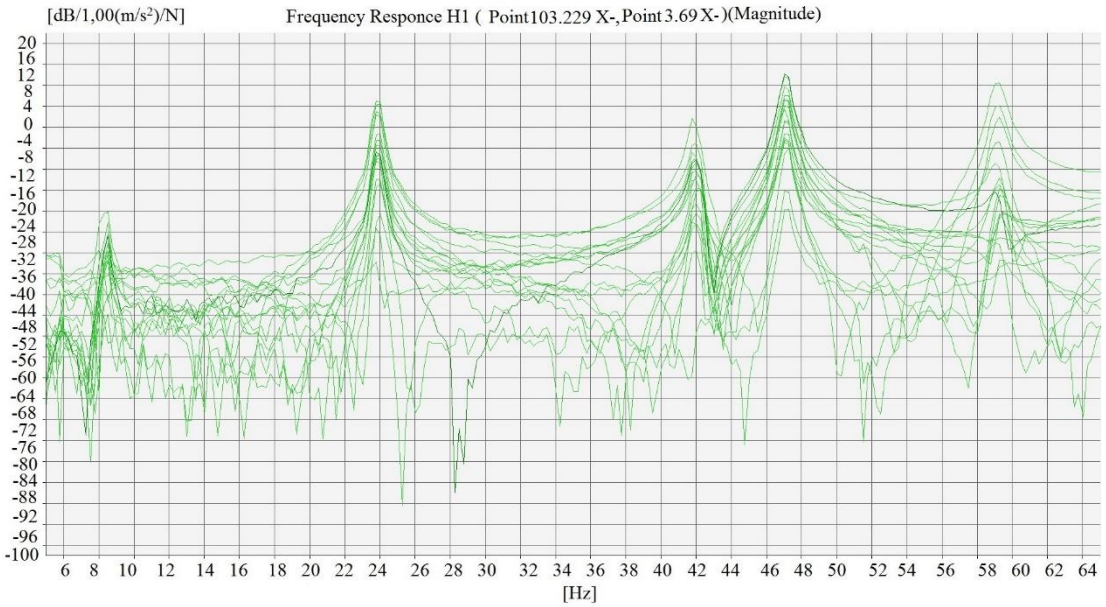

Figure 3.38. Accelerance FRFs of Force Transducer (Modal Shaker) and the Uniaxial Accelerometer #4 (4508 B)

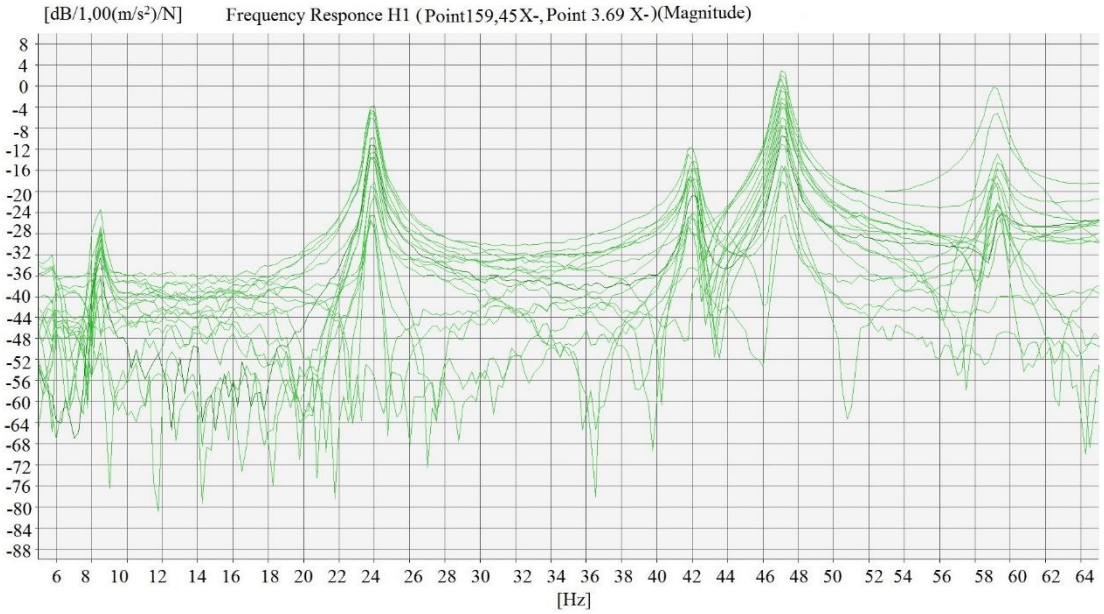

Figure 3.39. Accelerance FRFs of Force Transducer (Modal Shaker) and the Uniaxial Accelerometer #5 (4508 B)

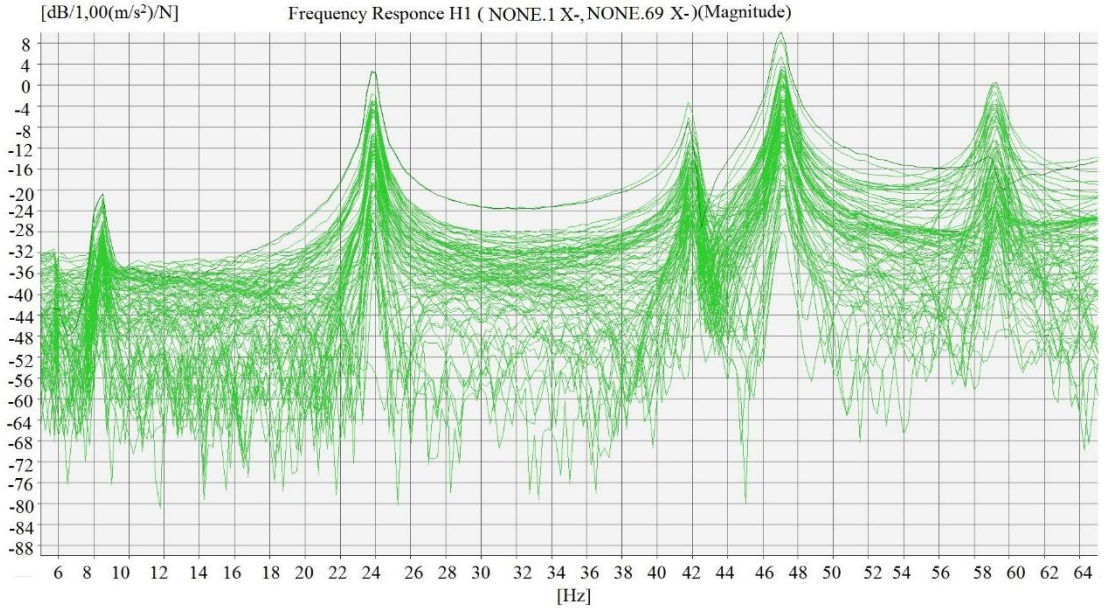

Figure 3.40. Accelerance FRFs of Force Transducer (Modal Shaker) and All Accelerometers

Here in these figures, the accelerometer #1 was positioned at points 1, 6, 11, 16, 21, 26, 31, 36, 41, 46, 51, 56, 61, 66, 71, 76, 81, 86 in each measurement. As all the accelerometers were rowed, accelerometer #2, #3, #4 and #5 were positioned at points 2, 7, 12, … , 87, at points 3, 8, 13, …, 83, at points 4, 9, 14, …, 84 and at

points 5, 10, 15, …, 85 respectively. By detecting the peak points of these FRF's the resonance frequencies are found and presented in Table 3.4. The corresponding mode shapes are also given in Figure 3.41-3.45.

Table 3.4. Resonance Frequencies obtained via Shaker with Accelerometers

Mode Shapes	Resonance Frequencies [Hz]
1st Out-of-plane Bending	8.25
2nd Out-of-plane Bending	23.75
2nd Out-of-plane Bending with 1st In-plane Bending Coupling	41.75
3rd Out-of-plane Bending	46.75
1st Torsion Coupling	58.75

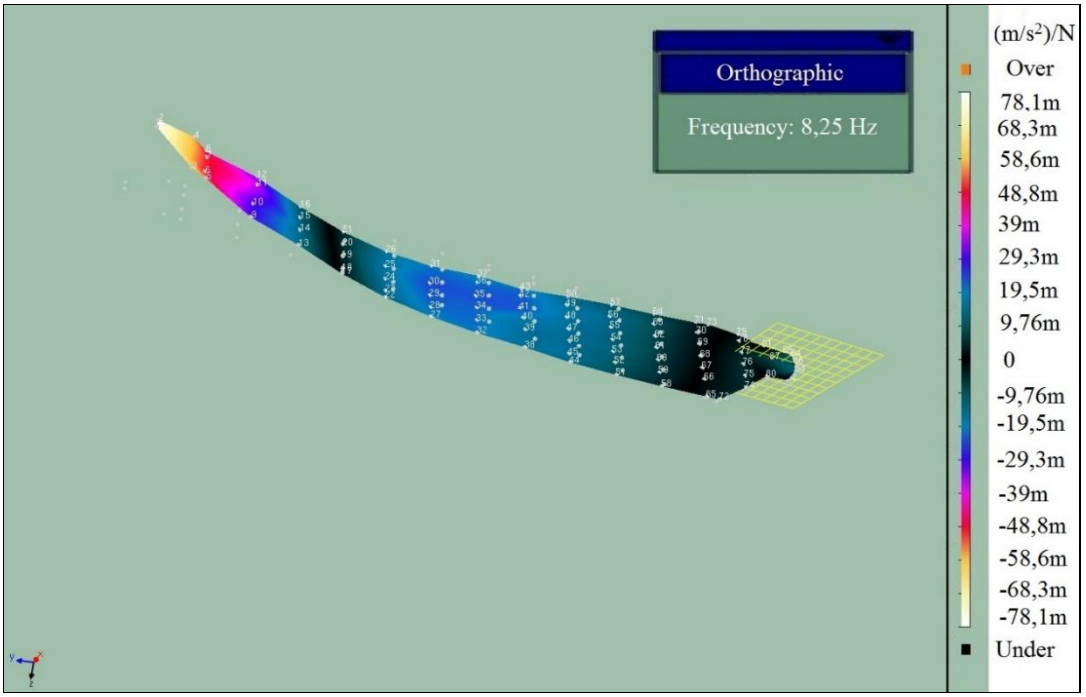

Figure 3.41. 1st Out-of-Plane Bending [8.25 Hz] - Shaker Test with Accelerometers

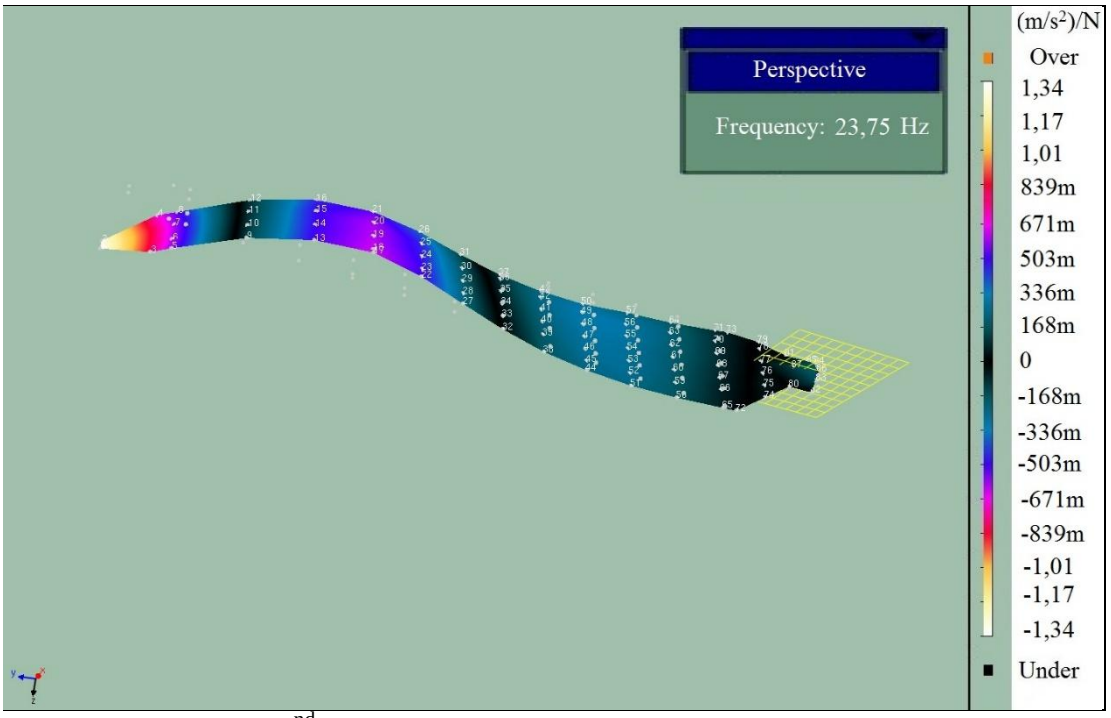

Figure 3.42. 2nd Out-of-Plane Bending [23.75 Hz] - Shaker Test with Accelerometers

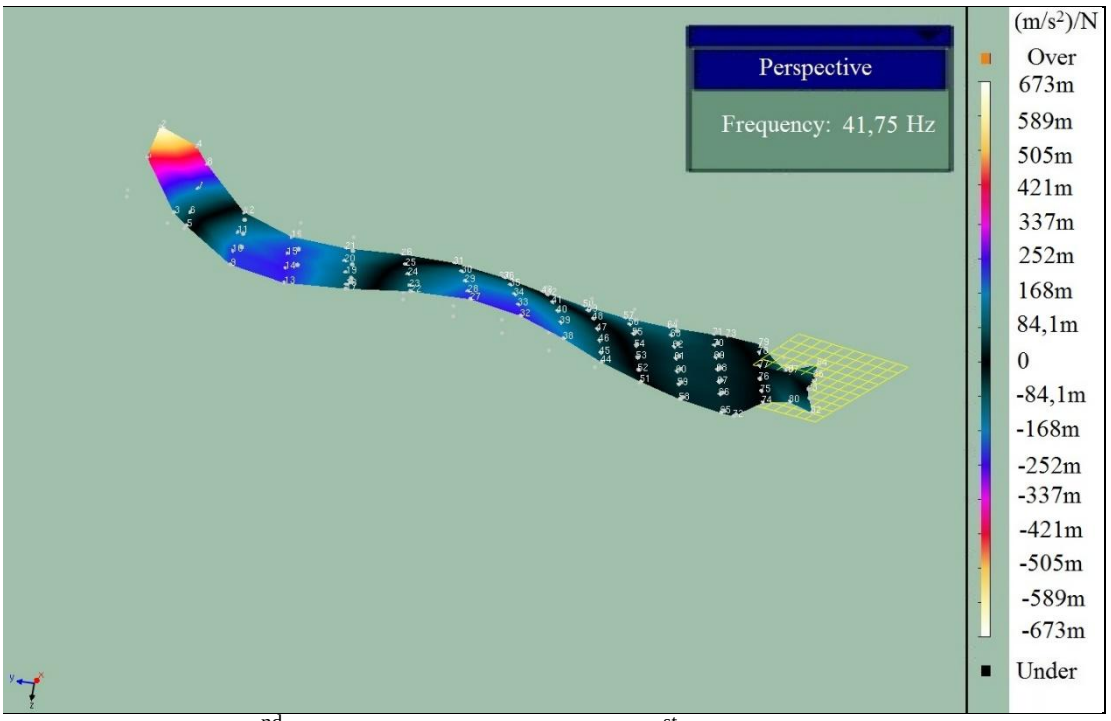

Figure 3.43. 2nd Out-of-Plane Bending with 1st In-Plane Bending coupling [41.75 Hz] - Shaker Test with Accelerometers

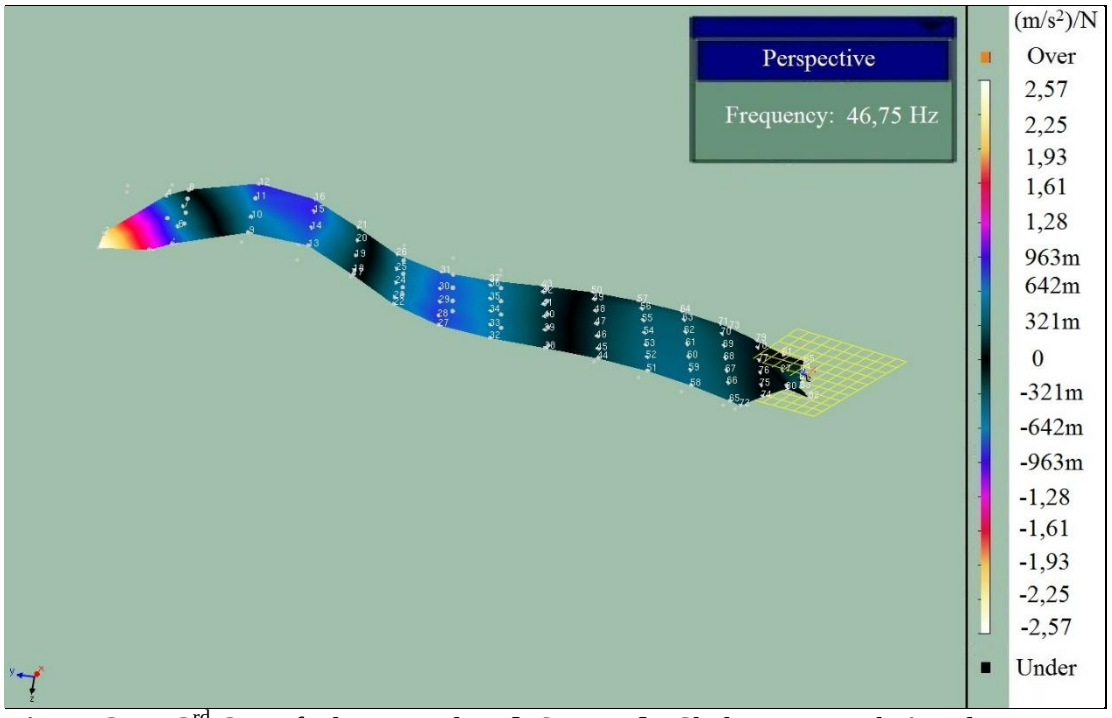

Figure 3.44. 3rd Out-of-Plane Bending [46.75 Hz] - Shaker Test with Accelerometers

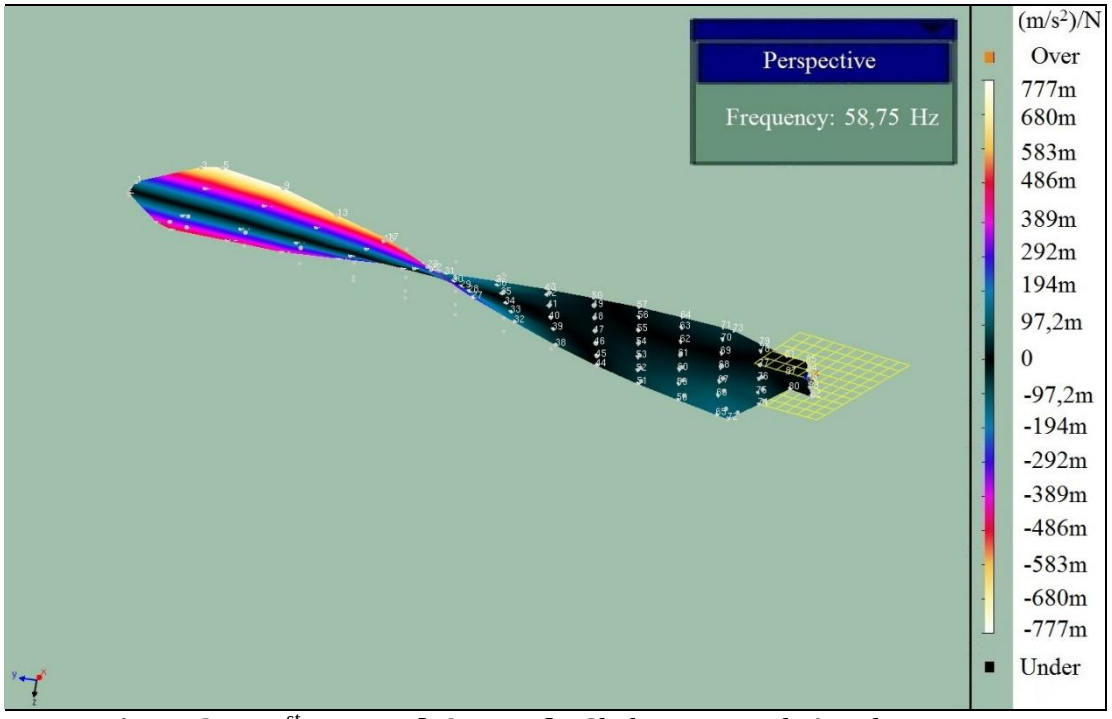

Figure 3.45. 1st Torsion [58.75 Hz] - Shaker Test with Accelerometers

3.5.2.2. Shaker with Scanning Laser Vibrometer Tests

The shaker with Scanning Laser Vibrometer test is based on the excitation coming from the electromechanical shaker and velocity measurement via Scanning Laser Vibrometer over the measurement points. The test structure was facing the Scanning Laser head from about 5m distance. Nonetheless, due to its pseudo-transparent surface there was not any possibility to detect the signal of the laser (i.e. a good reflection from the laser). Having bonded opaque aluminium stickers on all the measurement points, the test (Figure 3.46) was set by using PSV software [38] (Figure 3.47) with various setup parameters tabulated in Table 3.5. Then, the mobility FRF results of this particular test which is obtained from the combination of all the individual FRF graphs as a composite mobility FRF is presented in Figure 4.48. By detecting the peak points of these FRF's, the resonance frequencies are found and presented in Table 3.6. The corresponding mode shapes are also given in Figure 3.49-3.53.

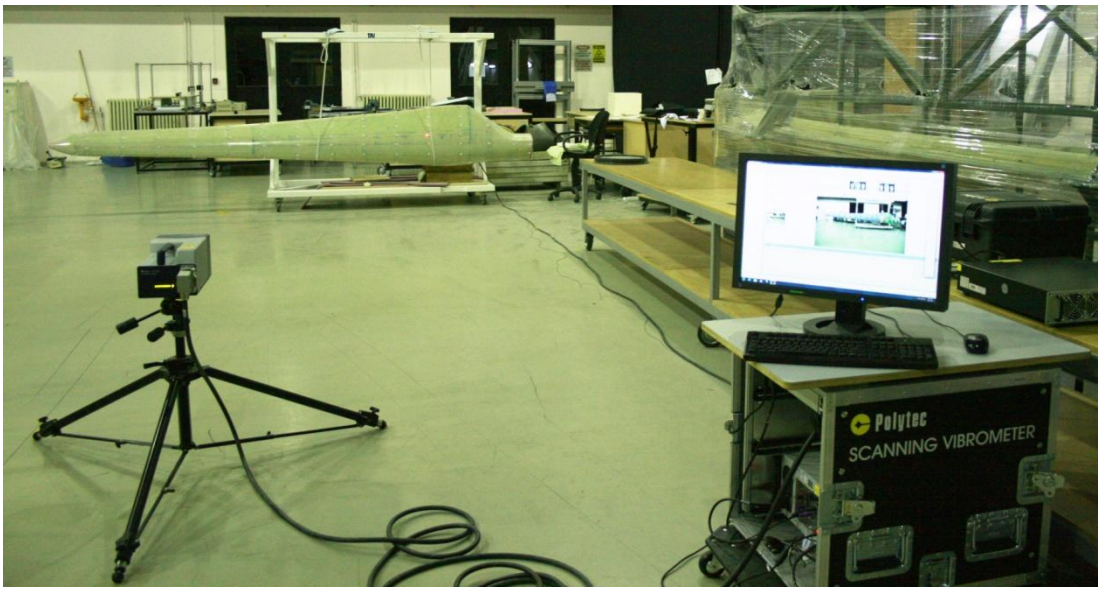

Figure 3.46. Test Setup for the Shaker and Scanning Laser Vibrometer

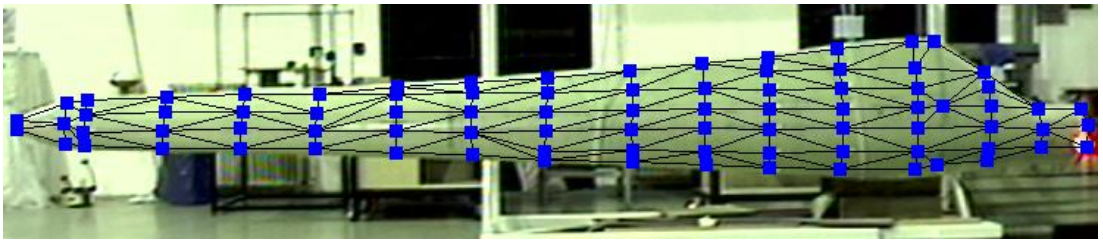

Figure 3.47. PSV Measurement Points

Table 3.5. The PSV Software Regulations

Parameter	Values
Number of Averages	5 complex
Filters	None
Bandwidth	0.4 [KHz]
Range	0-0.1 [KHz]
Sample Frequency	1.024 [KHz]
Sample Time	8 [s]
Resolution	125 [mHz]
FFT Lines Total	3200
FFT Lines used	800
Overlap	0 %
Windowing	Rectangular
Vibrometer Controler (VC)	OFV-5000
Velocity of the VC	VD-04 10 [mm/s/V]
Max. Frequency of the VC	250 [KHz]
Wave Form	Periodic Chirp of 0.3 Amplitude

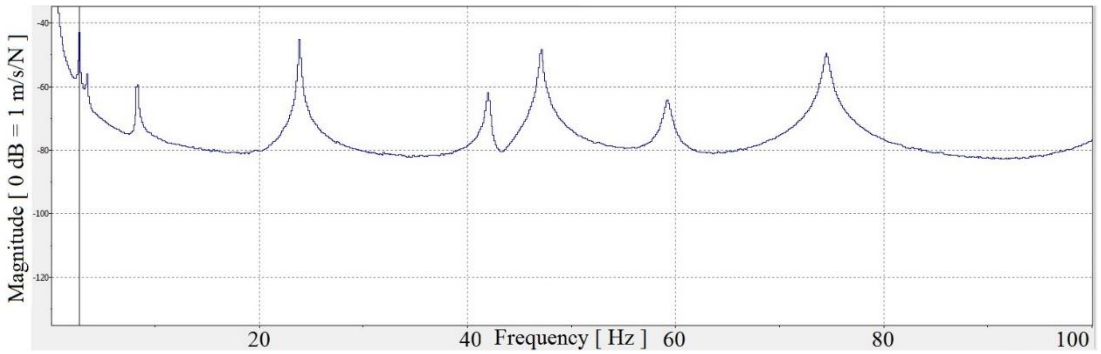

Figure 3.48. The Composite Mobility FRF Graph obtained from the PSV Software

Table 3.6. Resonance Frequencies Obtained via Shaker with Laser Vibrometer

Mode Shapes	**Resonance Frequencies [Hz]**
1st Out-of-plane Bending	8.38
2nd Out-of-plane Bending	23.88
2nd Out-of-plane Bending with 1st In-plane Bending Coupling	42.00
3rd Out-of-plane Bending	47.13
1st Torsion	59.25

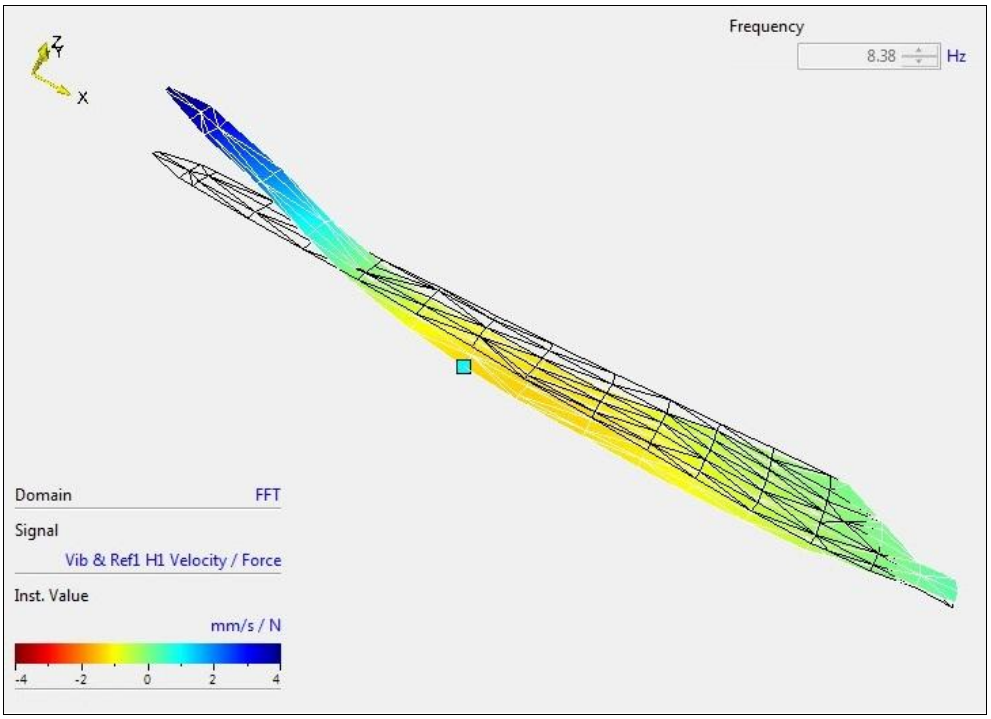

Figure 3.49. 1st Out-of-Plane Bending [8.38 Hz] - Shaker Test with Laser Vibrometer

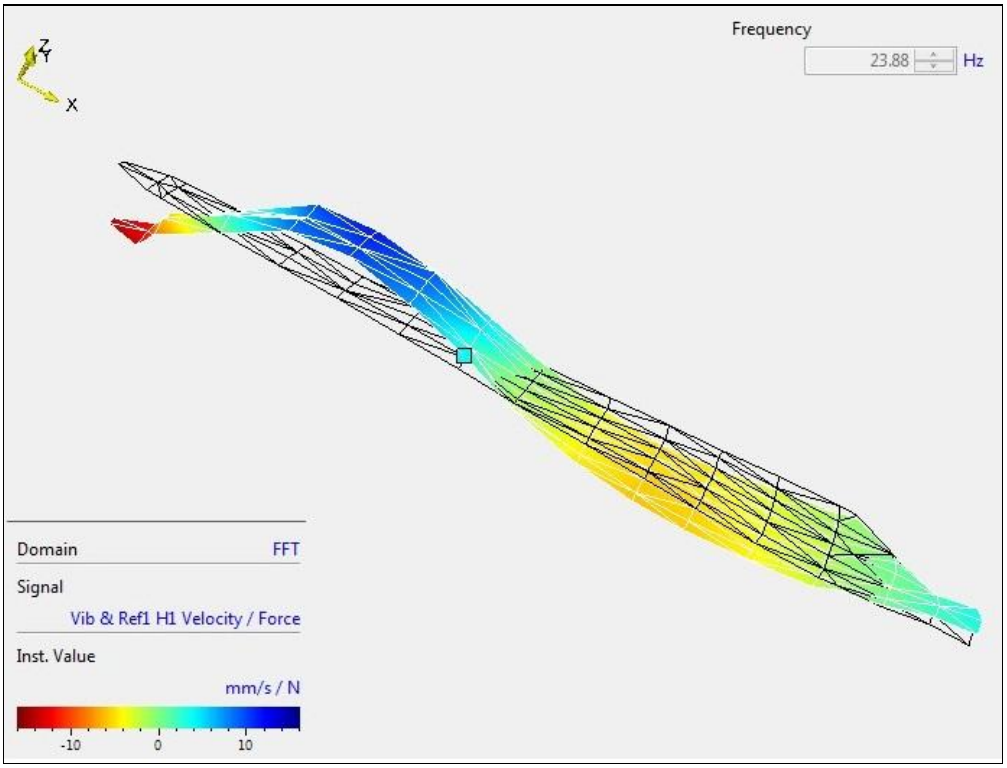

Figure 3.50. 2nd Out-of-Plane Bending [23.88 Hz] - Shaker Test with Laser Vibrometer

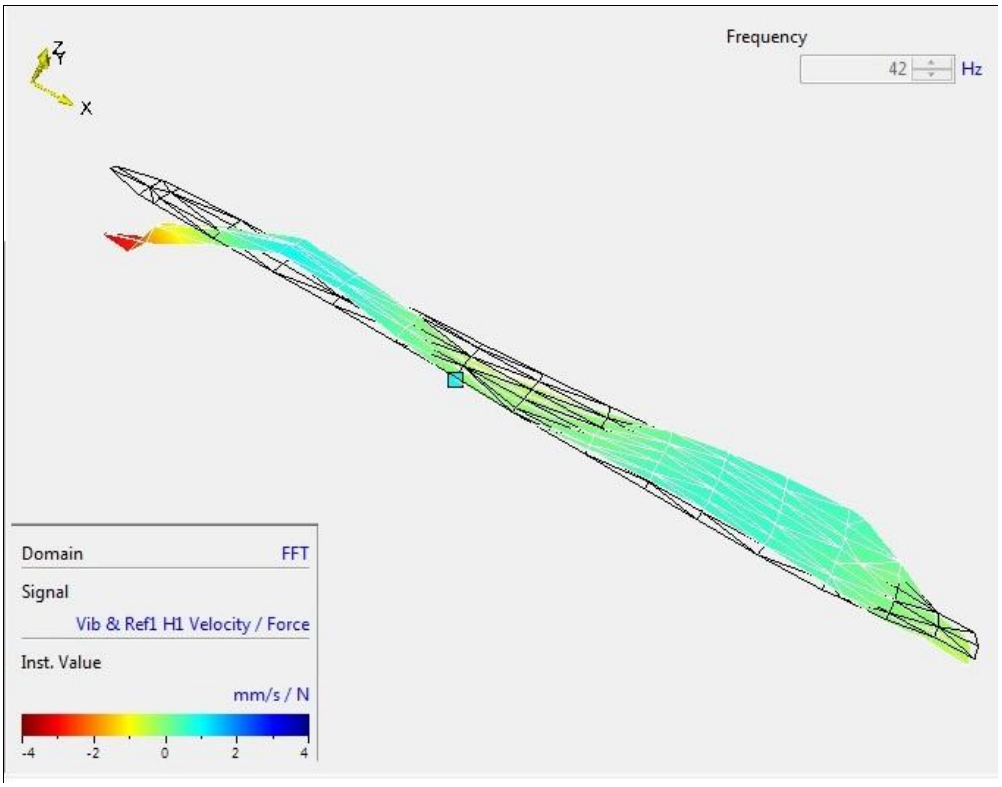

Figure 3.51. 2nd Out-of-Plane Bending with 1st In-Plane Bending Coupling [42.00 Hz] - Shaker Test with Laser Vibrometer

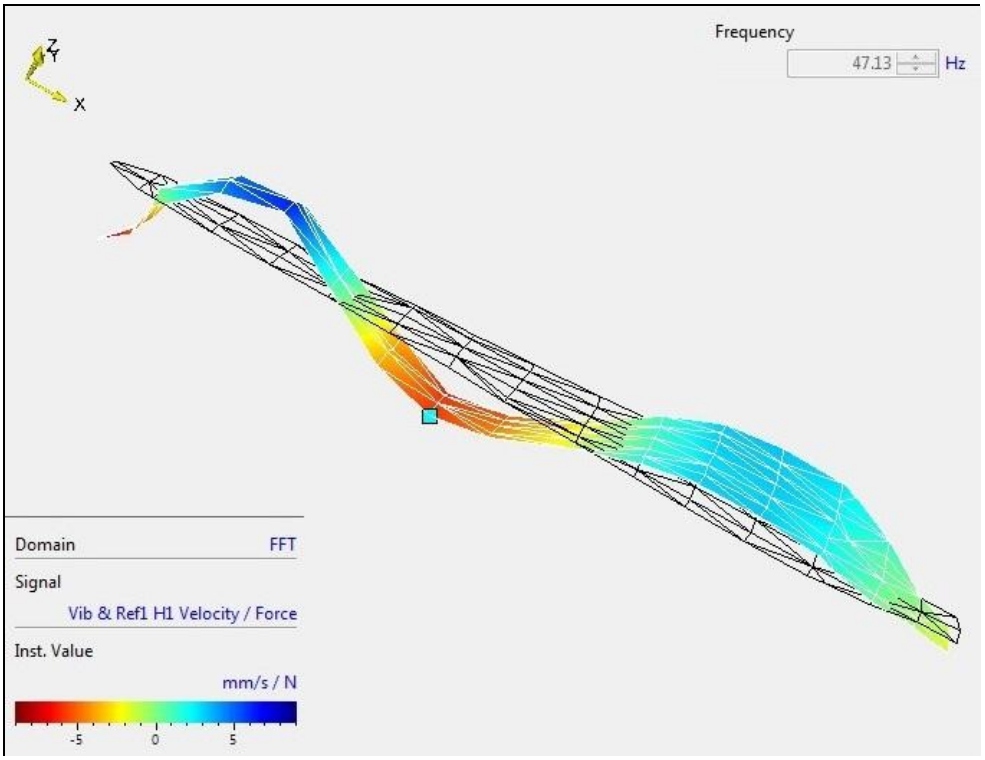

Figure 3.52. 3rd Out-of-Plane Bending [47.13 Hz] - Shaker Test with Laser Vibrometer

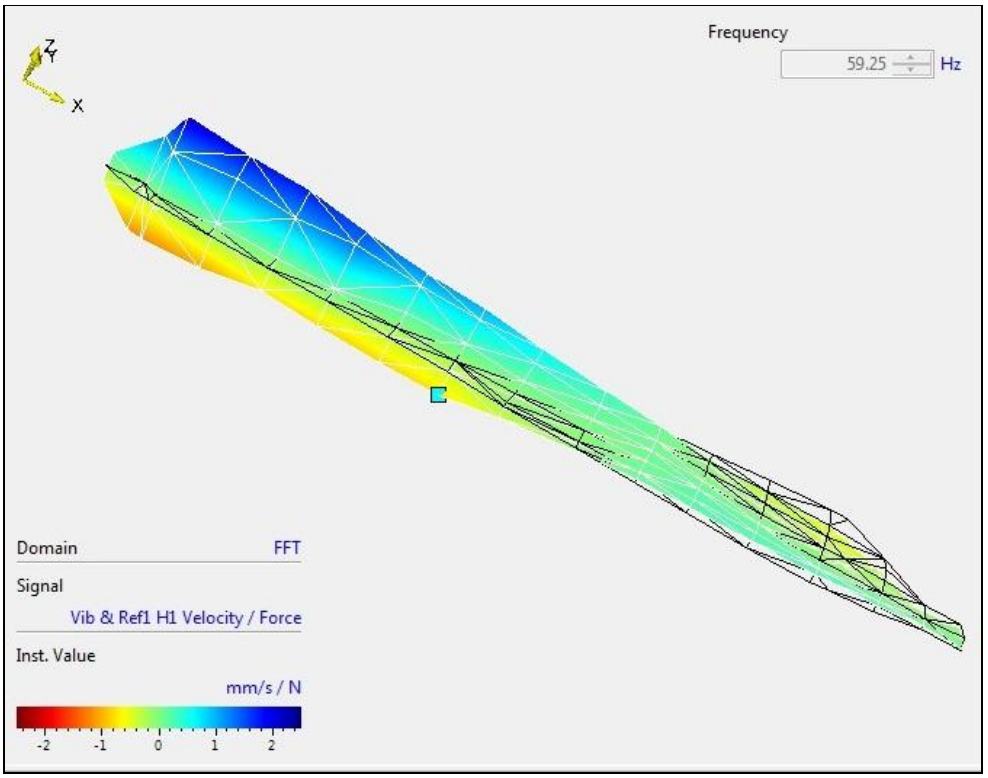

Figure 3.53. 1st Torsion [59.25 Hz] - Shaker Test with Laser Vibrometer

3.6.Conclusion

Having completed the modal tests, the comparison of the results are tabulated in Table 3.7.

Table 3.7. Comparison of the Modal Tests Results

Mode Shapes	Resonance Frequencies [Hz]		
	Hammer with Accelerometer	**Shaker with Accelerometer**	**Shaker with Laser Vibrometer**
1st Out-of-plane Bending	8.25	8.25	8.38
2nd Out-of-plane Bending	23.75	23.75	23.88
2nd Out-of-plane Bending and 1st In-plane Bending Coupling	41.75	41.75	42.00
3rd Out-of-plane Bending	47.00	46.75	47.13
1st Torsion	59.00	58.75	59.25

As it can been seen from the above table that the modal test results for all three setups are very close to each other regarding both resonance frequencies and the corresponding mode shapes.

CHAPTER 4

FINITE ELEMENT MODELLING AND ANALYSES OF THE WIND TURBINE BLADE

4.1. Introduction

In the project of METUWIND - Center For Wind Energy, the design of aerodynamically optimized and structurally light and reliable rotor blade is the primary aim. For this purpose, a blade is designed according to IEC 61400-2 which includes an internal hat shaped spar beam structure, a joint design at the hub as well as composite shells. In this section, the modal analyses are performed numerically on a 5-m long horizontal axis composite wind turbine blade by using MSC Patran/Nastran commercial finite element software as a tool. First, the required data regarding the general geometrical parts are gathered and then the airfoil geometries are created at various sections along the span of the blade by using CATIA software to obtain the suction and the pressure side of the blade. Following the material property selection, the finite element modelling of the blade is performed via MSC Patran software with various meshes created on each structural part considering 2-D shell type for all the blade surfaces. Then, the boundary conditions are assigned as fixed at the root and/or left as free and the normal mode dynamic analyses which are aiming to cover the first three out-of-plane bending and the first torsional natural frequencies and their corresponding mode shapes of the blade are performed. Fixed-free case simulates the behaviour of the blade while connected to the main turbine structure, via the hub joint, in its working condition. Free-free case was used to discretely observe the dynamic of the blade by avoiding its coupling with boundary structure.

4.2. Modelling Procedures of the Blade

In this section, the modelling details of the blade including all its surfaces, selection of materials regarding different staking sequence of laminates, as well as the analyses details and the corresponding results are discussed.

4.2.1. Geometric Modelling of the Blade Sections

The geometric modelling of the blade is performed in CATIA [30] environment with the airfoils of the type NACA 23014 (Figure 4.1) which are the basis of the drawings provided by the aerodynamic design having each different cord length and twist angle along the blade span of the blade. They start from a pitch down angle (20.6°) at (0.5 m) from the root until reaching the horizontal position at the tip (5 m) and are located at around 10 stations along the span after a cylindrical geometry of diameter (0.289 m) at the root (0 - 0.2 m). Then, the transition surfaces between the airfoils are designed via "multi-sections surface" tool [30]. After drawing each airfoil in its related position, hat shaped spar position is then located for each airfoil cross-section where two shear webs starting from 0.5 m from the root and extending up to 4 m as the main load carriers. These two shear webs are also perpendicular to the chord of each airfoil and located at 50% and 85% of the airfoil from the trailing edge chord, respectively. Following this, the width of each of the suction flanges are designated at 7% of the airfoil cord, which is shown in Figure 4.2, and all the surfaces of the blade are finalised.

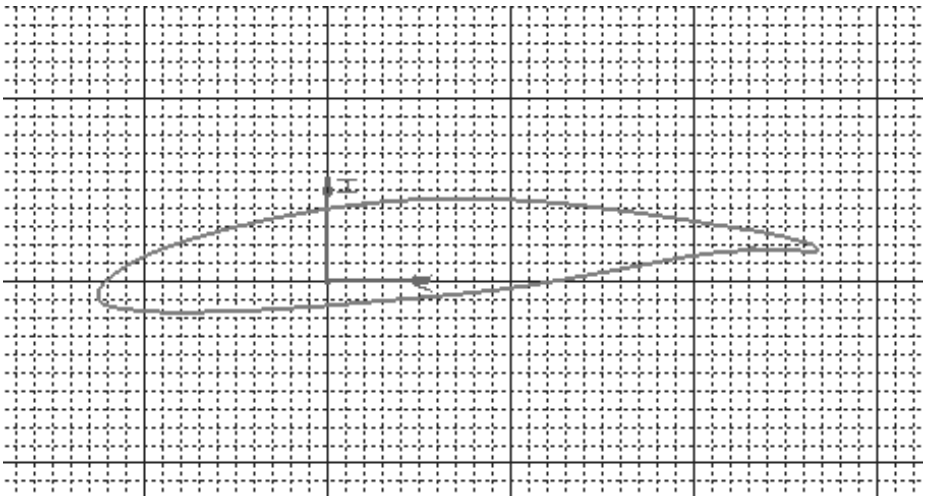

Figure 4.1. NACA 23014 Airfoil at 3.0 m from the Root of the Blade

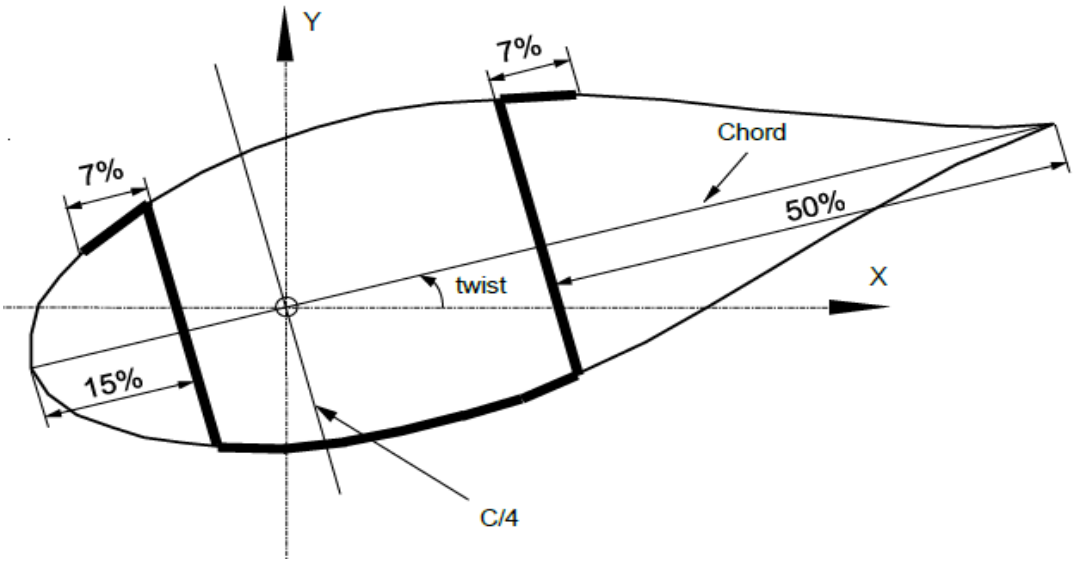

Figure 4.2. Positioning of the Spars

4.2.2. Solid Modelling of the Blade

The modelling of the blade is performed as mentioned by using surface geometries following the airfoil drawings at different sections and the transition areas in between. Each surface section of the design has its specific material lamination properties (explained in details in Section 4.3.1). By taking this into consideration, the airfoil positions are chosen precisely to divide the areas as desired and shown in Figure 4.3. In other word, the area at the root part, including the skin and the shear webs, has a thicker and stronger cross-section to handle a bigger moment at this particular station. Then, the layer staking sequence is decreased, from the root part, until having a relatively thinner thickness at the blade tip in order to achieve an optimum engineering design with the lightest and strongest way possible. In addition, that decrease of layers was made gradually to prevent possible delamination between the laminates.

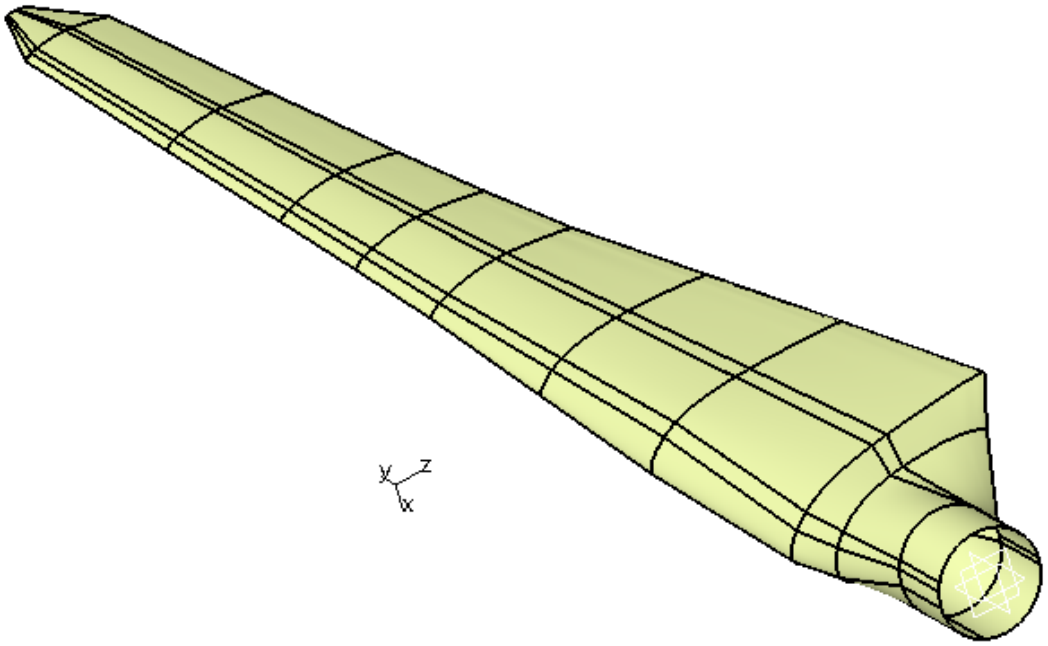

(a)

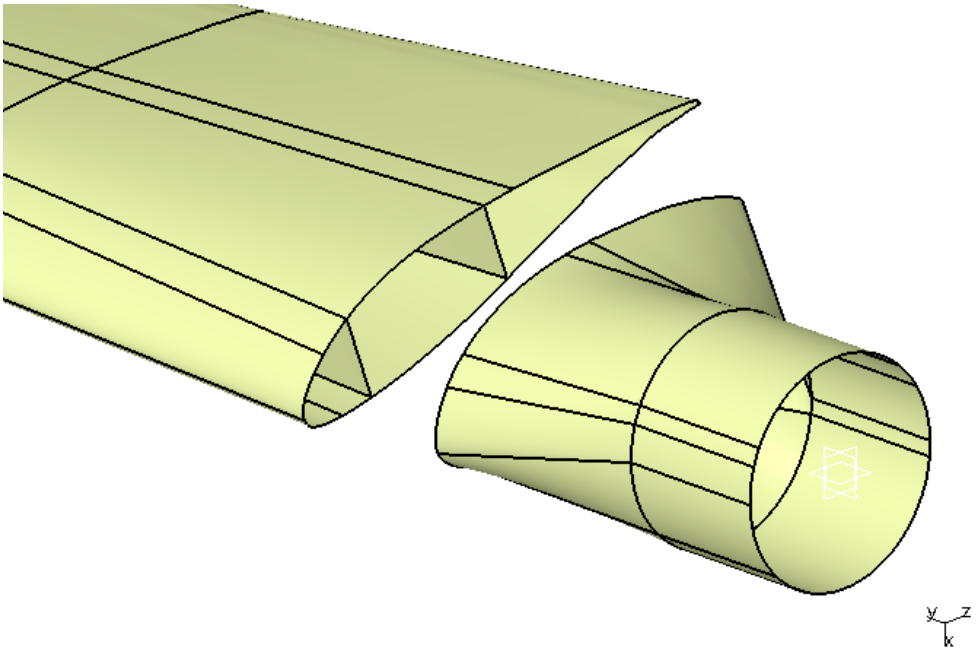

(b)

Figure 4.3. Solid Model of the Blade (a) Isometric View (b) Cross-sectional Zoom View to the Root Part

4.2.3. Solid Modelling of the Root Part of the Blade

At the root, inside the composite cylindrical part, there exists a hub joint steel frame having an outside diameter of 273 mm and 12 hollow studs located at a diameter of 245 mm. The studs are of length of 200 mm and 24 mm in diameters with internal thread that are held equidistant by means of two steel perforated annular disks. They are of M16x1.5 type quality 8.8 studs and they are distributed along the bolt-hole circle of the hub as given in Figure 4.4. The steel frame structure after its placement in the blade root is covered with adhesive putty, balsa wood and glass fibre reinforced plastic unidirectional strips.

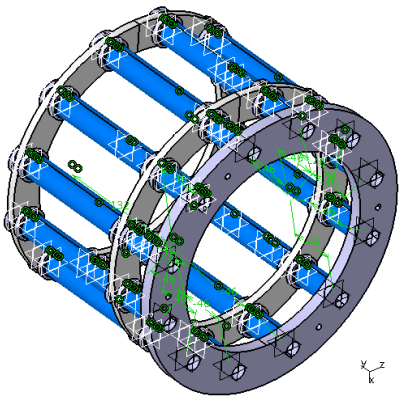

Figure 4.4. The Hub Joint Steel Frame

4.2.4. Material Modelling

The basic materials that are used are in the analyses comprise; two different glass fabrics which are to be applied using hand lay-up wet lamination with Epoxy resin, namely; METYX L600E10C-0 of 623 g/m^2, is unidirectional with parallel continuous fibres and METYX XL800E10F-[0/45/-45] of 835 g/m^2, is a tri-axial architecture with fibres in 0, +45° and -45° directions in a ratio of 2:1:1. Polymeric foam, which is the commercial Divinycell H45 of DIAB group as core material in sandwich constructions, and steel. For the surface finishing, two different protection materials are used; transparent gel coat and a layer of chopped strand mat of 300 g/m^2 CSM 300. The properties of each are shown in Table 4.1. For a lamination stacking sequence (Figure 4.5), a surface section in the interval labelled as D3 (Figure 4.6) is chosen as an example at the blade upper surface of the blade where all section properties and dimensions are given in meters.

There are more examples provided regarding the lamination stacking sequence used in the blade manufacturing and given in Appendix A.

Table 4.1. Basic Material Properties

Property	Unidirectional (UD)	Divinycell H45	Steel	Gel Coat	CSM 300
ρ [kg/m^3]	1896	48	7850	1200	1896
E_1 [GPa]	24.84	55.10^{-3}	210	3.98	9.14
E_2 [GPa]	9.14	55.10^{-3}	-	-	-
G_{12} [GPa]	2.83	15.10^{-3}	-	-	-
ν_{12}	0.29	0.4	0.3	0.34	0.29

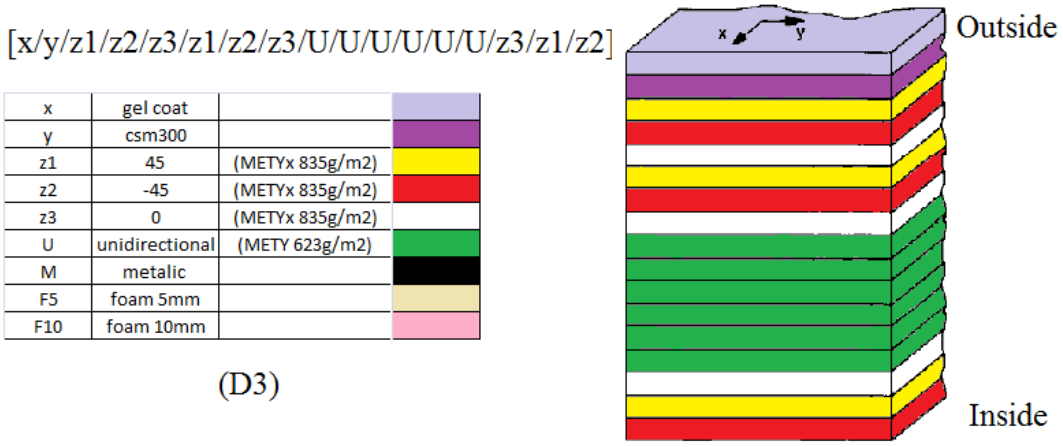

Figure 4.5. Lamination Staking Sequence at the Upper Surface of the Blade in Interval D3

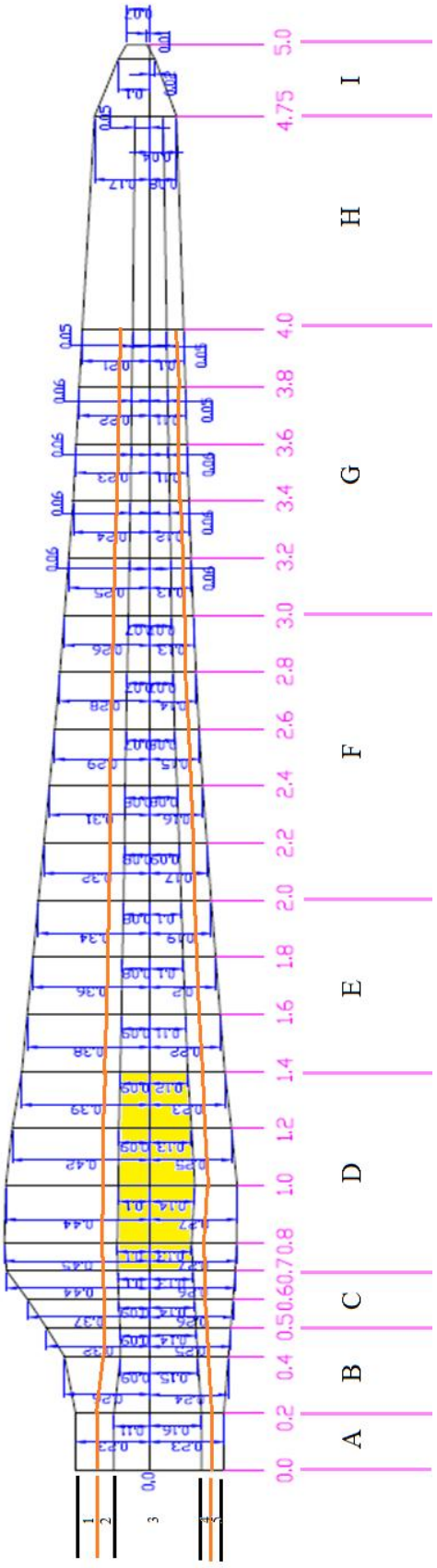

Figure 4.6. Upper Surface Sections of the Blade

4.3. Finite Element Modelling of the Blade

In this section, the construction of the blade model is explained in details by defining the material properties, mesh densities, boundary conditions and finally different type of analyses for different blade types are performed and the results of these analyses are presented.

4.3.1. Construction of the Blade Model

The designed geometry is then imported to MSC Patran/Nastran finite element modelling and analysis tool. Defining the dimension as metric, materials are created as isotropic for steel, gel coat and CSM300, and orthotropic for the fiber glass and foam core as mentioned.

Following this step, materials are set for the laminate applied on the surface. The laminate sequence in MSC Patran environment previously presented (i.e. namely (D3)), has, for example, 17 different layer having total thickness of 0.0084 m. Noting that for the unidirectional and triaxial fibreglass laminates same material properties are applied nonetheless thickness and layer orientation differs considerably. The thickness for +45 and -45 degree for triaxial lamina is of 2.38×10^{-4} m and its 4.83×10^{-4} m for 0 degree layer. The thickness for the unidirectional one is of 7.16×10^{-4} m.

The layer sequencing is based on the manufacturing blue prints [3] given from the designers as interim reports to project METUWIND - Center For Wind Energy. Referring to these manufacturing blue prints, the blade is cut into 9 sections in span-wise direction and 5 sections in longitudinal direction making a total of 45 different surfaces for each side of the blade. This then makes 90 different laminates in total for the whole blade and is presented in Table 4.2. The letters and the numbers appeared in this table can also be seen in Figure 4.6 which previously presents the section D3 chosen as an example at the blade upper surface of the blade.

On the other hand, the Appendix A, presents the 13th, 14th and 15th layers for the lower (i.e. pressure) side of the blade as an example for the layer stacking sequence, Figure A.1. Additionally, the web of the spars (i.e. chassis) of the blade which extends from 0.5 m to 4.0 m is considered in three different continuous sections as 0.5 m to 0.7 m, 0.5 m to 1.4 m, and 0.5 m to 4.0 m. Figures A.2 to Figure A.4, show the layer sequences for the spar (i.e. chassis) of the blade for the aforementioned section intervals [3].

Table 4.2. Section Divisions for the Blade Span

Distance from root [m]	**0-0.2**	**0.2-0.5**	**0.5-0.7**	**0.7-1.4**	**1.4-2.0**	**2.0-3.0**	**3.0-4.0**	**4.0-4.75**	**4.75-5.0**
Longitudinal Cross Sections	A1	B1	C1	D1	E1	F1	G1	H1	I1
	A1	B1	C1	D1	E1	F1	G1	H1	I1
	A2	B2	C2	D2	E2	F2	G2	H2	I2
	A3	B3	C3	D3	E3	F3	G3	H3	I3
	A4	B4	C4	D4	E4	F4	G4	H4	I4
	A5	B5	C5	D5	E5	F5	G5	H5	I5

The sequences of the layers are defined from outside to inside for both covers and spars and presented for a standard airfoil cross section (Figure 4.7) to show how the blueprint numbering, is actually counted. The concept of layer sequencing is of manufacturing issue and therefore the surface of contact between the spar upper flange and the spar lower flange are bonded respectively to the upper and the lower surface. While creating that surface bonded by glue, both layer sequences for the spar and the covers are considered and modelled accordingly.

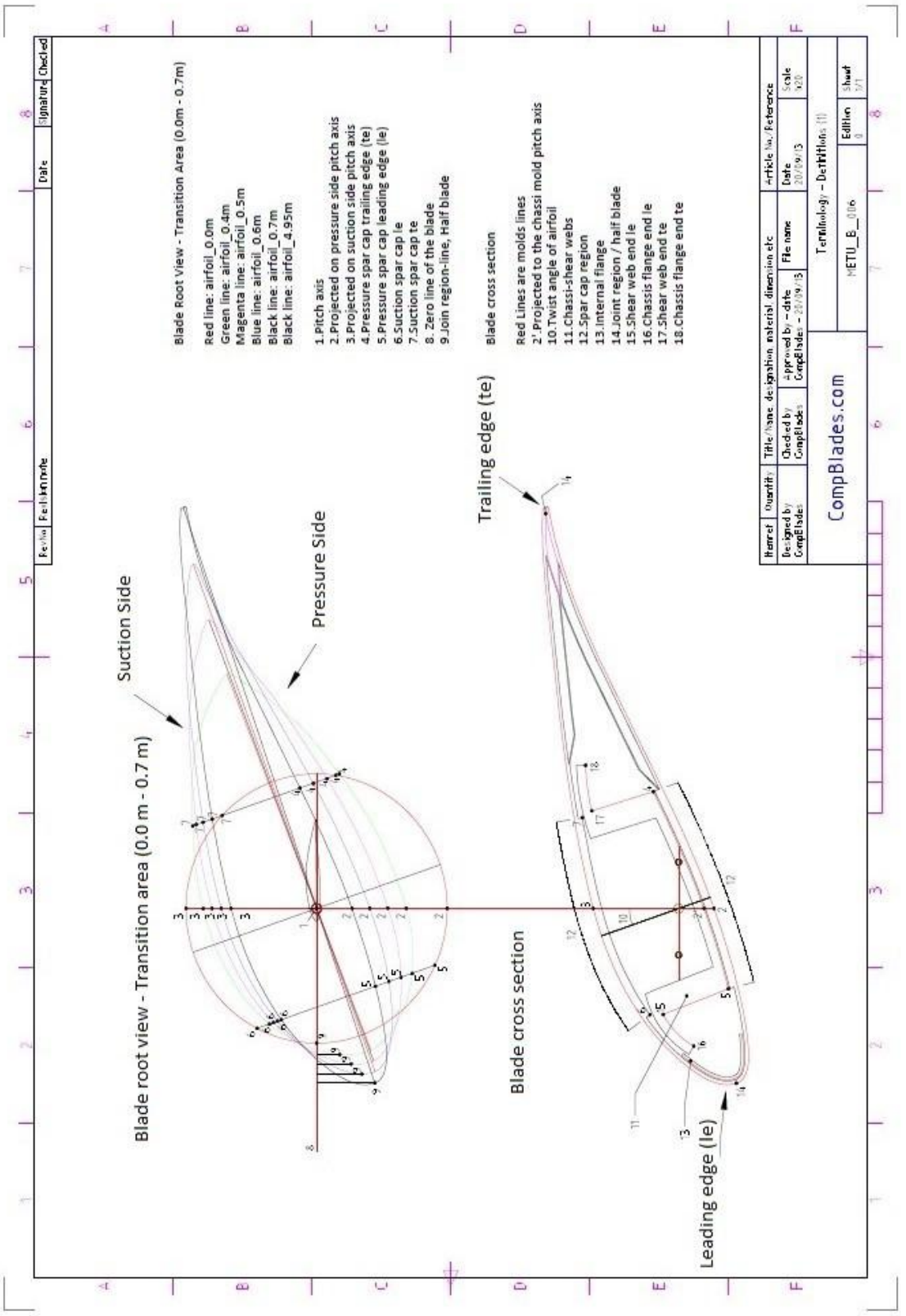

Figure 4.7. A Standard Airfoil Cross Section Showing the Direction of Sequence

For the composite part of the model, linear layered structural 2-D shell elements (QUAD4) are selected which are defined by four nodes having six degrees of freedom in each one. The complicated hub joint steel frame structure (Figure 4.4) is then modelled as a simplified hollow cylindrical section (Figure 4.8) to be a part of the root laminate for the sake of the simplicity in the finite element modelling and analysis. This new simplified design of the root had also been provided by the design blue prints.

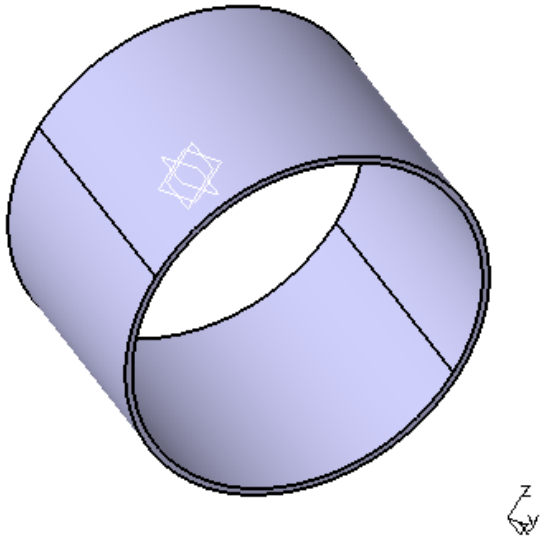

Figure 4.8. The Hub Joint Steel Frame Simplified Model

The blade mass and the centre of gravity coordinates measured from the root of the beam are then deduced by using the final model of the blade and it is tabulated in Table 4.3.

Table 4.3. Static Properties of the Blade

Properties	**Values**
Mass [kg]	74.81
CG_x [m]	0.019
CG_y [m]	0.039
CG_z [m]	1.580

Hybrid type mesh is constructed by using 2-D shell QUAD4 elements by knowing the fact that this type of mesh, unlike iso-mesh, is completely able to generate a full cover of any surface by cutting it to square element in total and triangle segments at specific locations such as corners and edges. Three different mesh densities namely: coarse, fine, and the finest are tabulated in Table 4.4 and used for the mesh independency test. These meshes are constructed after creating laminates and applying them to each individual surface section. The finest mesh density for the blade surface is shown in Figure 4.9. The boundary condition for the fixed-free case, made at the root by assigning zero to all degrees of freedom applied to the associated line, is shown in Figure 4.10. Figure 4.11, on the other hand, presents the three chosen mesh densities of the blade for comparison purposes. The three dimensional view of the blade including the inner spars is then presented in Figure 4.12.

Table 4.4. Mesh Density and Related Properties

	Coarse Mesh	**Fine Mesh**	**Finest Mesh**
Average Element Edge length [m]	0.089	0.045	0.010
Number of Elements	921	2949	57299
Number of Nodes	814	2787	56614
Degree of Freedom	4884	16722	339684

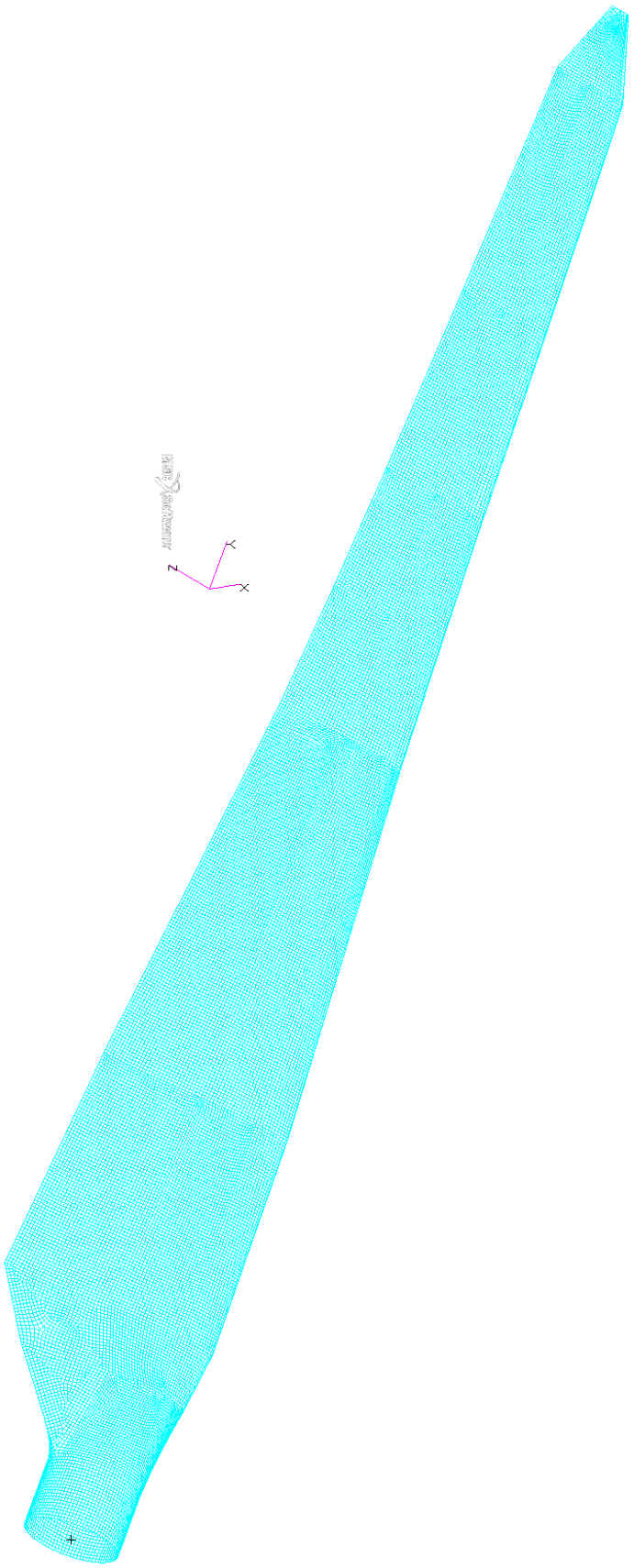

Figure 4.9. The Finest Mesh of the Blade

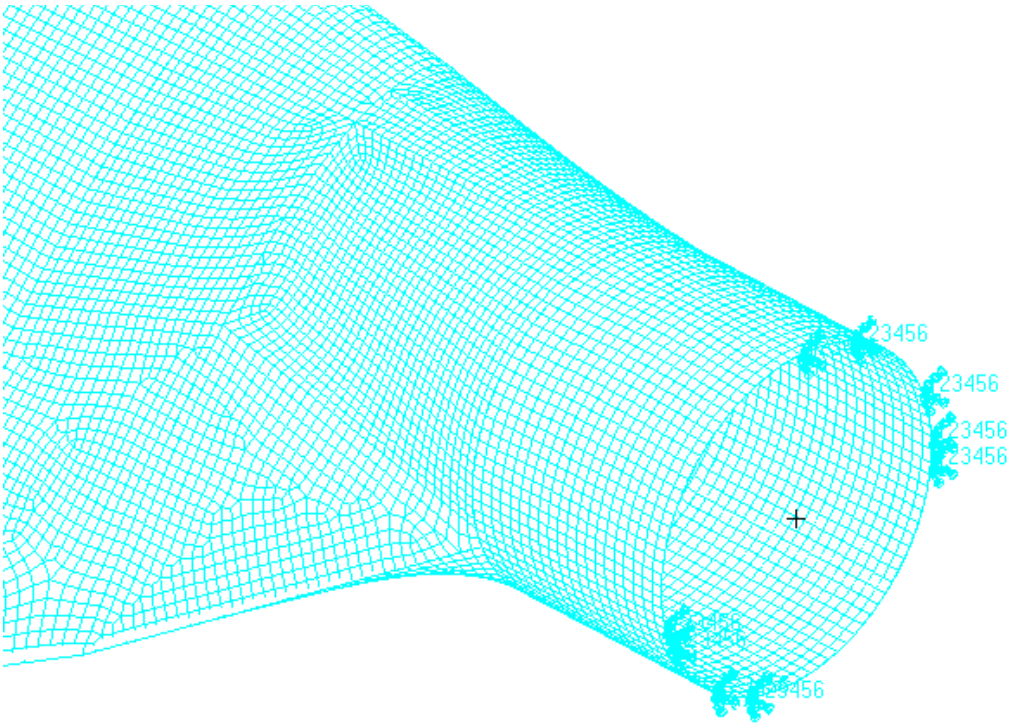

Figure 4.10. Boundary Condition, Zoomed View

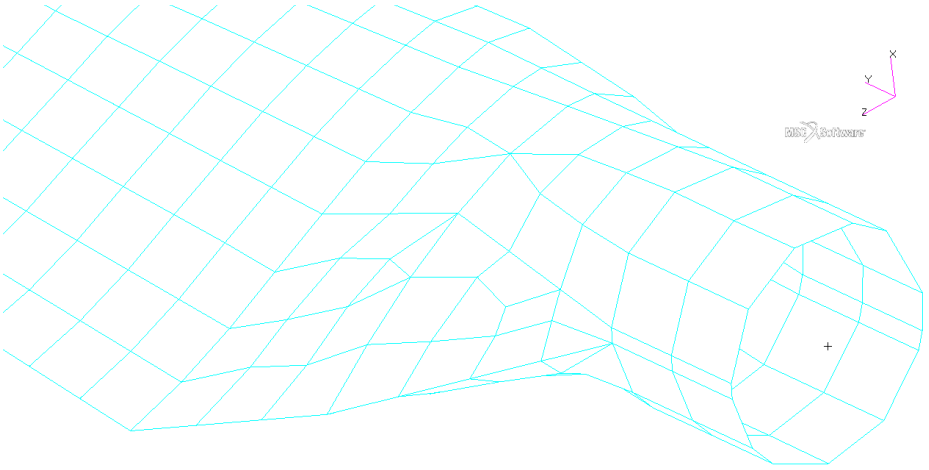

(a)

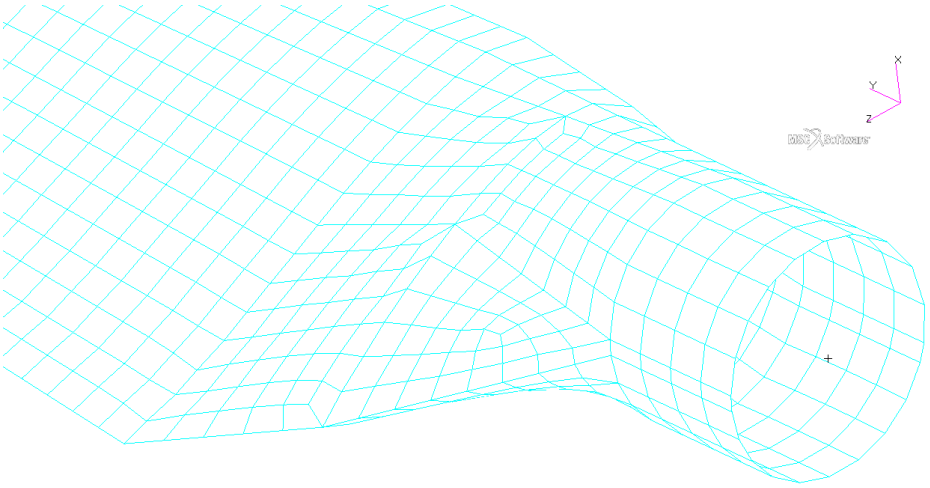

(b)

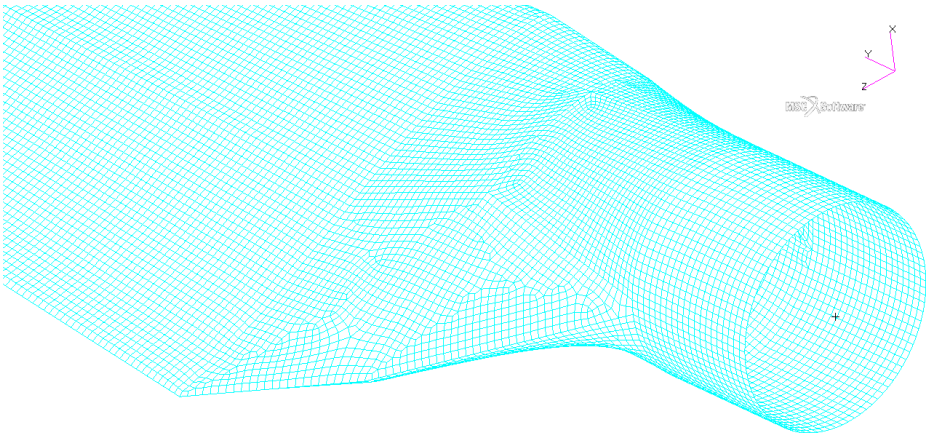

(c)

Figure 4.11. Three Different Mesh Sizes (a) Coarse (b) Fine (c) Finest - Zoom view at the root

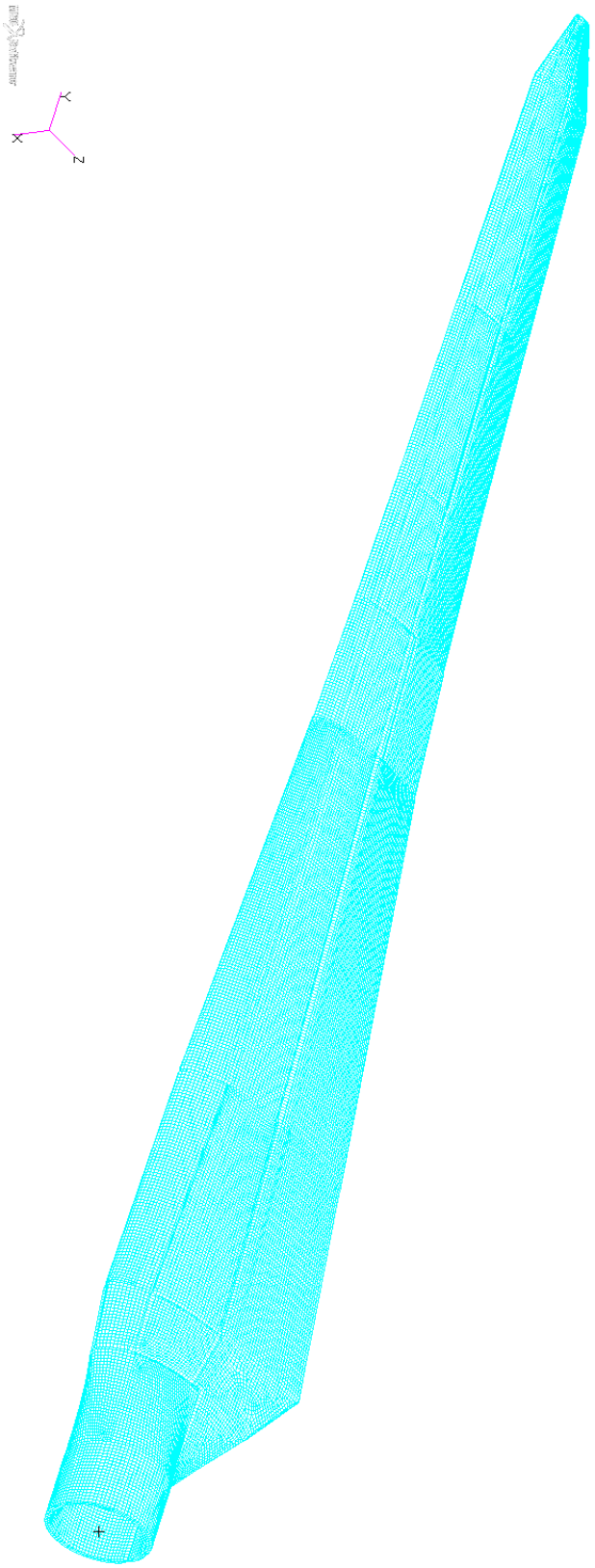

(a)

Figure 4.12. Three-Dimensional View of the Blade (a) Isometric View (b) Front View

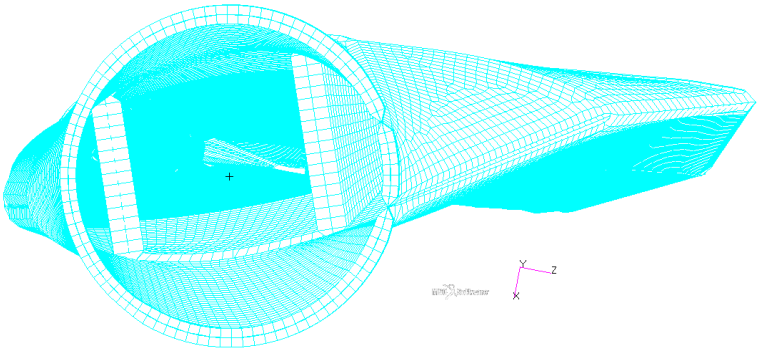

(b)

Figure 4.12. (continued)

4.3.2. Normal Mode Dynamic Analysis: Free – Free Case

In order to find the natural frequencies and the corresponding mode shapes, (Table 4.5, Figure 4.13 to Figure 4.17), 'normal modes' analysis type is performed in MSC Patran/Nastran environment, for the previously mentioned free-free boundary condition. In this analysis, the focus was mainly on the first three out-of-plane bending, two in-plane bending and the first torsional modes of the blade. It is observed from the dynamic analysis results that the mode shapes are coupled regarding the "2nd Out-of-plane Bending and 1st In-plane Bending" and "2nd In-plane Bending and 1st Torsional" ones.

Table 4.5. Natural Frequencies for Three Different Mesh Densities – Free-Free Case

Mode Shapes	Natural Frequencies [Hz]		
	Coarse Mesh	Fine Mesh	Finest Mesh
1st Out-of-plane Bending	10.92	11.13	11.20
2nd Out-of-plane Bending	29.37	30.11	30.28
2nd Out-of-plane Bending & 1st In-plane Bending	47.20	47.38	47.55
3rd Out-of-plane Bending	56.14	56.91	57.18
1st Torsion	62.47	67.33	68.44

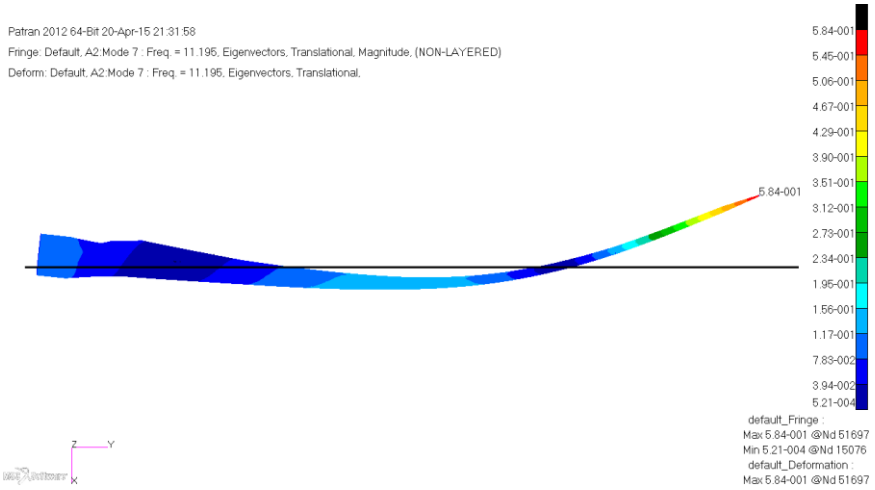

Figure 4.13. 1st Out-of-Plane Bending [11.20 Hz]

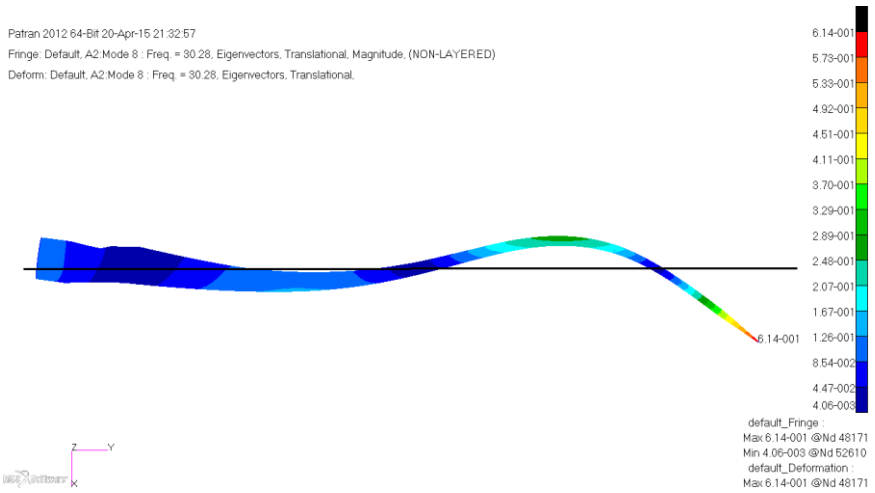

Figure 4.14. 2nd Out-of-Plane Bending [30.28 Hz]

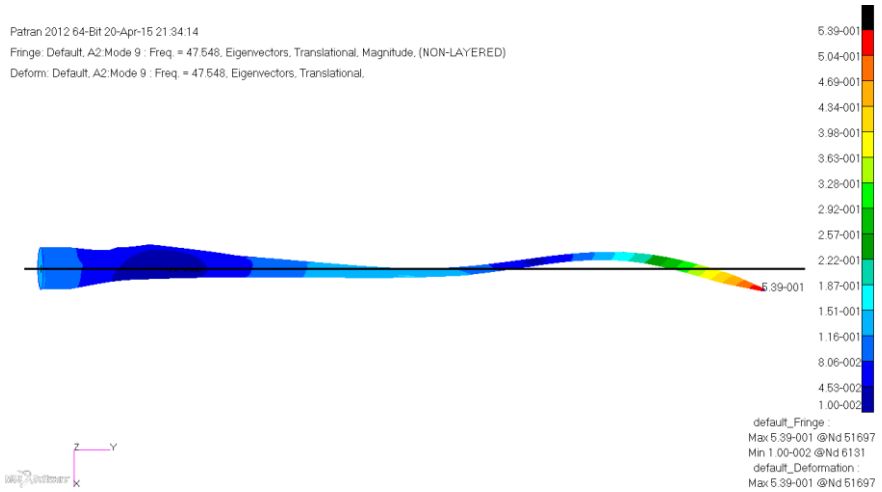

(a)

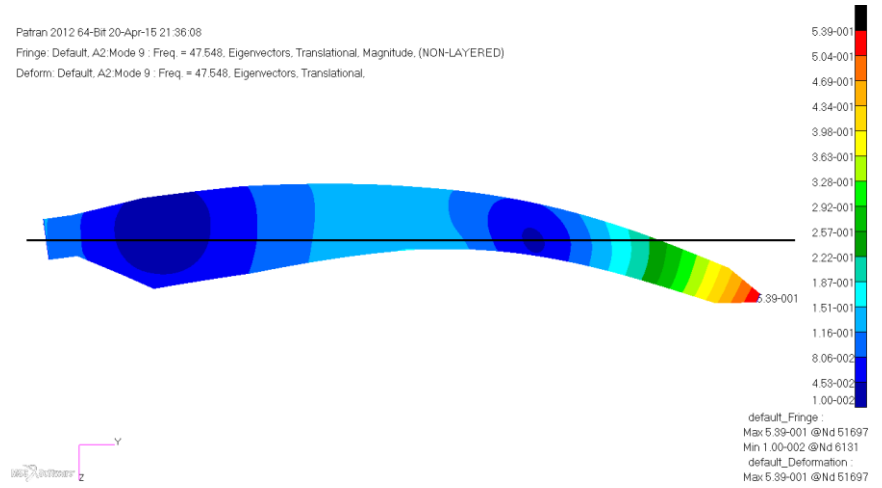

(b)

Figure 4.15. 2nd Out-of-Plane Bending and 1st In-Plane Bending Coupling [47.55 Hz] (a) Side View (b) Top View

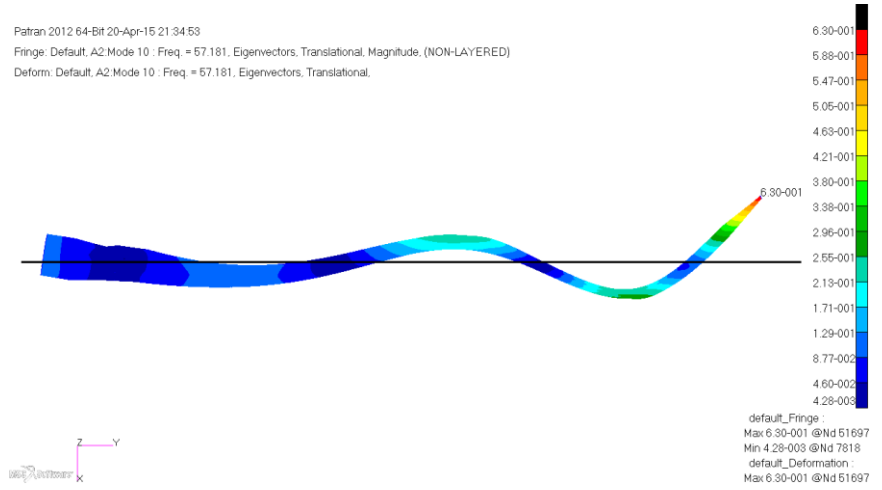

Figure 4.16. 3rd Out-of-Plane Bending [57.18 Hz]

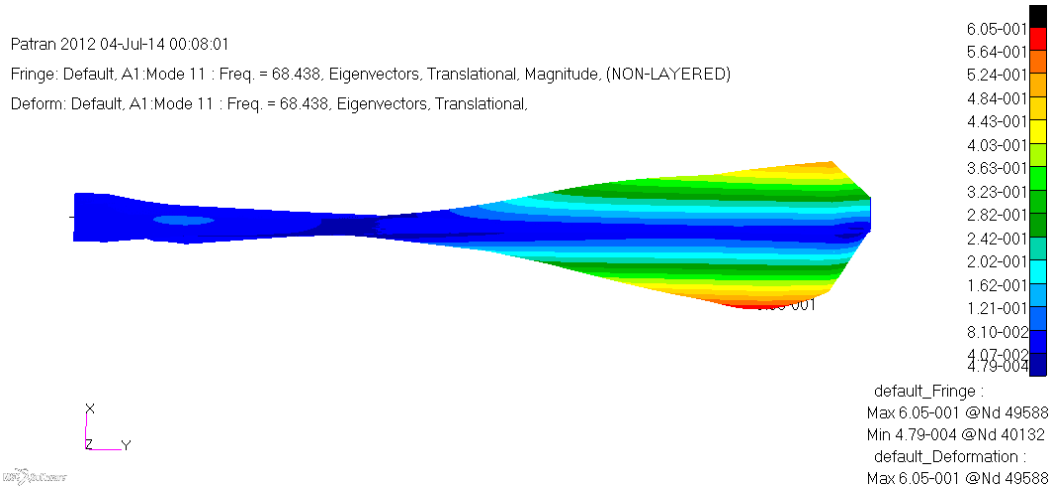

Figure 4.17. 1st Torsion [68.44 Hz]

4.3.3. Normal Mode Dynamic Analysis: Fixed – Free Case

In order to find the natural frequencies and corresponding mode shapes, 'normal modes' analysis type is also performed in MSC Patran/Nastran environment, this time, for the fixed-free condition (Table 4.6, Figure 4.18 to Figure 4.22).

Table 4.6. Natural Frequencies for Three Different Mesh Densities – Fixed Free Case

Mode Shapes	Natural Frequencies [Hz]		
	Coarse Mesh	**Fine Mesh**	**Finest Mesh**
1st Out-of-plane Bending	5.01	5.06	5.09
2nd Out-of-plane Bending and 1st In-plane Bending Coupling	13.66	13.70	13.80
2nd Out-of-plane Bending	17.33	17.56	17.71
3rd Out-of-plane Bending	36.37	37.16	37.49
2nd In-plane Bending and 1st Torsion Coupling	51.71	51.89	52.17

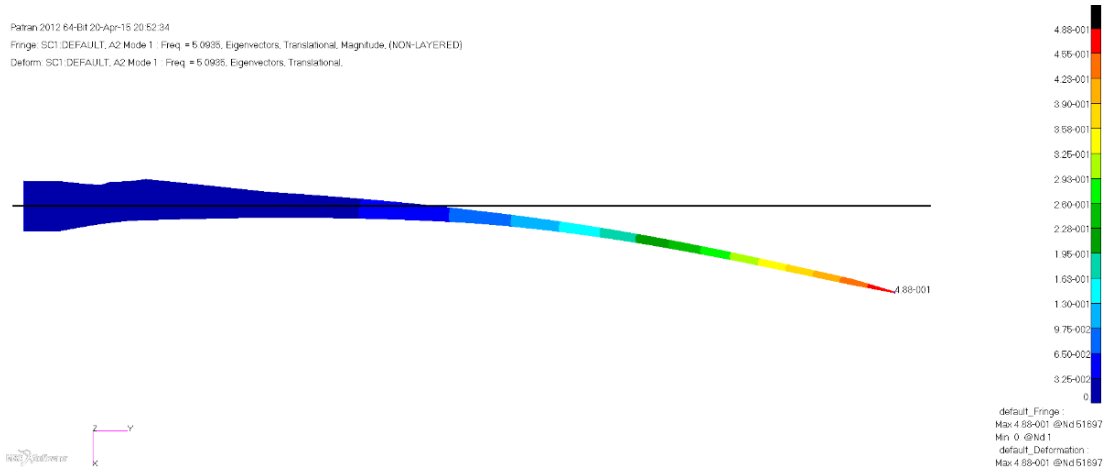

Figure 4.18.1st Out-of-Plane Bending [5.09 Hz]

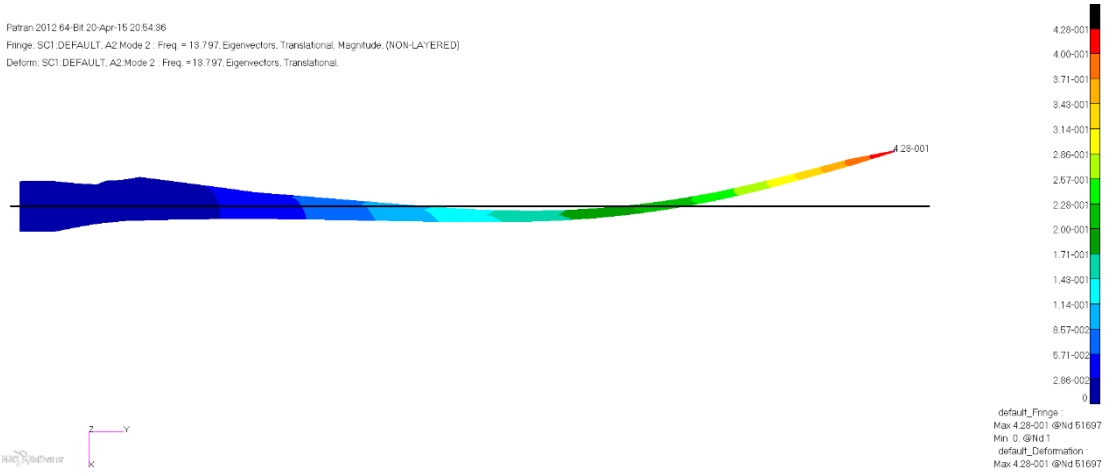

(a)

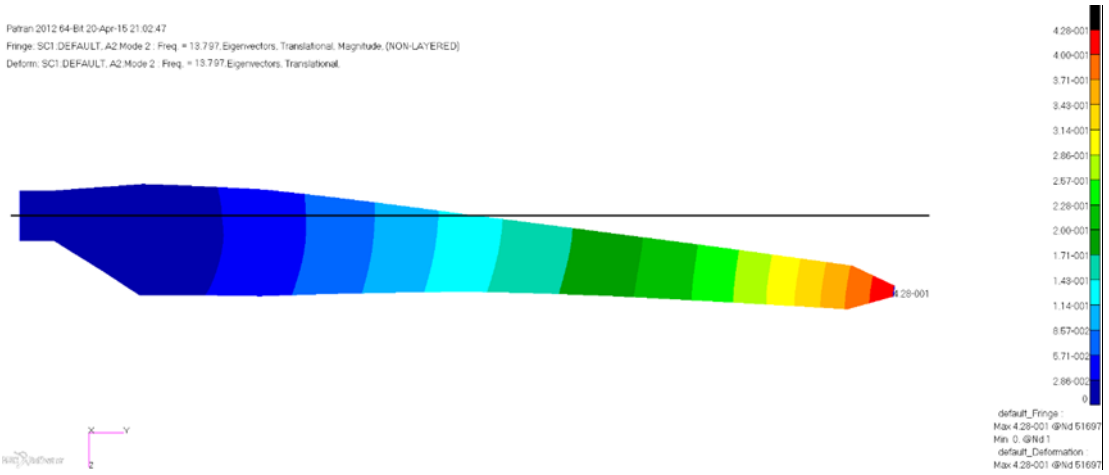

(b)

Figure 4.19. 2nd Out-of-Plane Bending and 1st In-plane Bending Coupling [13.80 Hz]

(a) Side View (b) Top View

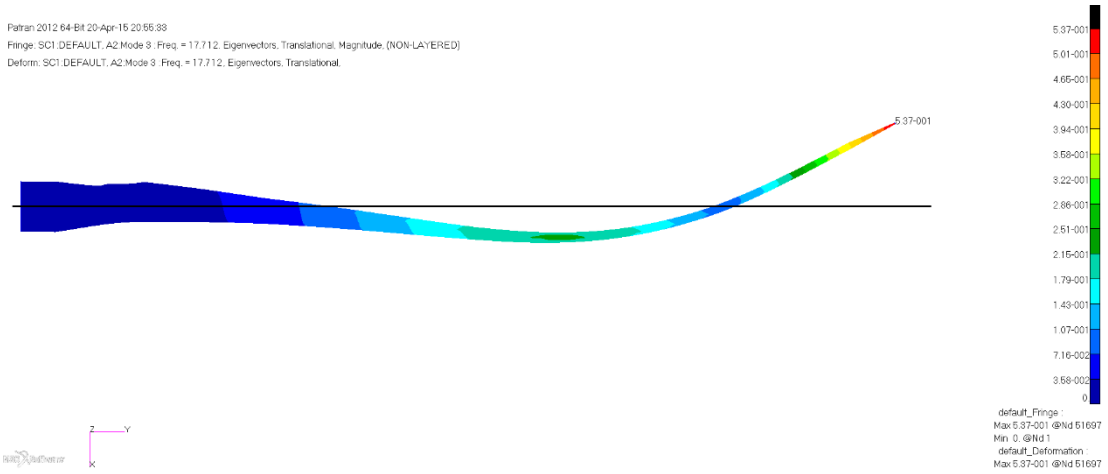

Figure 4.20. 2nd Out-of-Plane Bending [17.71 Hz]

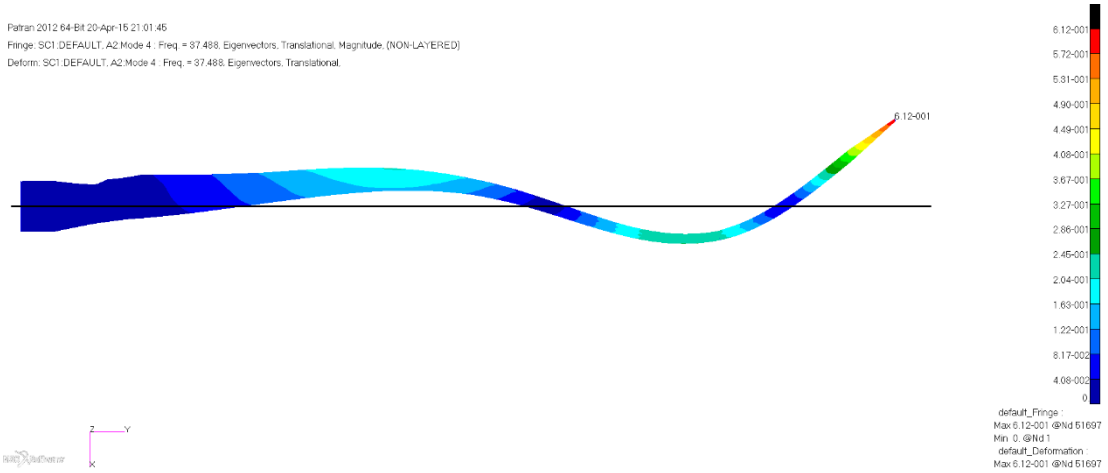

Figure 4.21. 3rd Out-of-Plane Bending [37.49 Hz]

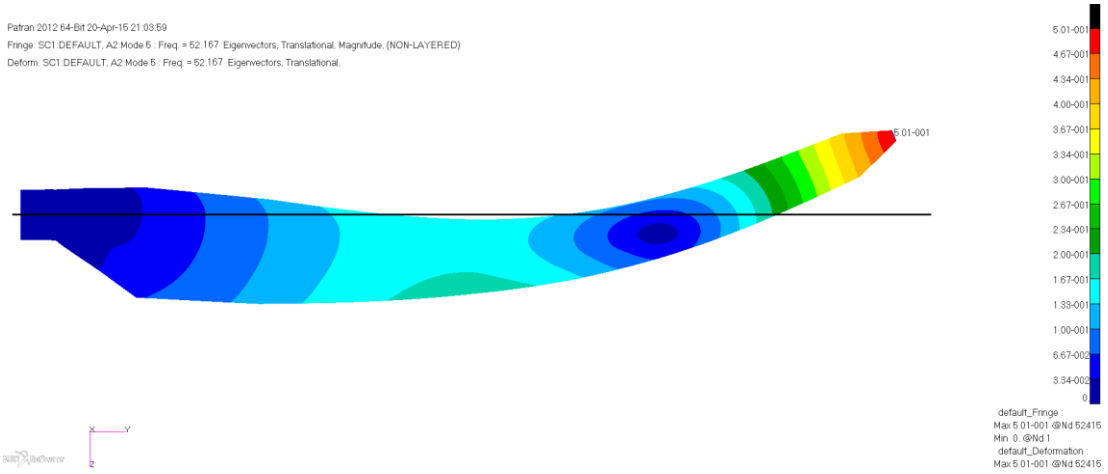

(a)

Figure 4.22. 2nd In-Plane Bending and 1st Torsion Coupling [52.17 Hz].

(a) Top View (b) Front View

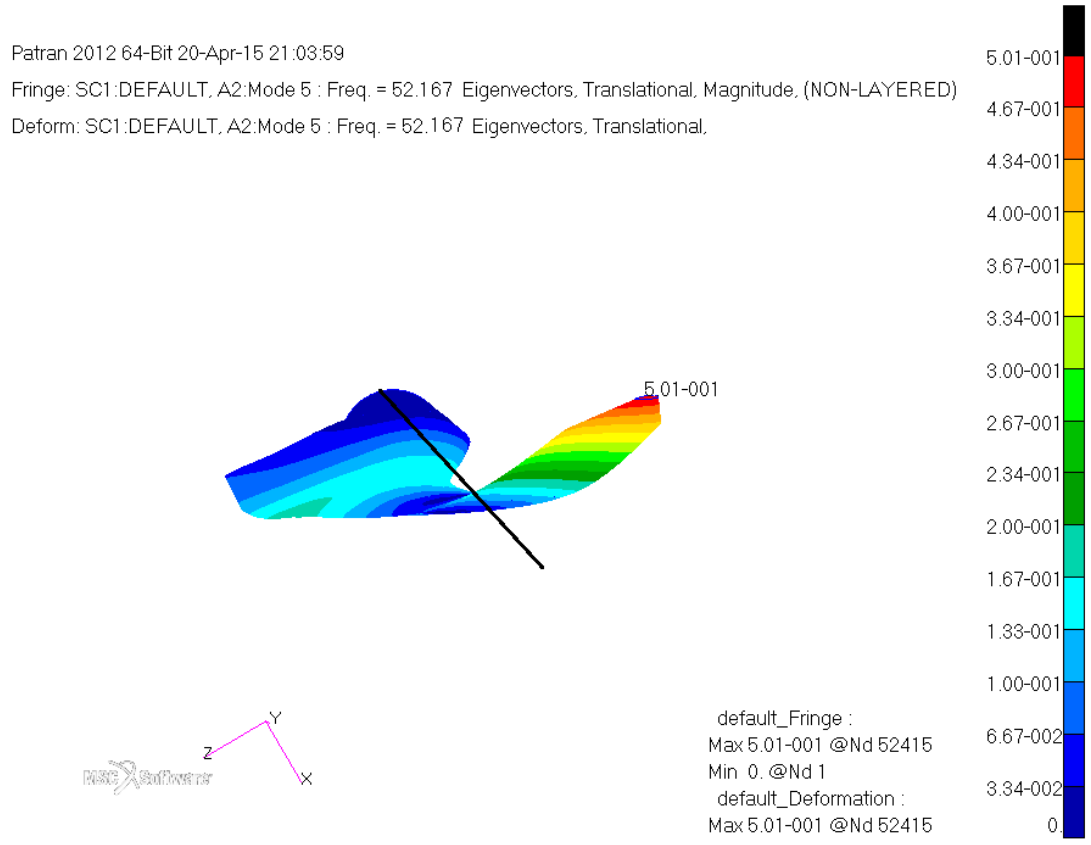

(b)

Figure 4.22. (continued)

4.4.Conclusion

In this chapter, an optimised horizontal axis 5-meter-long wind turbine rotor blade is modelled by using the airfoil geometries created at various sections along the span of the blade. The obtained geometry is then transferred to finite element modelling environment and the material properties are assigned. For the investigation of both the dynamic and static behaviour of the blade, various analyses are performed regarding the finite element mesh independency check and for a diversity of boundary conditions. Now, in order to compare the Modal Tests Results with the FEM ones for Free-Free case, the results of these tests are tabulated in the following Table 4.7.

Table 4.7. Comparison of the Modal Tests Results with the FEM – Free-Free Case

Mode Shapes	Resonance (and/or Natural) Frequencies [Hz]			
	Hammer with Accelerometer	**Shaker with Accelerometer**	**Shaker with Laser Vibrometer**	**FEM**
1st Out-of-plane Bending	8.25	8.25	8.38	10.11
2nd Out-of-plane Bending	23.75	23.75	23.88	27.69
2nd Out-of-plane Bending and 1st In-plane Bending Coupling	41.50	41.75	42.00	43.38
3rd Out-of-plane Bending	47.00	46.75	47.13	52.44
1st Torsion	59.00	58.75	59.25	60.58

As it can be seen from the above table, there are some discrepancies between the experimental and the finite element analyses results and therefore this low fidelity FEM of the blade must be updated in order to reach a high fidelity one.

CHAPTER 5

MODEL UPDATE OF THE WIND TURBINE BLADE

5.1. Introduction

As it can be concluded from the previous Chapters 3 and 4 that the modal test results do not perfectly match with the finite element analysis ones and this lack of accuracy is assumed to be due to various assumptions made during the construction of the model. Thus, in order to reach a high fidelity reliable finite element model, some criteria in the modelling must be reconsidered and the low fidelity FEM should be updated. Therefore, in this chapter an update of the model by using FEMTools [5] software is performed.

5.2. Model Updating

At first, the model updating is performed by using MSC© Patran/Nastran software. By comparing the FEM and the real blade, it was found that the weight of the finite element model (74.81 kg) and that of the actual blade (81.50 kg) were different. This difference was considered to be due to the weight of the excessive adhesive paste (assumed to be the difference in weights 6.69 kg) used during the manufacturing of the blade.

5.2.1. Finite Element Modelling and Analysis with Mass of Adhesive

The same mesh and surface properties used in previous studies are also used in this new model; nonetheless, adhesive paste now was distributed homogenously, by trying to simulate the production of the blade. The spatial locations for the

adhesive paste were at the contact edges of the upper and lower surface, as well as, at the contact surfaces of the inside hat shaped spar with the surrounding surfaces in contact. This modelling approach can be better understood by considering the Figure 5.1 (edited by the previously shown Figure 4.2 in Chapter 4) where the red dots represent the adhesive paste and by the Figure 5.2 where both the lower and the upper surface views of the FEM are presented. The lumped masses used in the FEM for the points at the aforementioned geometrical locations are calculated by dividing the total mass of the used adhesive (i.e. 6.69 kg) over the total number of points considered (i.e. 64). Therefore, unit lumped mass is calculated as 0.10453125 kg.

Then, the normal mode dynamic analysis is performed on free-free boundary condition by considering only the finest mesh density in FEM. The results of this particular analysis, namely; with and without adhesive compared with the modal test results involving shaker with accelerometers and are tabulated in Table 5.1. The corresponding mode shapes of the blade with mass of the adhesive can be found in Appendix B. As all three modal tests results were quite close to each other, the shaker with accelerometer results are chosen with no specific intention.

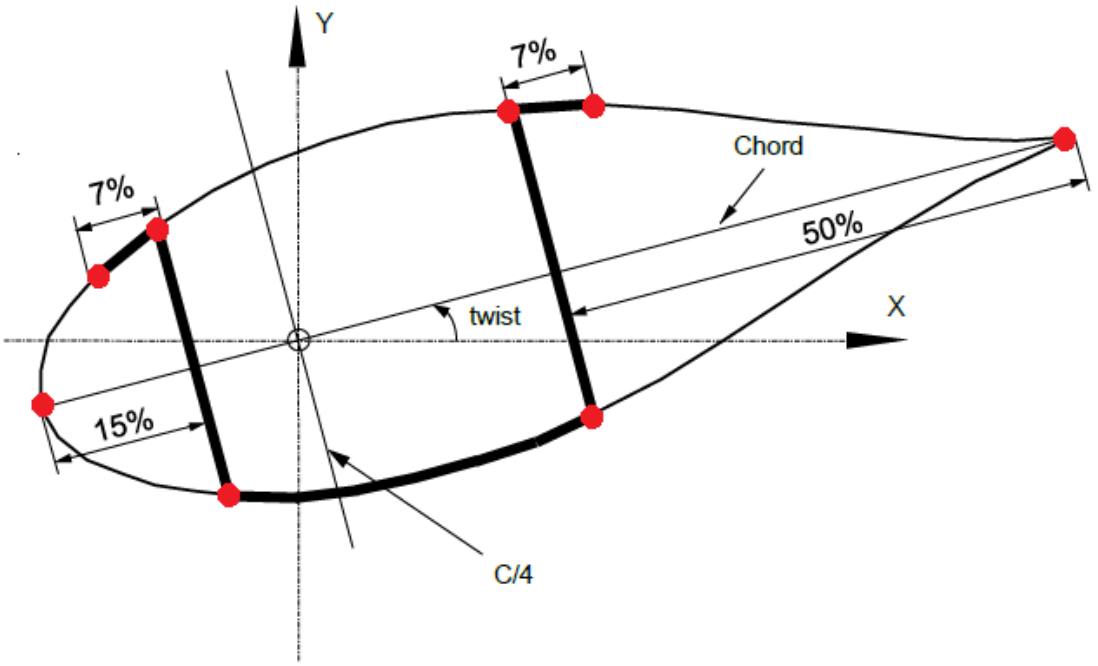

Figure 5.1. Positioning of the Adhesive Paste

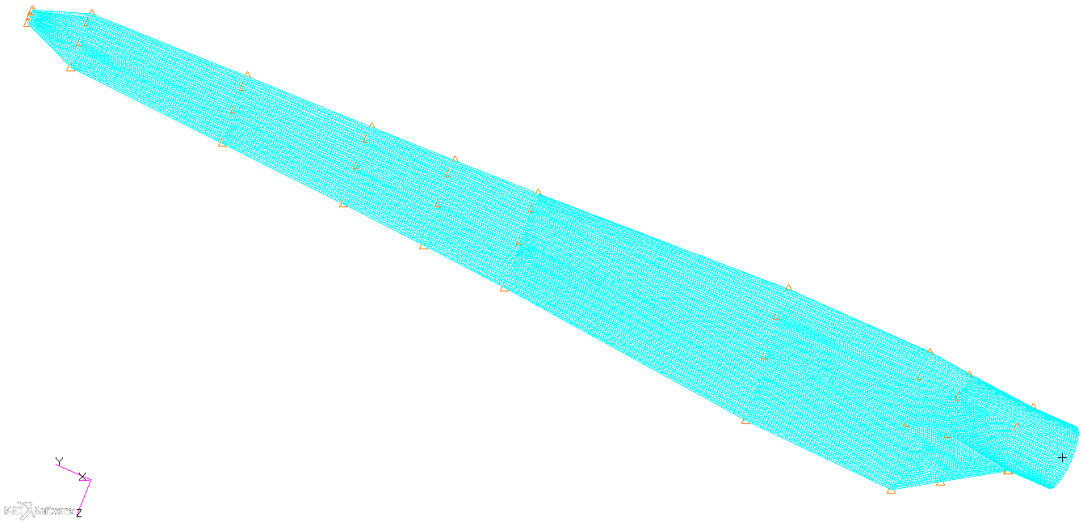

(a)

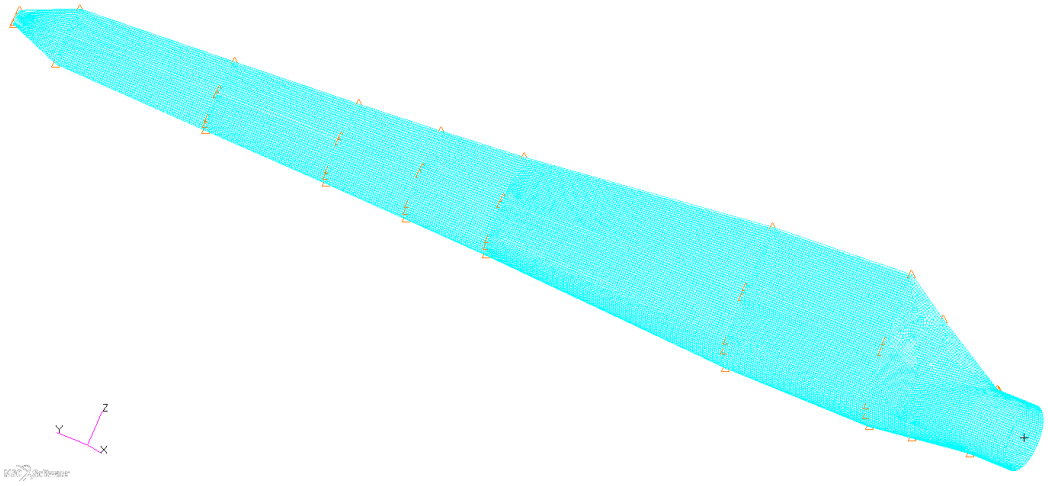

(b)

Figure 5.2. New Finite Element Model with the adhesive addition (a) lower surface view (b) upper surface view

Table 5.1. Natural Frequencies of the Blade with and without Adhesive – Free-Free Case

Mode Shapes	Resonance (and/or Natural) Frequencies [Hz]		
	Without Adhesive	**With Adhesive**	**Shaker with Accelerometer**
1st Out-of-plane Bending	11.20 (35.75)*	10.11 (22.55)	8.25
2nd Out-of-plane Bending	30.28 (27.49)	27.69 (16.59)	23.75
2nd Out-of-plane Bending and 1st In-plane Bending Coupling	47.55 (13.89)	43.38 (3.90)	41.75
3rd Out-of-plane Bending	57.18 (22.31)	52.44 (12.17)	46.75
1st Torsion	68.44 (16.49)	60.58 (3.11)	58.75

()* Percentage difference between the test and the FEA

It can be seen from the above Table 5.1 that the addition of the adhesive to FEM improved the dynamic analyses results by providing closer values to the ones obtained from the modal test.

5.2.2. Modal Assurance Criterion Comparison

Modal Assurance Criterion is a technique for comparing mode shapes, computed from analytical (or numerical) model, with modes identified from measured data experimentally by respecting the following equation:

$$MAC^{\langle i,j \rangle} = \frac{\left| \left[\left(S^{\langle i \rangle T} \cdot u^{\langle j \rangle} \right)^2 \right] \right|}{\left(S^{\langle i \rangle T} \cdot S^{\langle i \rangle} \right) \cdot \left(u^{\langle j \rangle T} \cdot u^{\langle j \rangle} \right)}$$

where “S” represents one data series, “u” representing another data series, and “i”&“j” letters representing the corresponding mode number. This criterion has values laying between 0 and 1 only, where 1 represents a perfect match, while 0 means a non-coherent result between the two selected modes.

Now, in relation to the research study, the Modal Assurance Criteria are obtained to compare the mode shapes of the modal tests and that of the FEA. These MACs are presented in Figure 5.3 by comparing the FEA and Shaker Modal Test Results (MAC matrix values from Table 5.2) and Figure 5.4 by comparing the FEA and Impact Hammer Test Results (MAC matrix values in Table 5.3) both for Out-of-Plane excitation tests. The numbers (i.e. 1,2,3,4 and 5) in those tables correspond to the aforementioned mode shapes, respectively. (i.e. 1st Out-of-plane Bending, 2nd Out-of-plane Bending, 2nd Out-of-plane Bending and 1st In-plane Bending Coupling, 3rd Out-of-plane Bending and 1st Torsion).

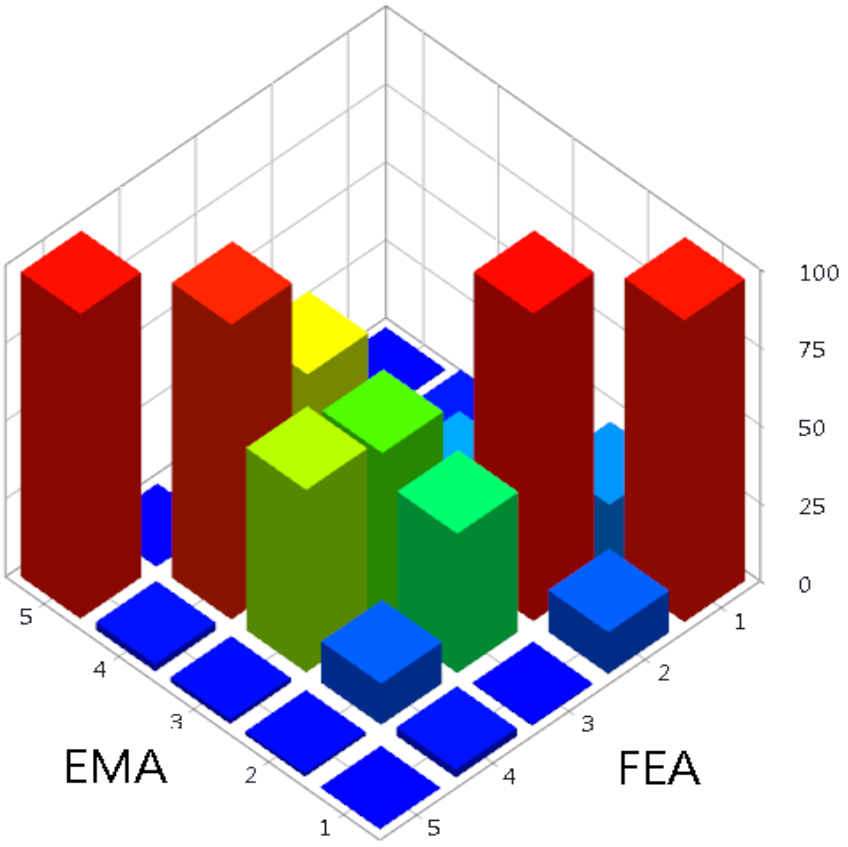

Figure 5.3. Cross MAC Matrix between FEA and Modal Test Shaker Results – Graphical Representation

Table 5.2. Cross MAC Matrix between FEA and Modal Test Shaker Results - Values

		Test Results				
		1	2	3	4	5
FEA Results	1	96.9	20.8	5.7	3.7	0.4
	2	13.5	98.8	23.8	15.0	2.2
	3	0.5	44.8	53.8	62.1	3.7
	4	2.7	13.3	58.6	94.7	0.2
	5	0.2	1.2	1.7	2.4	97.9

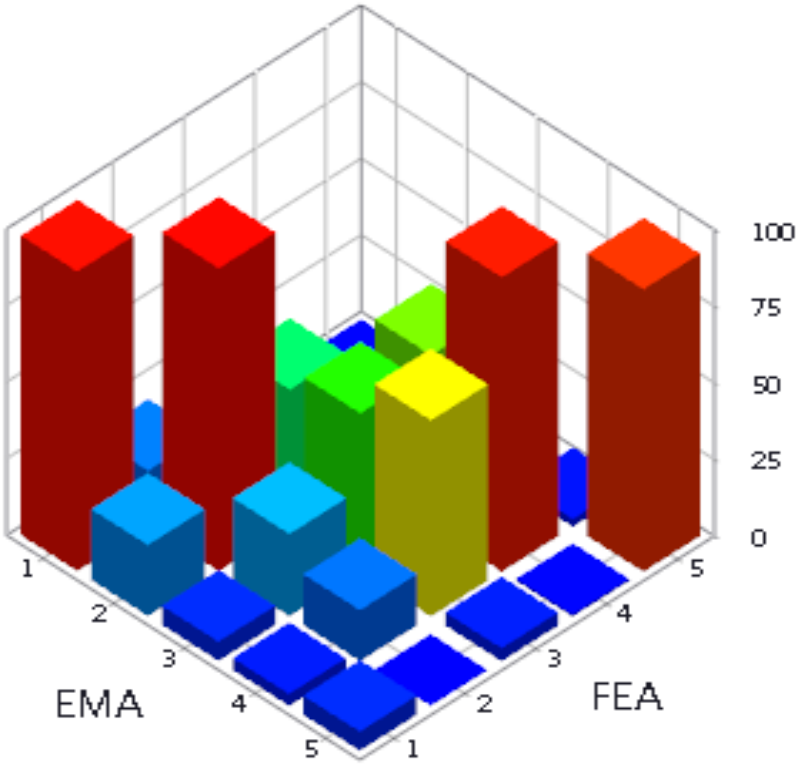

Figure 5.4. Cross MAC Matrix between FEA and Modal Test Impact Hammer Results – Graphical Representation

Table 5.3. Cross MAC Matrix between FEA and Modal Test Impact Hammer Results - Values

		Test Results				
		1	2	3	4	5
FEA Results	1	97.9	23.2	6.4	3.9	6.3
	2	18.2	99.0	26.9	16.7	0.2
	3	0.3	44.7	51.7	64.0	4.3
	4	4.4	13.8	56.0	96.1	0.7
	5	0.5	1.0	2.9	2.6	92.3

From the MACs above, it can be concluded that the FEA results show better correlation with the modal test results obtained from Shaker with Accelerometer data and therefore this test data is used for further model updates via FEMTools software. Additionally, the third mode inaccuracy is supposed to be due to the incompatibility between the mode shape of the third mode and the Out-of-Plane excitations as that mode shows majorly an In-Plane behaviour. For a better understanding, Figure 5.5 represents the MAC between the FEA and Impact Hammer Test Results for the third mode for In-Plane Excitation with a MAC value 98.6%.

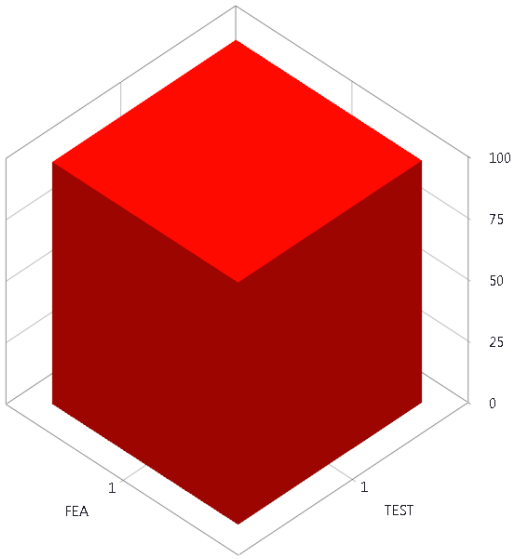

Figure 5.5. Cross MAC Matrix between FEA and Modal Test Impact Hammer Results for the Third Mode – In-Plane Excitation

5.2.3. FEMTools Model Updating Analyses

FEMTools, being a reliable multitask finite element analyser, is used at this stage to import, update and export the FEM already designed in MSC Patran. Figure 5.6 presents the blade model in FEMTools environment.

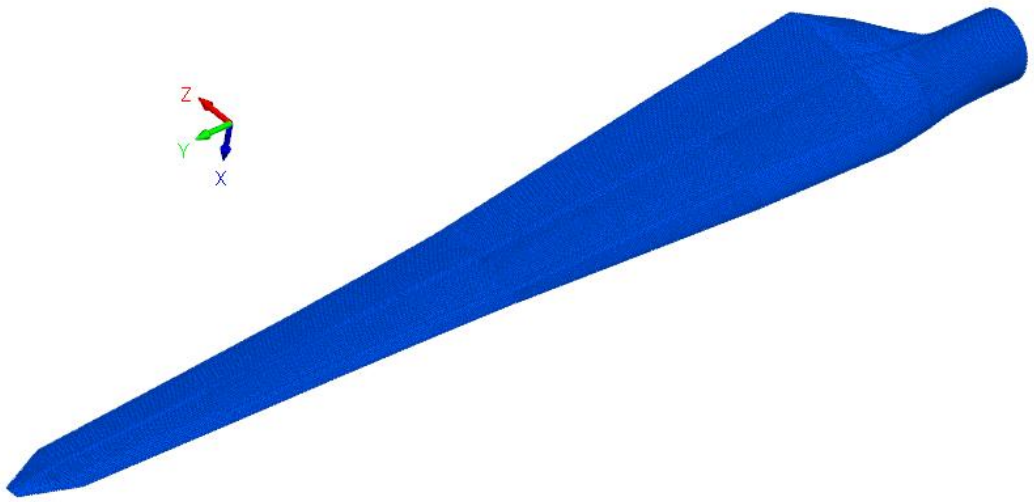

Figure 5.6. The Blade's FEM in FEMTools Environment

In order to update the FEM, it is essential to get the FEA and Modal Models results together into same environment. Thus, Figure 5.7 represents the imported model of the modal test 2-D blade, while Figure 5.8 shows the two models being bound together in order to share their data which are all in FEMTools environment.

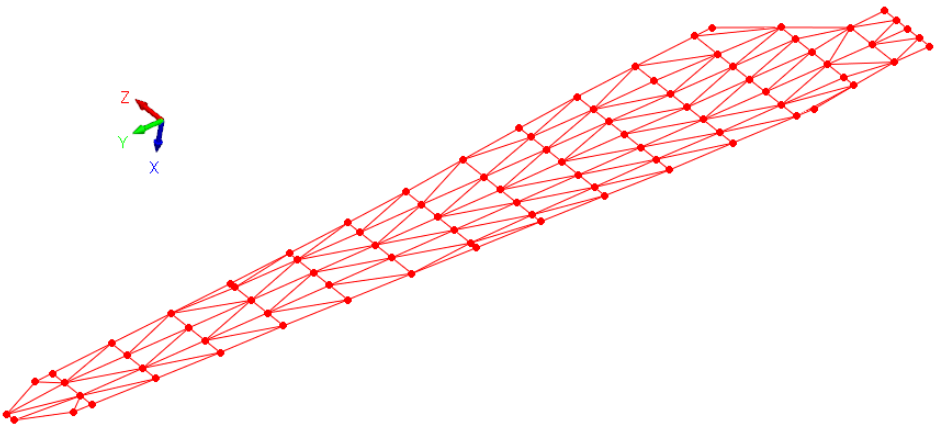

Figure 5.7. The Blade's Test Model in FEMTools Environment

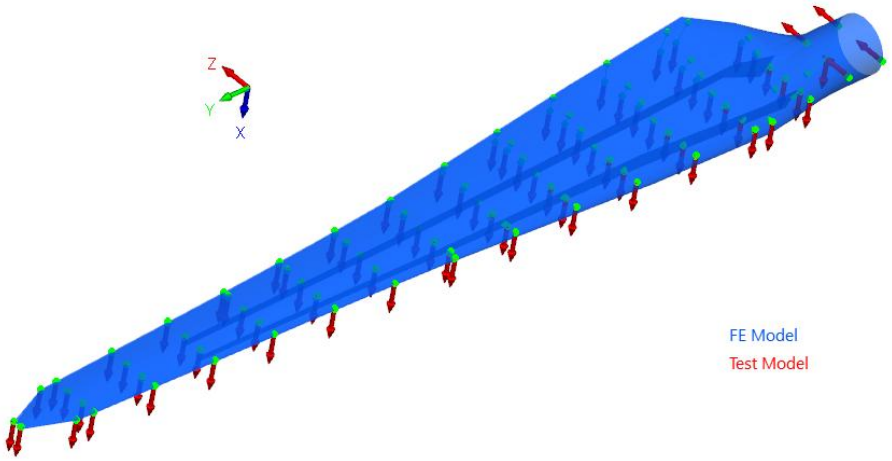

Figure 5.8. The Blade's FE and Test Models in FEMTools Environment

Two different types of model updating routines are considered either by redistributing the adhesive paste by also keeping its total mass constant (i.e. 6.69 kg) or by changing the stiffness parameters of the composite material in a particular range.

In the first model update, the maximum mass per previously defined nodes (shown in Figure 5.1 and 5.2) is given up to a five times changeability (i.e. maximum 500% variation corresponding to an addition of a maximum mass of 0.523 kg) assumed to be the logical quantity of adhesive to be put in the designated areas. This particular update is performed, at first, by considering the Shaker-with-Accelerometer test data for the Out-of-Plane excitation (named as FEMTools Update-1a and the results summarised in Table 5.4) and then by also including the In-Plane mode which is obtained by using Hammer-with-Accelerometer test data (named as FEMTools Update-1b and the results summarised in Table 5.5). The mode shapes obtained after these updates are presented in the Appendix C section. The change in parameters in these updates are presented for FEMTools Update-1a and FEMTools Update-1b in Figures 5.9-5.10 and Figures 5.11-5.12, respectively.

In the second model update (named as FEMTools Update-2) the stiffness parameters of the composite material are changed in the range of interest shown in Table 5.6 [31]. The correlation coefficient (i.e. the stopping criterion for the iterations – namely; CCABSOLUTE) in the update runs of FEMTools is set and it measures the

weighted absolute relative difference between resonance frequencies via the following equation:

$$CC = \frac{1}{C_R}\sum_{i=1}^{N} C_{R_i}\frac{\Delta f_i}{f_i};\ C_R = \sum_{i=1}^{N} C_{R_i}$$

where; (f_i) is the natural frequencies, (C_R) is the response confidences used in the Bayesian objective and N is the number of modes interested.

Table 5.4. Natural Frequencies of the Blade: FEMTools Update-1a

Mode Shapes	Resonance (and/or Natural) Frequencies [Hz]		
	With Adhesive	**FEMTools Update-1a**	**Shaker with Accelerometer**
1st Out-of-plane Bending	10.11 (22.55)*	9.92 (20.24)	8.25
2nd Out-of-plane Bending	27.69 (16.59)	26.70 (12.42)	23.75
2nd Out-of-plane Bending and 1st In-plane Bending Coupling	43.38 (3.90)	42.55 (1.91)	41.75
3rd Out-of-plane Bending	52.44 (12.17)	50.30 (7.59)	46.75
1st Torsion	60.58 (3.11)	59.50 (1.27)	58.75

()* Percentage difference between the test and the FEA

Table 5.5. Natural Frequencies of the Blade: FEMTools Update-1b

Mode Shapes	Resonance (and/or Natural) Frequencies [Hz]		
	With Adhesive	**FEMTools Update-1b**	**Shaker with Accelerometer**
1st Out-of-plane Bending	10.11 (22.55)*	9.72 (17.82)	8.25
2nd Out-of-plane Bending	27.69 (16.59)	27.04 (13.85)	23.75
2nd Out-of-plane Bending and 1st In-plane Bending Coupling	43.38 (3.90)	41.83 (0.19)	41.75
3rd Out-of-plane Bending	52.44 (12.17)	51.08 (9.26)	46.75
1st Torsion	60.58 (3.11)	59.10 (0.59)	58.75

()* Percentage difference between the test and the FEA

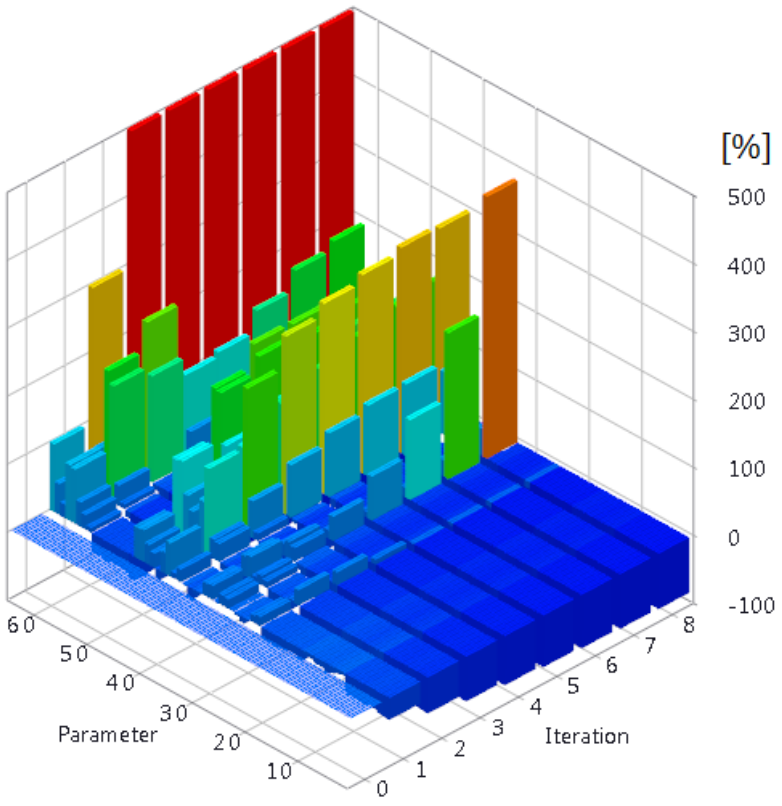

(a)

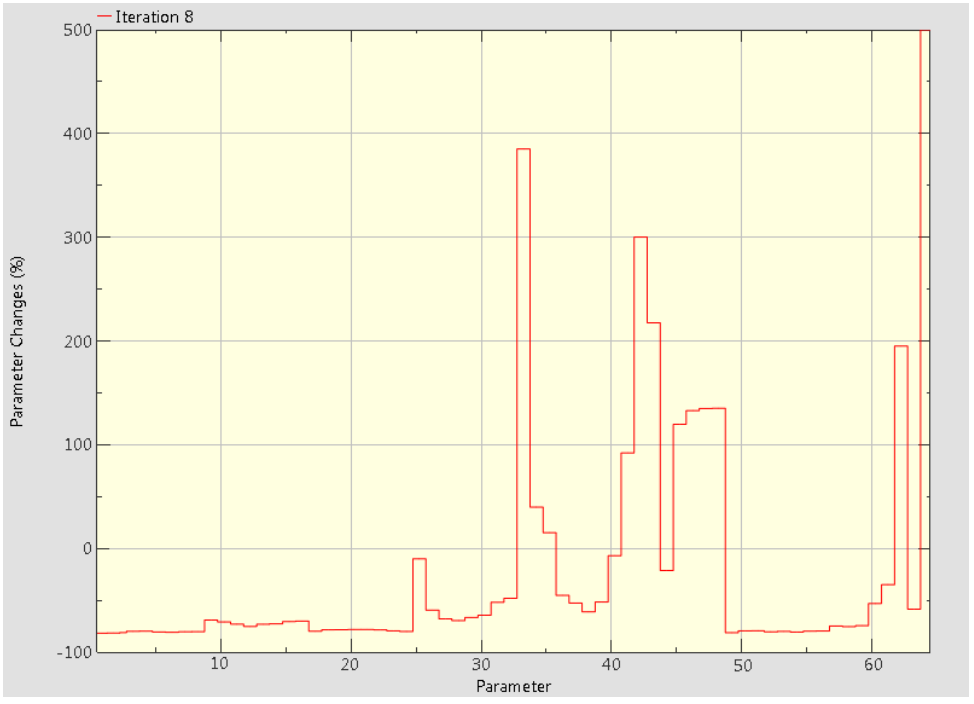

(b)

Figure 5.9. Parameter Changes: FEMTools Update-1a (a) 3D view (b) 2D view of the last iteration at the convergence

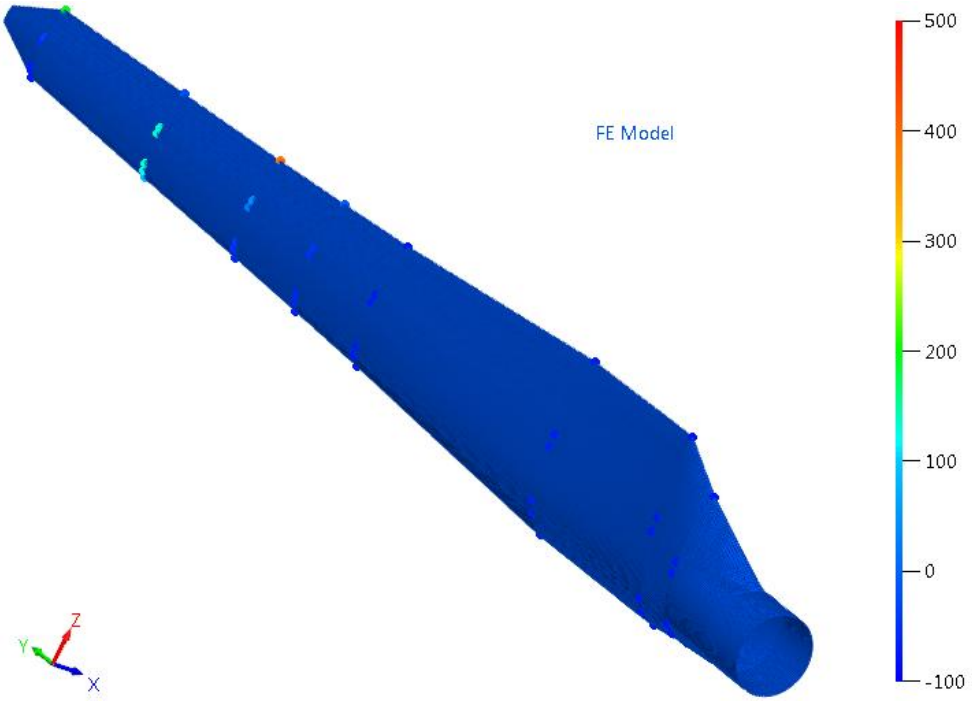

(a)

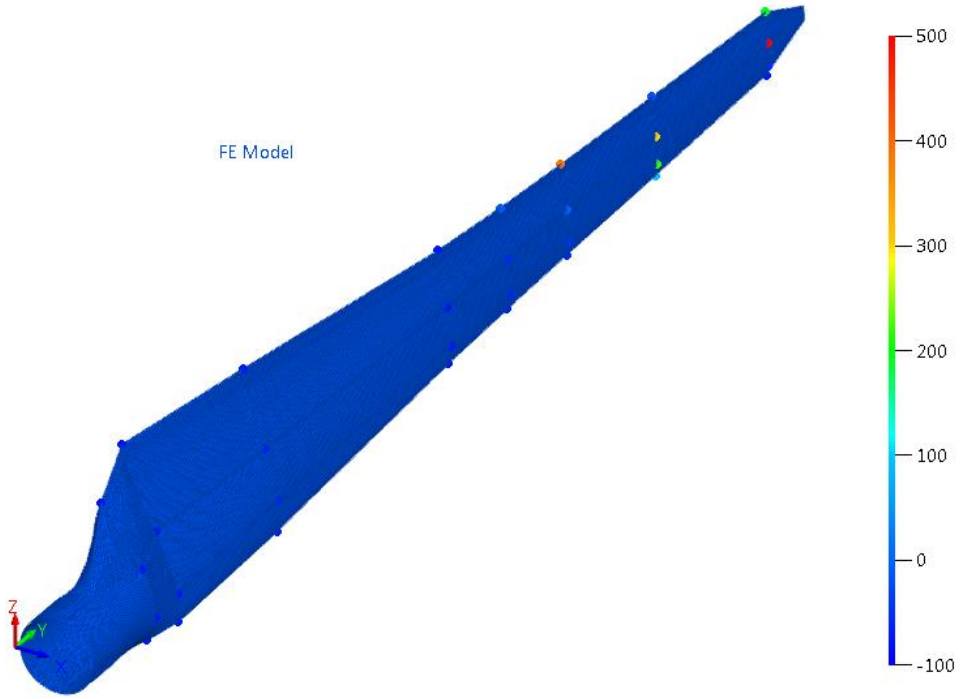

(b)

Figure 5.10 Parameter Changes over the Blade: FEMTools Update-1a
(a) Upper Side (b) Lower Side

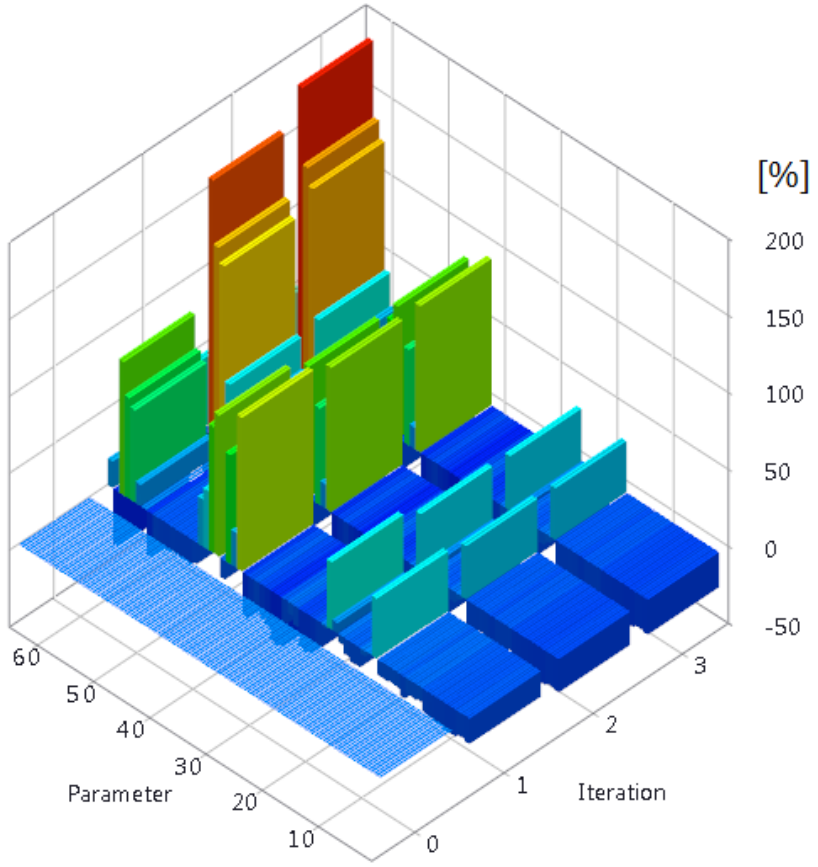

(a)

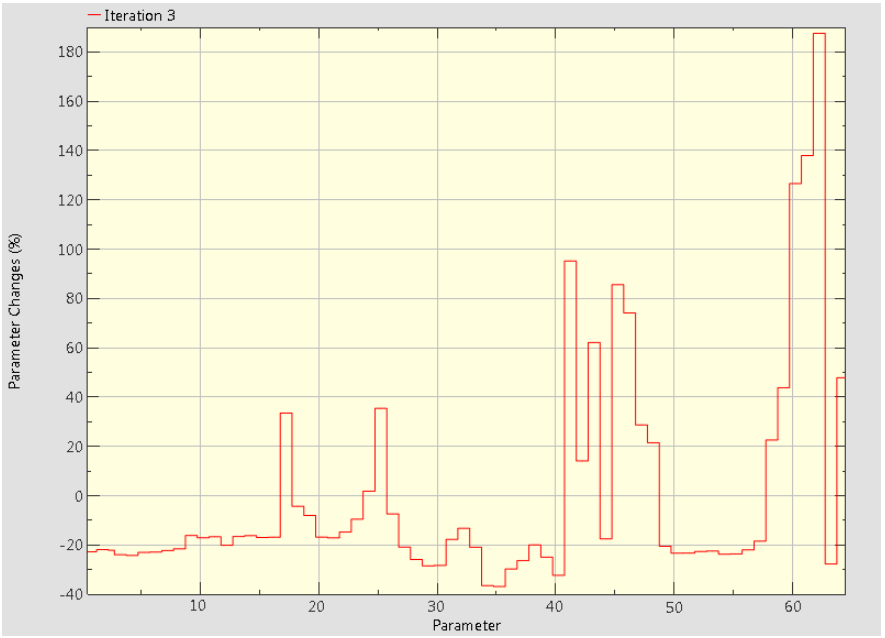

(b)

Figure 5.11. Parameter Changes: FEMTools Update-1b (a) 3D view (b) 2D view of the last iteration at the convergence

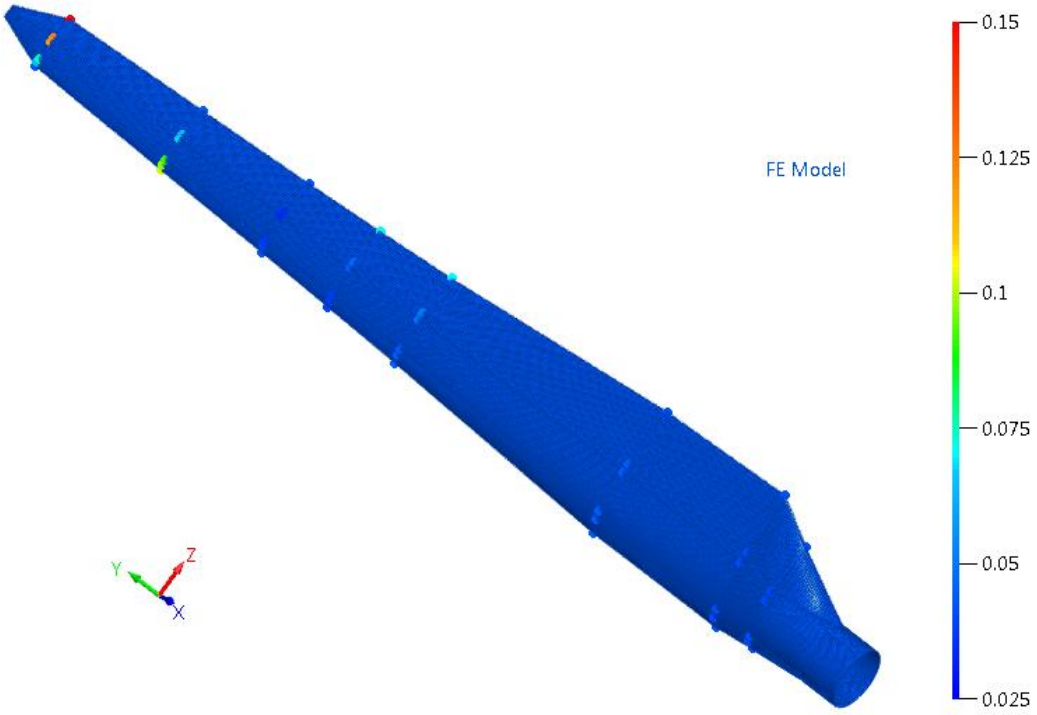

(a)

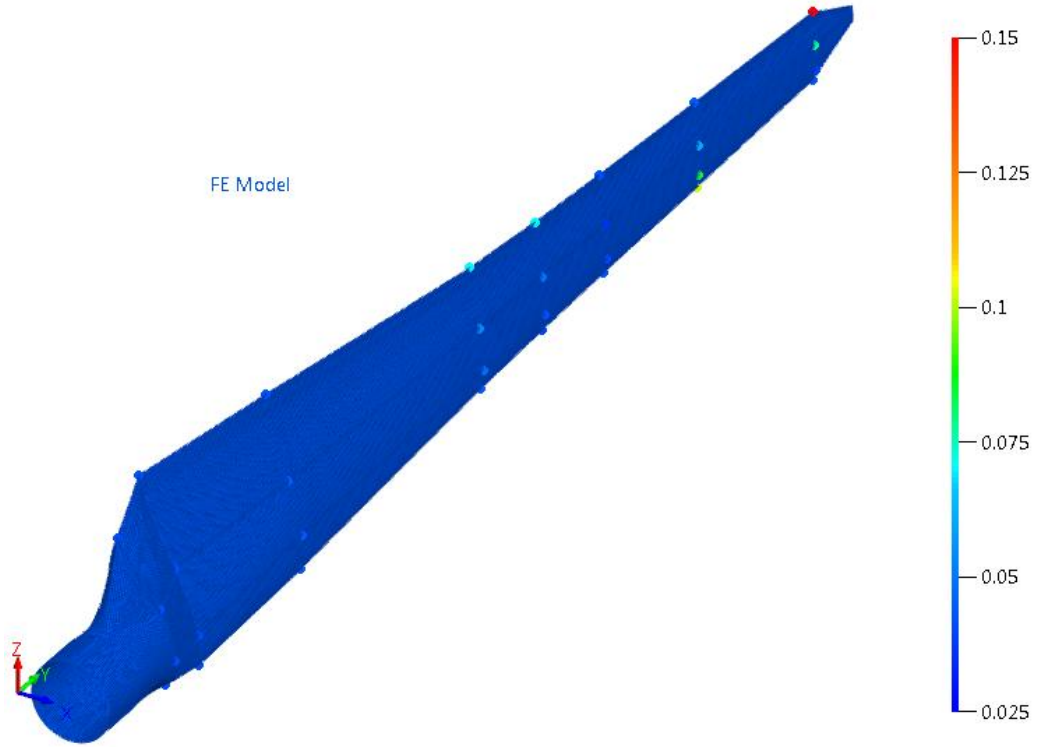

(b)

Figure 5.12 Parameter Changes over the Blade: FEMTools Update-1b
(a) Upper Side (b) Lower Side

Table 5.6. Glass Epoxy Composite Mechanical Properties Ranges [31].

Mechanical Properties (GPa)	**23 °C**	**Values used Originally**	**-60 °C**
Longitudinal modulus Ex (Parameter 1)	19.94	24.84	28.65
Transverse modulus Ey (Parameter 2)	5.83	9.14	11.03
Shear modulus Gxy (Parameter 3)	2.11	2.83	4.21

This particular update is performed, at first, by considering the Shaker-with-Accelerometer test data for the Out-of-Plane excitation (named as FEMTools Update-2a and the results summarised in Table 5.7) and then by also including the In-Plane mode which is obtained by using Hammer-with-Accelerometer test data (named as FEMTools Update-2b and the results summarised in Table 5.8). The change in parameters in these updates are presented for FEMTools Update-2a and FEMTools Update-2b in Figure 5.13 and Figure 5.14, respectively.

Table 5.7. Natural Frequencies of the Blade: FEMTools Update-2a

Mode Shapes	**Resonance (and/or Natural) Frequencies [Hz]**		
	With Adhesive	**FEMTools Update-2a**	**Shaker with Accelerometer**
1st Out-of-plane Bending	10.11 (22.55)*	9.23 (11.88)	8.25
2nd Out-of-plane Bending	27.69 (16.59)	25.29 (6.58)	23.75
2nd Out-of-plane Bending and 1st In-plane Bending Coupling	43.38 (3.90)	39.89 (-4.45)	41.75
3rd Out-of-plane Bending	52.44 (12.17)	47.99 (2.65)	46.75
1st Torsion	60.58 (3.11)	56.85 (-3.23)	58.75

()* Percentage difference between the test and the FEA

Table 5.8. Natural Frequencies of the Blade: FEMTools Update-2b

Mode Shapes	Resonance (and/or Natural) Frequencies [Hz]		
	With Adhesive	**FEMTools Update-2b**	**Shaker with Accelerometer**
1st Out-of-plane Bending	10.11 (22.55)*	9.71 (17.69)	8.25
2nd Out-of-plane Bending	27.69 (16.59)	26.58 (11.92)	23.75
2nd Out-of-plane Bending and 1st In-plane Bending Coupling	43.38 (3.90)	41.75 (0.00)	41.75
3rd Out-of-plane Bending	52.44 (12.17)	50.38 (7.76)	46.75
1st Torsion	60.58 (3.11)	58.70 (-0.09)	58.75

()* Percentage difference between the test and the FEA

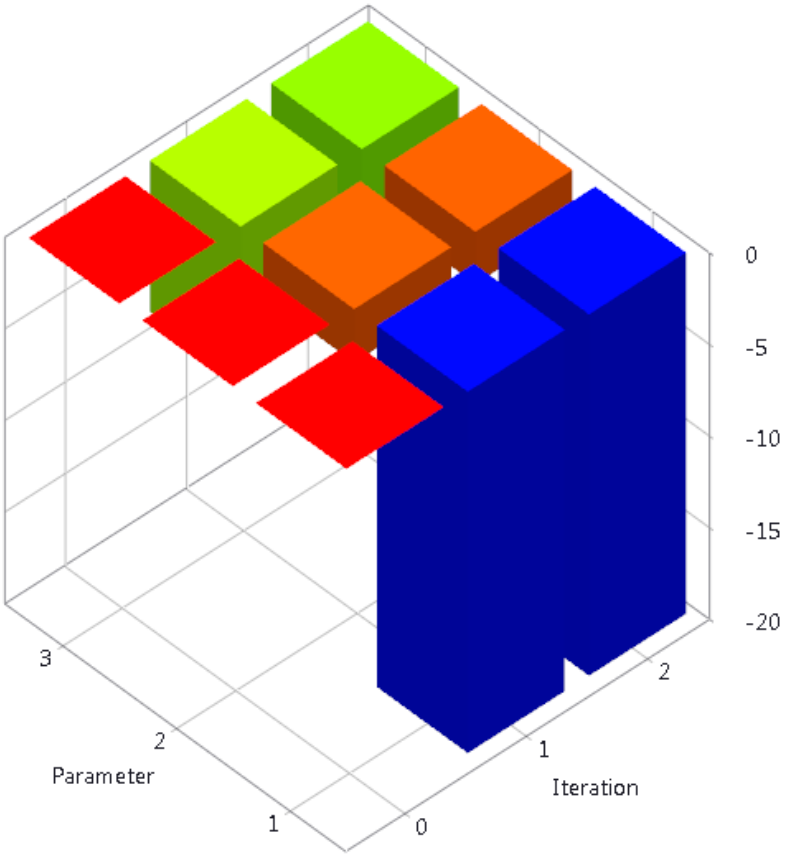

(a)

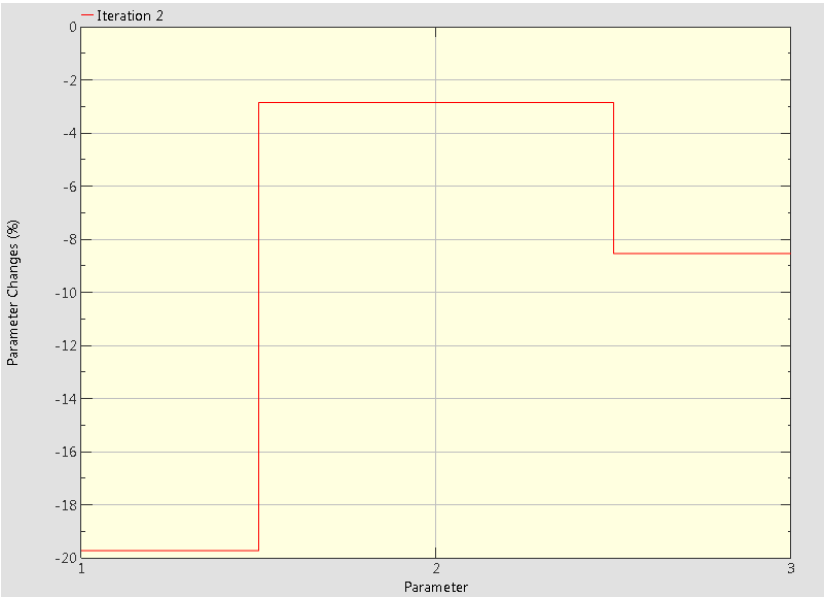

(b)

Figure 5.13. Parameter Changes: FEMTools Update-2a (a) 3D view (b) 2D view of the last iteration at the convergence

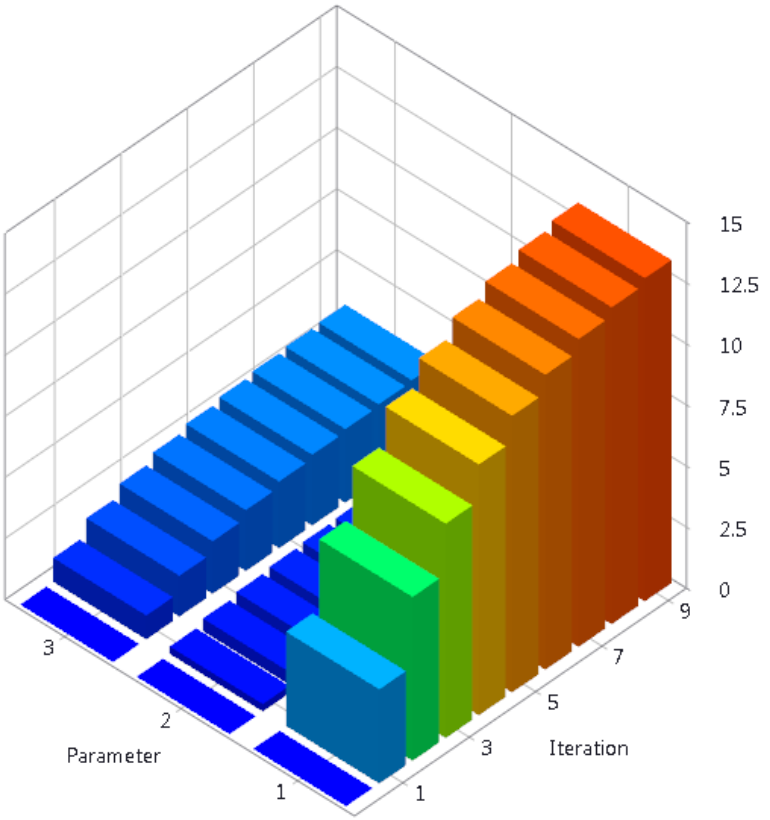

(a)

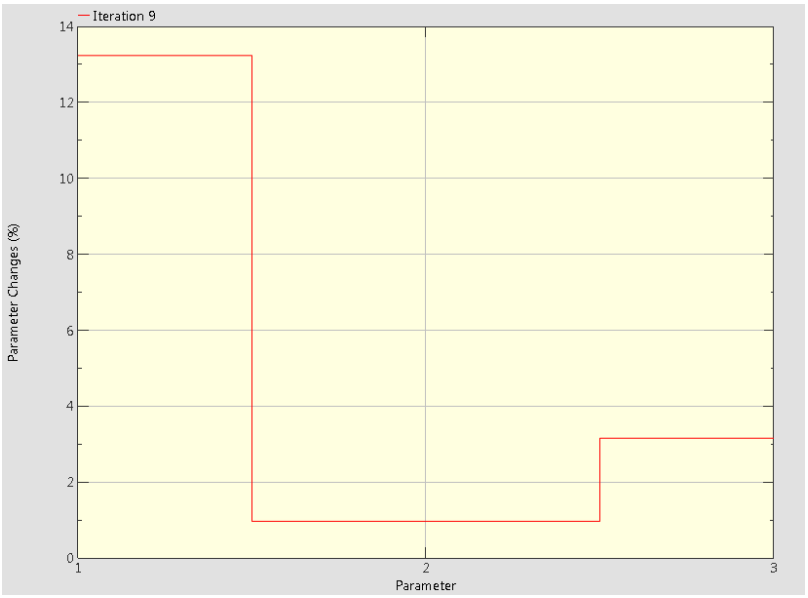

(b)

Figure 5.14. Parameter Changes: FEMTools Update-2b (a) 3D view (b) 2D view of the last iteration at the convergence

5.3. Conclusion

As a result, four updated finite element models are obtained either by redistributing the lumped masses (i.e. adhesive paste) or by altering the stiffness of the composite material. Those updates are performed first, by considering the Out-of-Plane modes only and then with the inclusion of the In-Plane mode as well. Having performed all the updates, Table 5.9 is constructed for the modes of the blade in the first three out-of-plane bending, the first torsional and the coupled one in order to summarize the results of the analyses. As it can be seen from the below table, while some of the natural frequencies of the blade get closer to the desired experimentally obtained values, some of them diverge depending on the type of the update.

Table 5.9. Natural Frequencies of the Blade: FEMTools Update Comparisons

	Resonance (and/or Natural) Frequencies [Hz]				
Mode Shapes	**1-a**	**1-b**	**2-a**	**2-b**	**Shaker with Accelerometer**
1st Out-of-plane Bending	9.92 (20.24)*	9.72 (17.82)	9.23 (11.88)	9.71 (17.69)	8.25
2nd Out-of-plane Bending	26.70 (12.42)	27.04 (13.85)	25.29 (6.58)	26.58 (11.92)	23.75
2nd Out-of-plane Bending and 1st In-plane Bending Coupling	42.55 (1.91)	41.83 (0.19)	39.89 (-4.45)	41.75 (0.00)	41.75
3rd Out-of-plane Bending	50.30 (7.59)	51.08 (9.26)	47.99 (2.65)	50.38 (7.76)	46.75
1st Torsion	59.50 (1.27)	59.10 (0.59)	56.85 (-3.23)	58.70 (-0.09)	58.75

()* Percentage difference between the test and the FEA

CHAPTER 6

CONCLUSIONS

6.1 General Conclusions

The main objective of this thesis is to obtain a high fidelity finite element model of a 5 meter long wind turbine blade. For this purpose, first, an experimental modal analysis is performed to extract the dynamic characteristics of the blade. Then, a low fidelity finite element model is created based on the supplied design and manufacturing blue prints. Following the normal mode structural dynamic analyses, the low fidelity finite element model is then updated by using FEMTools software based on the experimental results in order to obtain a high fidelity one.

It is observed from the results of the modal analyses performed on the updated models that while some of the natural frequencies of the blade get closer to the desired values, some of them diverge depending on the type of the updates performed. The observed discrepancies are thought to be due to both the effect of the boundary condition (i.e. modelled as free-free but hanged by restricting some degree of freedom by rubber bands) and the manufacturing uncertainties which are not taken into account during the modelling of this particular blade. It can also be seen from the analysis results that a good correlation between the high fidelity finite element model and the test results are finally achieved.

As a conclusion, the final form of the high fidelity finite element model of the 5 meter long wind turbine blade is now ready to serve as a benchmark for any future modification and/or correlation studies.

6.2 Recommendations for Future Work

The recommendations for future works of this study can be listed as follows:

- As the experimental work is performed on free-free boundary condition due to the non-existence of clamping mechanism, the modal tests can also be performed on a particular fixture in fixed-free condition. This case simulates the real behaviour of the blade while connected to the main turbine structure, via the hub joint, in its working condition.

- As the finite element model of the blade comprises 2-D shell elements for the composite material and lumped mass elements for the adhesive paste, a model can also be constructed by using 3-D solid elements.

- As the simplified 1-D models are generally preferred in complex and time consuming aeroelastic analyses, a further simplification can be made on the previously obtained high fidelity 3-D models.

REFERENCES

[1]-Yeniceli, S., Motivation of The Study. In *Design Optimization Of Whiffletree Systems For Wind Turbine Blade Testing* (1st Ed., Vol. 1, P. 12). Ankara: Middle East Technical University, 2014.

[2]-METUWIND [Online] [Cited: July 2014.] http://ruzgem.metu.edu.tr/en/

[3]-Philippidis, T. P., Roukis, G. A., *Structure design report of METUWIND small rotor blade*, Confidential Interim Report, unpublished, September 2013.

[4]- MSC PATRAN&NASTRAN [Online] [Cited: July 2014.] http://www.mscsoftware.com/product/

[5]-FEMtools[Online][Cited:July2014.] http://www.femtools.com/products/ftmu.htm

[6]-Alternative Power. [Online] Mariah Energy Development Corporation. [Cited: 10 June 2014.] http://www.mariah-energy.com/2011/01/top-10-countries-where-wind-turbines-are-used-most-efficiently-%E2%80%93-updated-article-with-new-information/.

[7]-Ata, R. (2013). The Current Situation of Wind Energy in Turkey. *Journal of Energy, 2013*(794095), p. 8. [Online] [Cited: 07 Aug 2014.]

[8]- Andy Darvill. 2014. "Energy Resources: Wind Power." [Online] [Cited: 04 March 2014.] (http://www.darvill.clara.net/altenerg/wind.htm).

[9]-Center of Energy. [Online] [Cited: 10 June 2014.] http://www.centreforenergy.com/AboutEnergy/Wind/Overview.asp?page=3.

[10]- KidWind. [Online] [Cited: 10 June 2014.] http://learn.kidwind.org/learn/wind_turbine_variables_bladedesign.

[11]- WWEA World Wind Energy Association. [Online] [Cited: 10 June 2014.] http://www.wwindea.org/technology/ch01/en/1_2_1_2.html.

[12]- Gizmag. [Online] [Cited: 10 June 2014.] http://www.gizmag.com/worlds-largest-wind-turbine-blades/23578/.

[13]- Nolet, S. C. (Director) (2011, January 20). Composite wind Blade engineering and Manufacturing. *Presented to Students and Faculty of: Massachusetts Institute of Technology - Independent Activities Period Mini-Course*. Lecture conducted from TPI Composites, Inc., Rhode Island. (presentation)

[14]- Scribd. [Online] [Cited: 10 June 2014.] http://www.scribd.com/doc/189207920/Composites-100-Years.

[15]- Jensen, F., Falzon, B., Ankersen, J., & Stang, H. (2006). Structural testing and numerical simulation of a 34 m composite wind turbine blade. *Composite Structures* (76), 52-61.

[16]- Branner, K., Blasques, J., Kim, T., Fedorov, V., Berring, P., Bitsche, R., & Berggreen, C. (2012, February 1). Anisotropic beam model for analysis and design of passive controlled wind turbine blades. *DTU Wind Energy E-Report*, 17-18.

[17]- Centraltrykkeri, J. (2002). *Guidelines for Design of Wind Turbines* (2nd ed., Vol. ISBN 87-550-2870-5, pp. 104 - 110). Copenhagen: Det Norske Veritas.

[18]- Mckittrick, L. R., Cairns, D. S., Mandell, J., Combs, D. C., Rabern, D. A. and Van Luchene, R. D. *Analysis of a composite blade design for the AOC 15/50 wind turbine using a finite element model,* p. 4, SANDIA report, Albuquerque, New Mexico 87185 and Livermore, California 94550, May 2001.

[19]- Asseff, N. S., *Design and finite element analysis of an ocean current turbine blade,* pp, 42-45, Florida Atlantic University, Boca Raton, Florida, August, 2009.

[20]- Yanbin, C., Lei, S. and Feng, Z., *Modal Analysis of wind turbine blade made of composite laminated plates*. pp. 225-228. Department of mechanical engineering, North China Electric Power University, Boading, China 2010.

[21]- Zhu, S. F., and Rustamov, I., *Structural design and finite element analysis of composite wind turbine blade, Vols 525-526,* pp. *225-228*, Key Engineering Materials, November 2012.

[22]- Chauhan, S., Tcherniak, D., Basurko, J., Salgado, O., Urresti, I., Carcangiu, C. E. and Rossetti, M., *Operational modal analysis of operating wind turbines: application to measured data*, Bruel&Kjaer Sound and Vibration Measurement A/S, Jacksorville, FL, XXIX International Modal Analysis Conference, 2011. (poster)

[23]- Larsen, G.C., Hansen, M. H., Baumgart, A. and Carlen I., *Modal analysis of wind turbine blades,* Riso National Laboratory, Roskilde, pp. 7-11, Denmark, February 2002.

[24]- Griffith, D. T., Smith, G., Casias, M., Reese, S. and Simmermacher, T. W., *Modal testing of the TX-100 wind turbine blade*, p. 9, Sandia National Laboratories, Albuquerque, New Mexico 87185 and Livermore, California 94550, March 2006.

[25]- Pabut, O., Allikas, G., Herranen, H., Talalaev, R. and Vene, K., *Model validation and structural analysis of a small wind turbine blade*, the 8th international DAAAM Baltic conference, Industrial Engineering pp. 19-21, Tallinn, Estonia, April 2012.

[26]- COMPBLADES, W/T Blade Repair & Maintenanceç, 2012. [Online] [Cited: August 2014.] http://www.compblades.com.

[27]- Product Data. Brüel & Kjaer, 2005. [Online] [Cited: August 2014.] http://www.bksv.com/

[28]- Agilent. Agilent 33120A Function/Arbitrary Waveform Generator Data Sheet. Agilent Technologies, 2004.

[29]- Polytec, PSV Scanning Vibrometer [Online] [Cited: August 2014.] http://www.polytec.com/us/products/vibration-sensors/vibrometer-software/psv-scanning-vibrometer-software/

[30]- Catia. [Online]. [Cited: 03 July 2014.] http://www.3ds.com/products-services/catia/#

[31]- Shokrieh M. M., Torabizadeh M. A., and Fereidoon A.. "Progressive Failure Analysis of Glass/epoxy Composites at Low Temperatures." *Strength of Materials* V.44: p. 317. , 2012.

APPENDIX A

Examples of the Layer Sequences of the Blade's Laminates

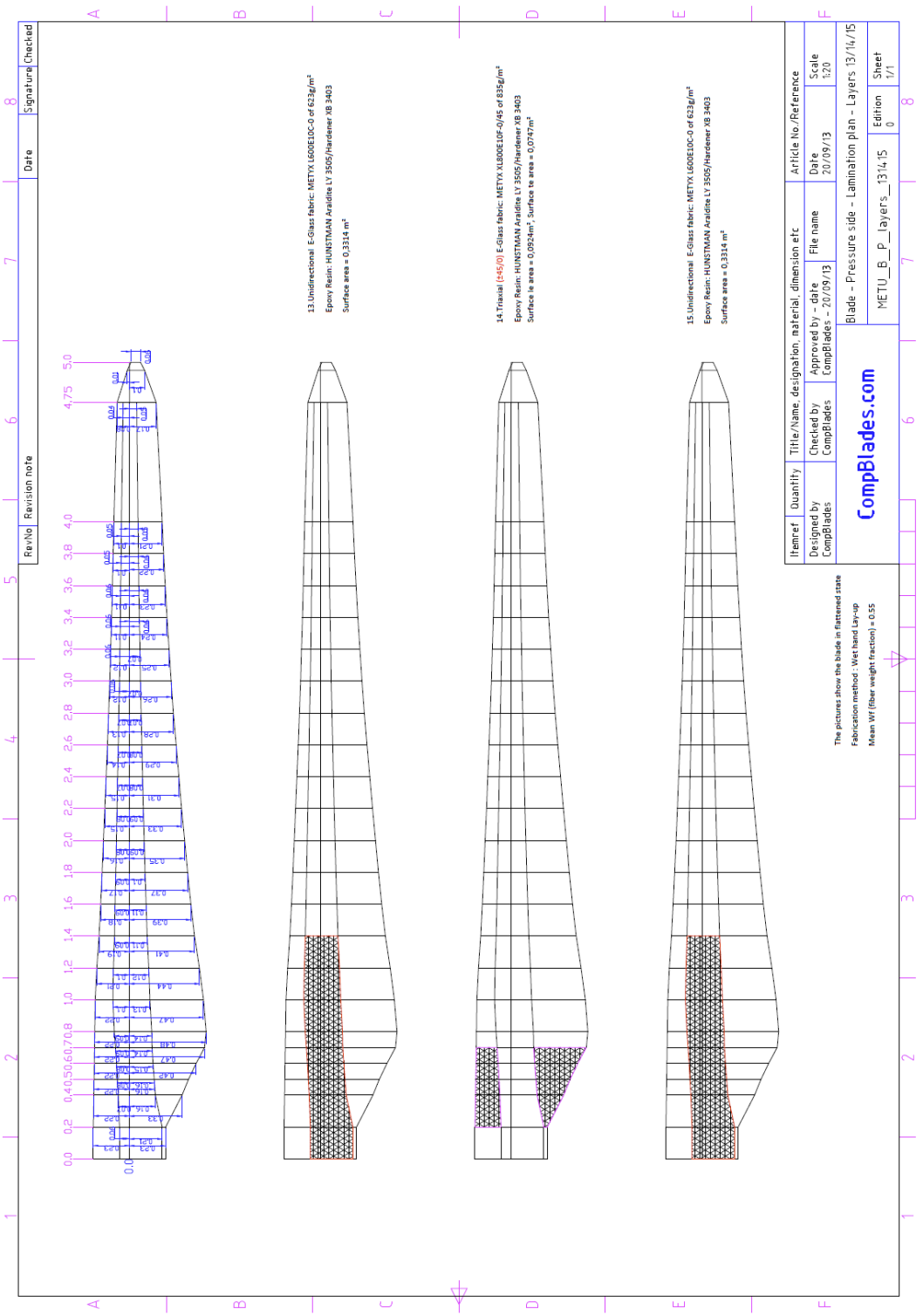

Figure A.1 The 13th, 14th and 15th Layer Sequences for the Lower (Pressure) Side of the Blade

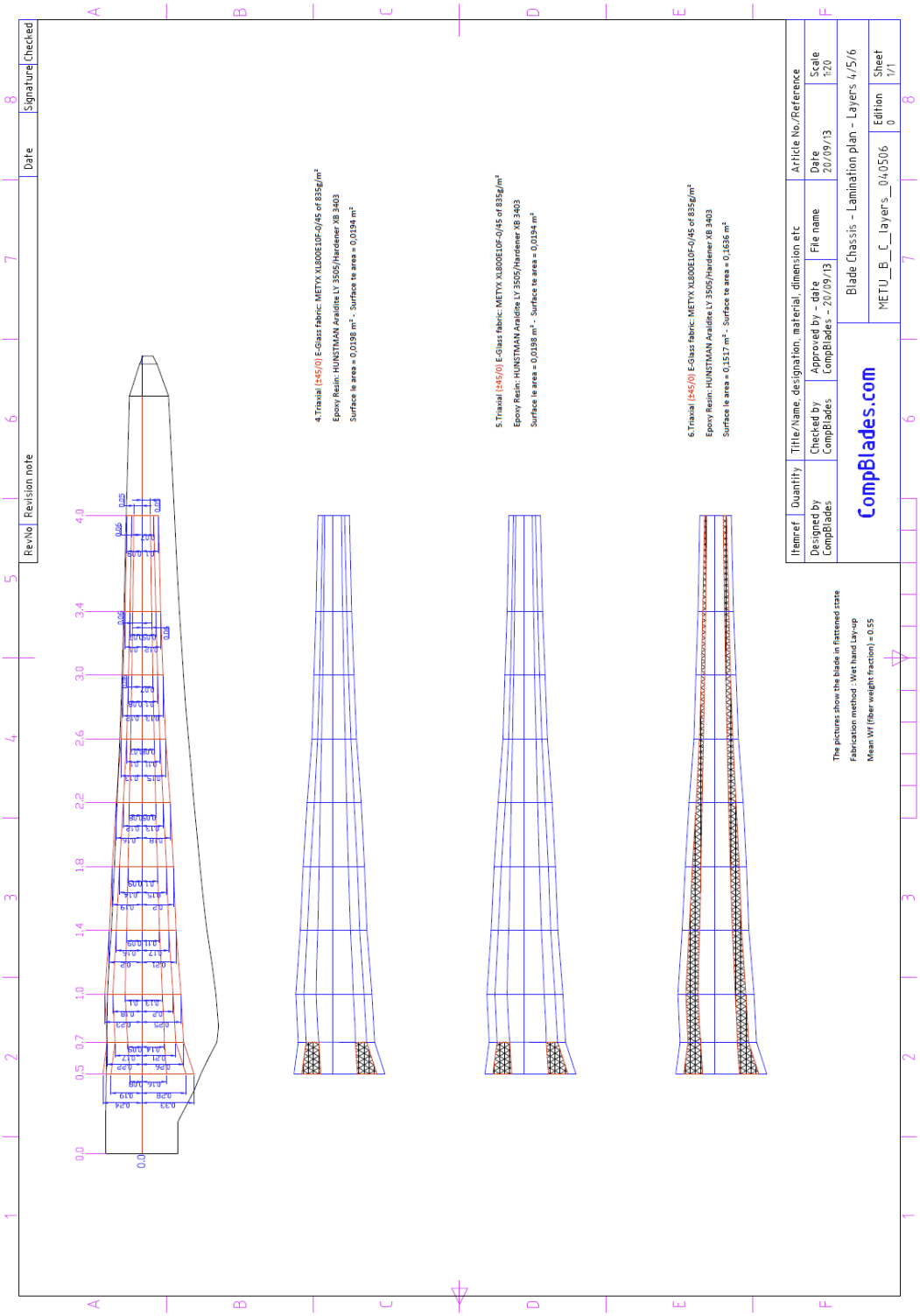

Figure A.2 Layer Sequences for the Spar (Chassis) of the Blade in Section 0.5 m to 0.7 m

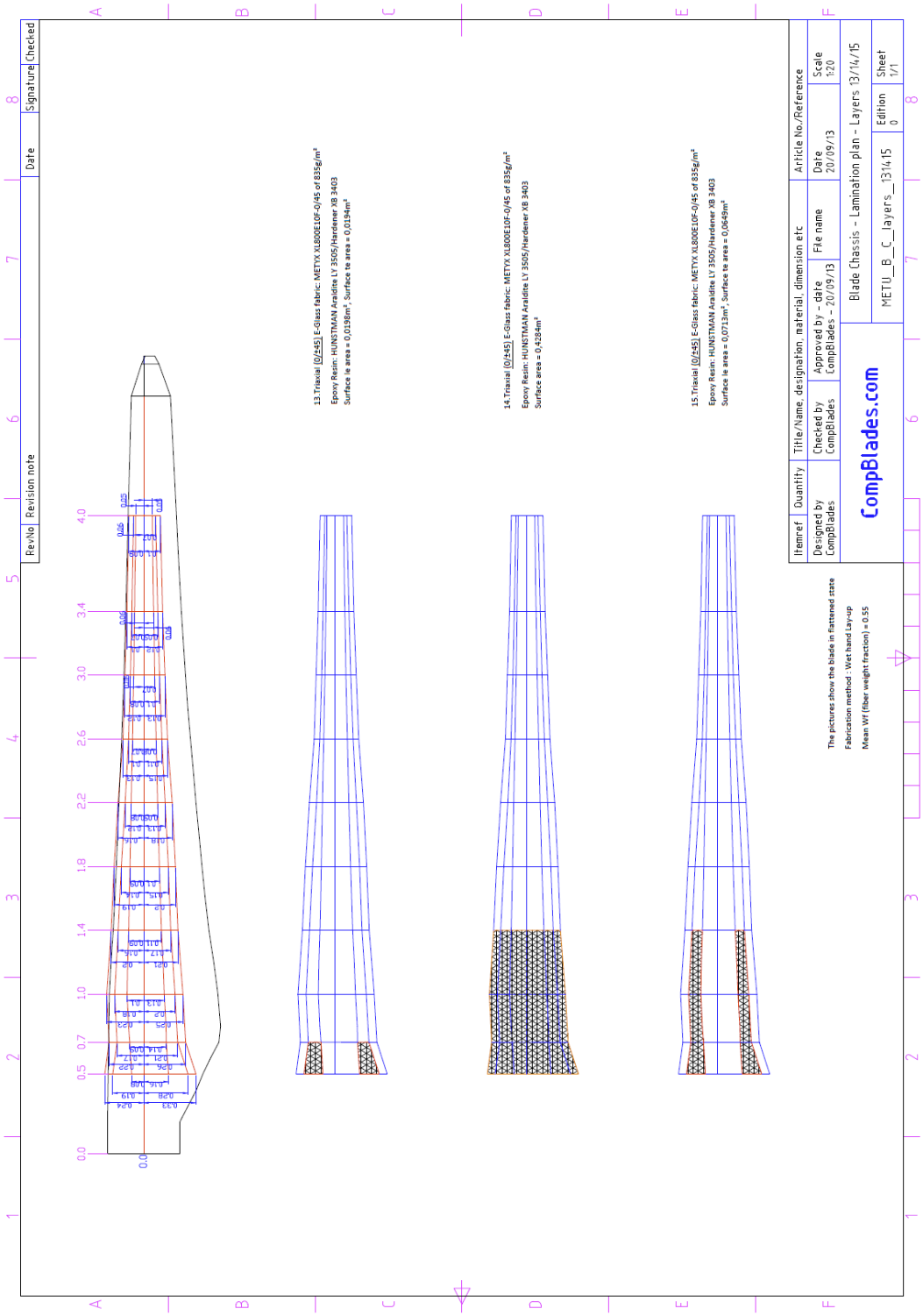

Figure A.3. Layer Sequences for the Spar (Chassis) of the Blade in Section 0.5 m to 1.4 m

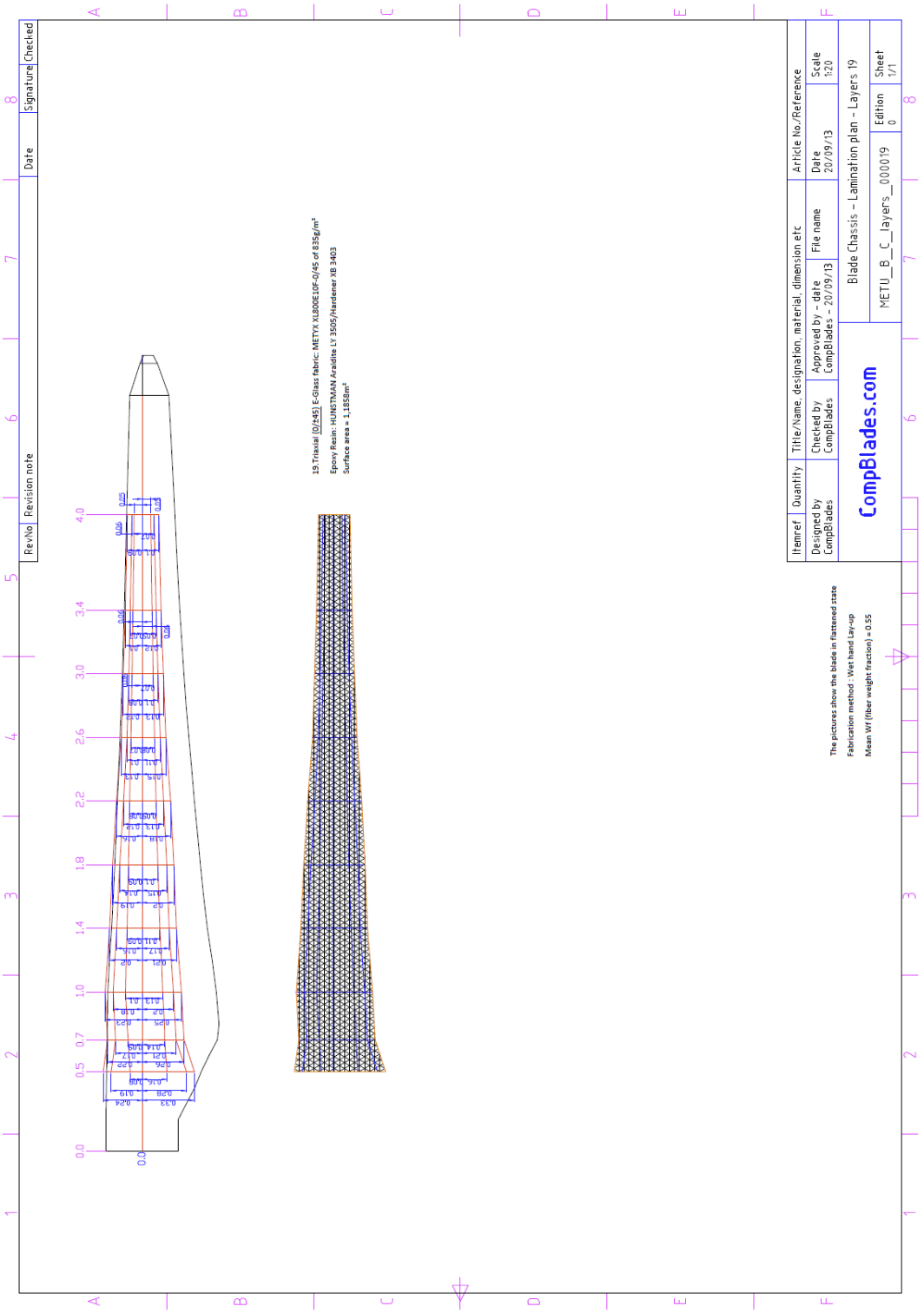

Figure A.4. Layer Sequences for the Spar (Chassis) of the Blade in Section 0.5 m to 4.0 m

APPENDIX B

Mode Shapes of the Blade with Mass of the Adhesive

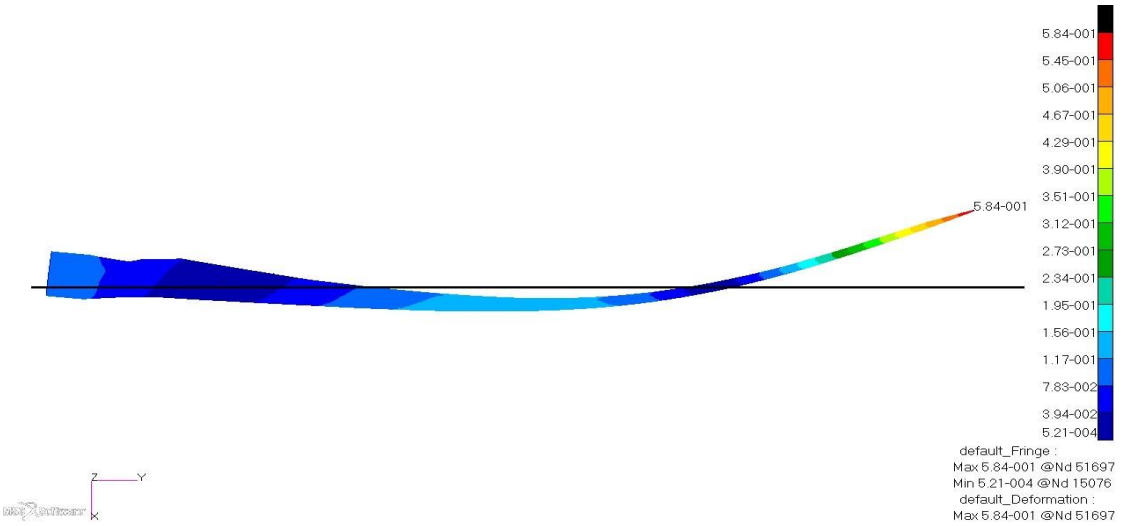

Figure B.1. 1st Out-of-Plane Bending [10.11 Hz]

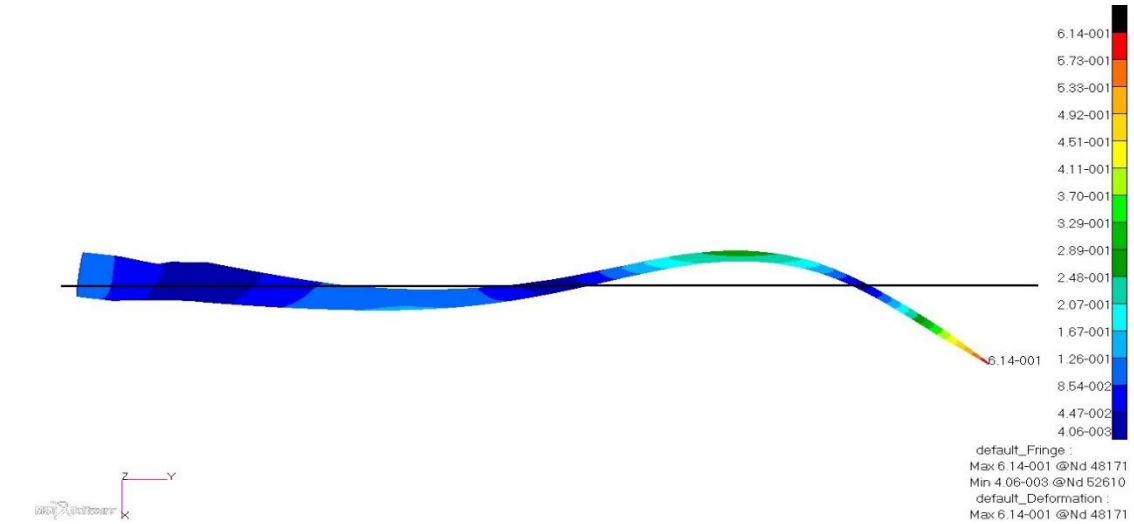

Figure B.2. 2nd Out-of-Plane Bending [27.69 Hz]

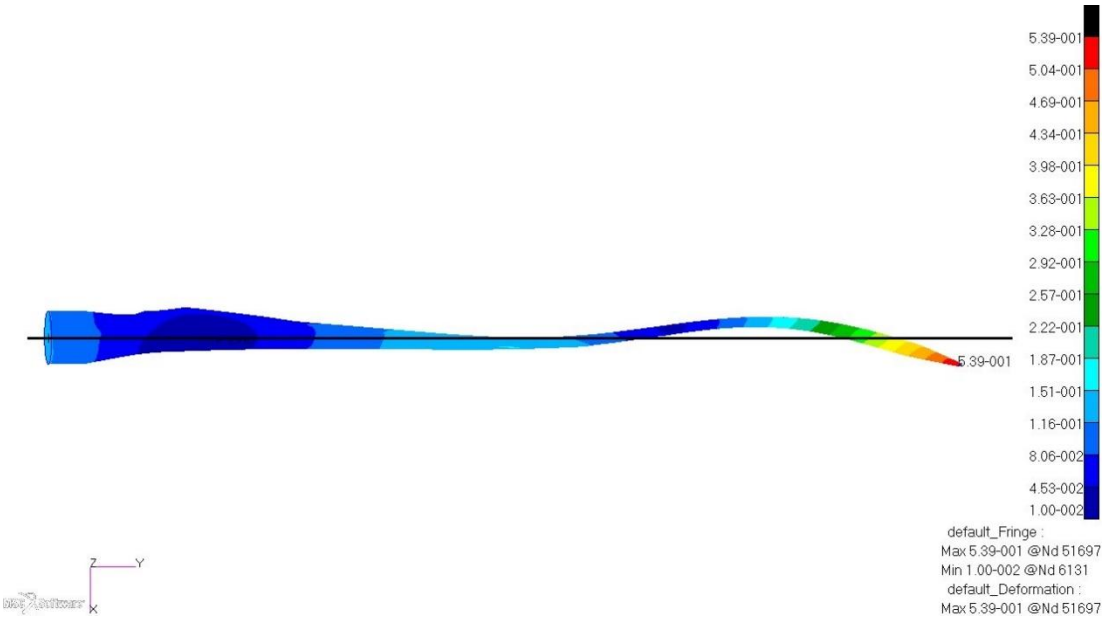

(a)

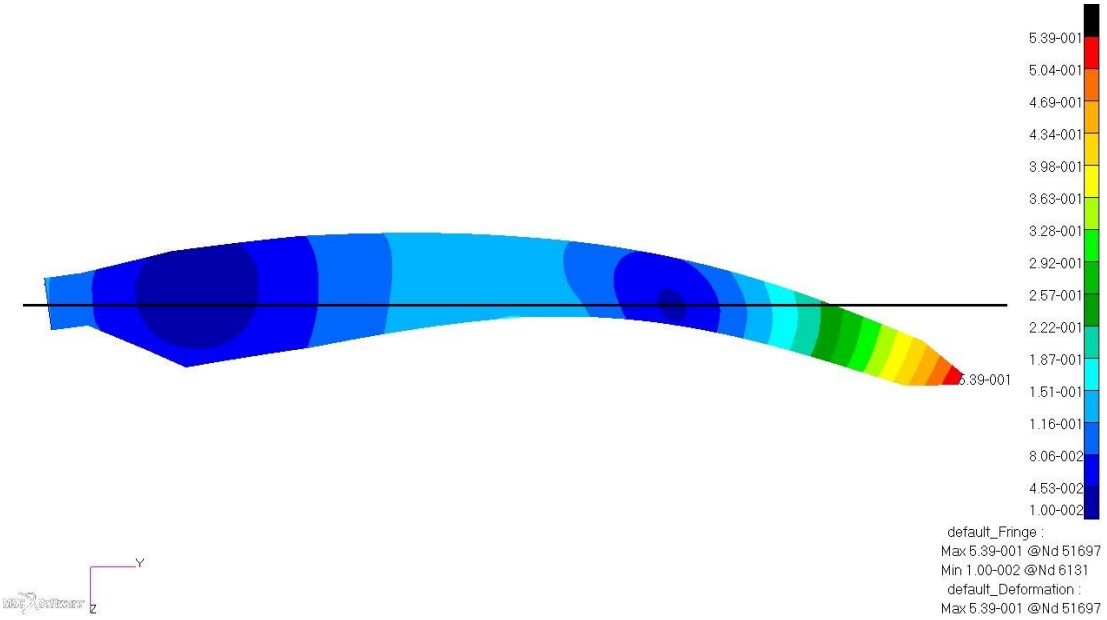

(b)

Figure B.3. 2nd Out-of-Plane Bending and 1st In-plane Bending Coupling [43.38 Hz]
(a) Side View (b) Top View

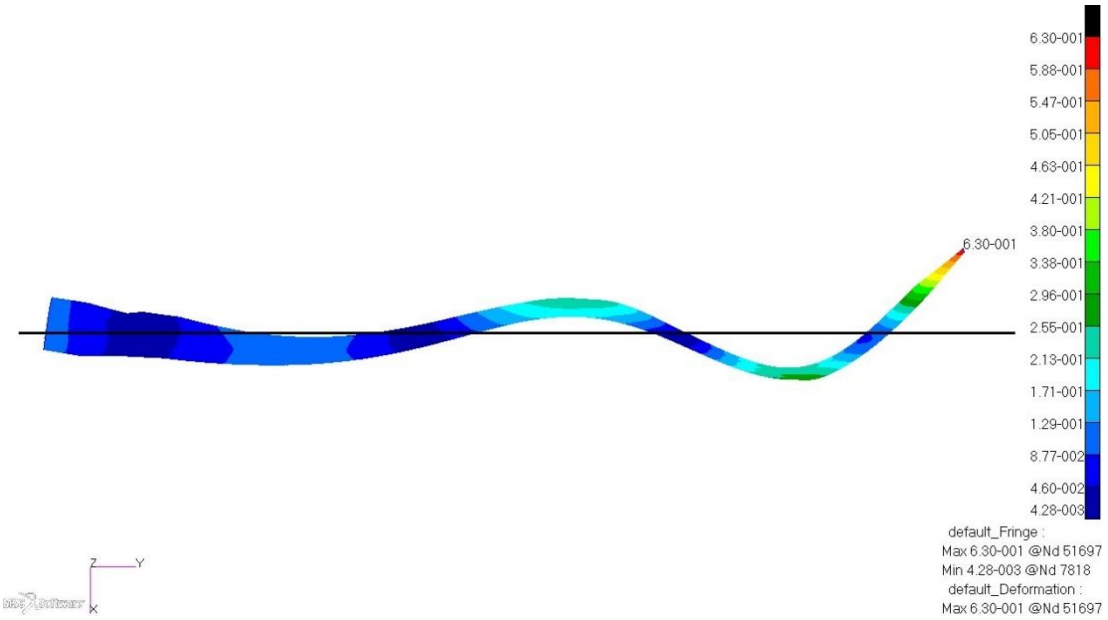

Figure B.4. 3rd Out-of-Plane Bending [52.44 Hz]

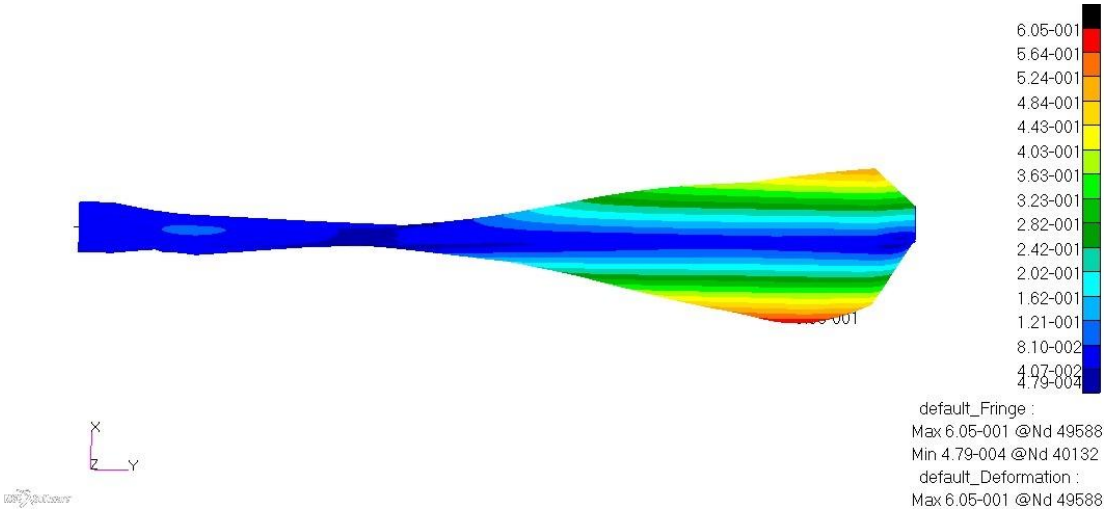

Figure B.5. 1st Torsion [60.58 Hz]

APPENDIX C

Mode Shapes of the Blade Obtained by using FEMtools

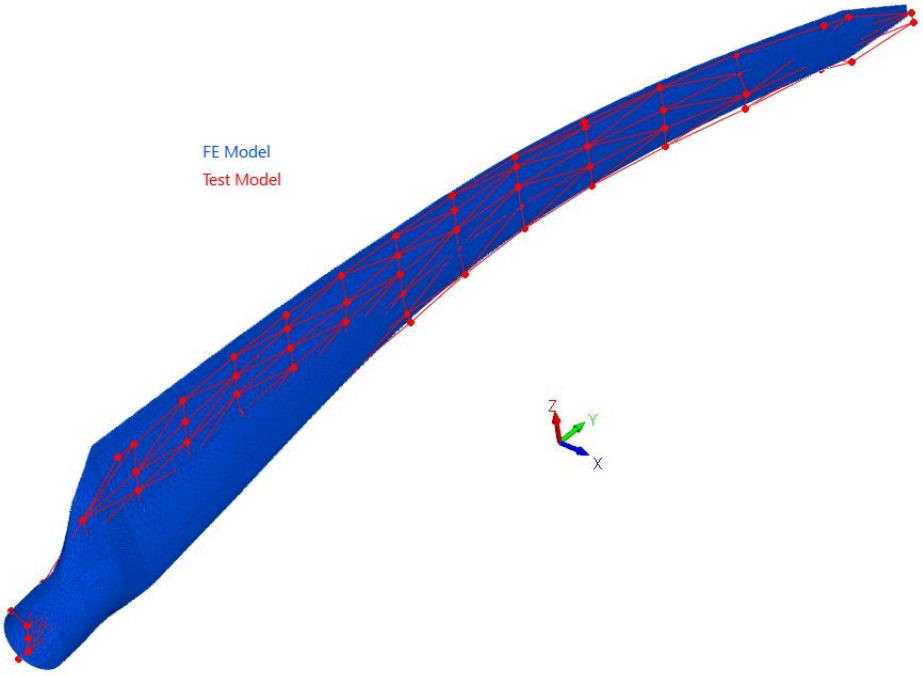

Figure C.1. 1st Out-of-Plane Bending [9.92 Hz] – FEMTools Updated.

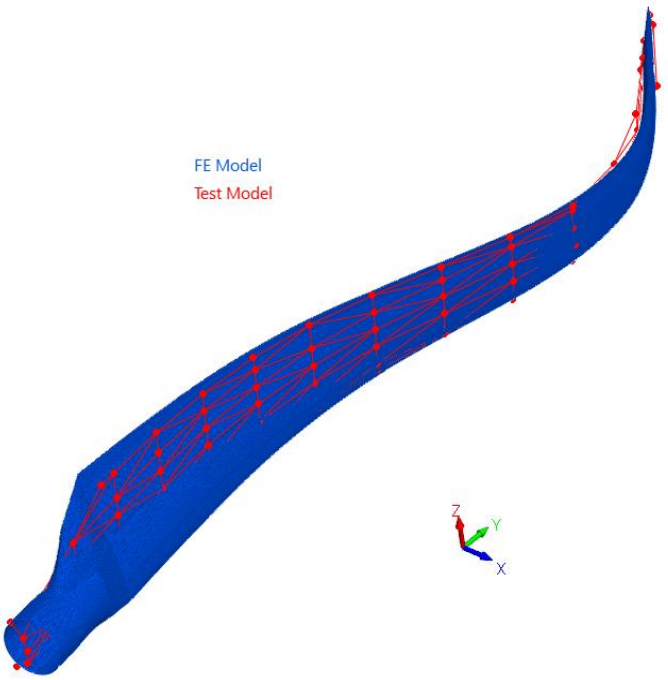

Figure C.2. 2nd Out-of-Plane Bending [26.67 Hz] – FEMTools Updated.

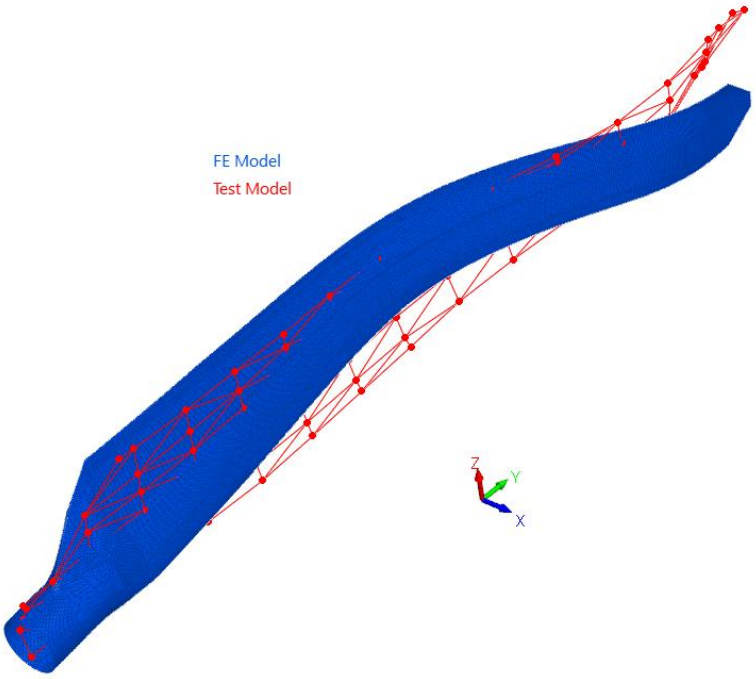

Figure C.3. 2nd Out-of-Plane Bending with 1st In-Plane Bending Coupling [42.55 Hz] – FEMTools Updated.

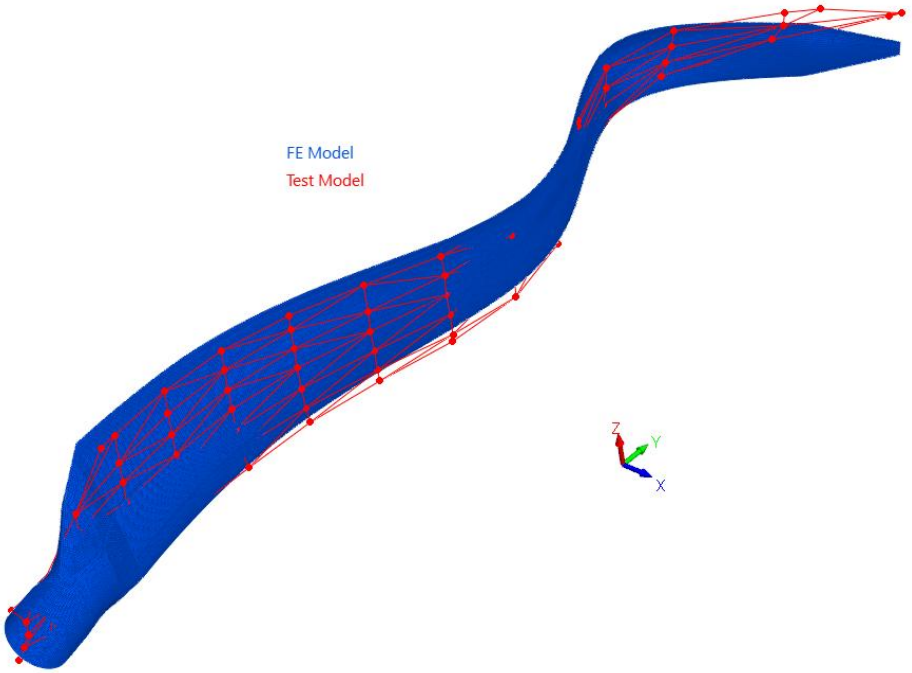

Figure C.4. 3rd Out-of-Plane Bending [50.30 Hz] - FEMTools Updated.

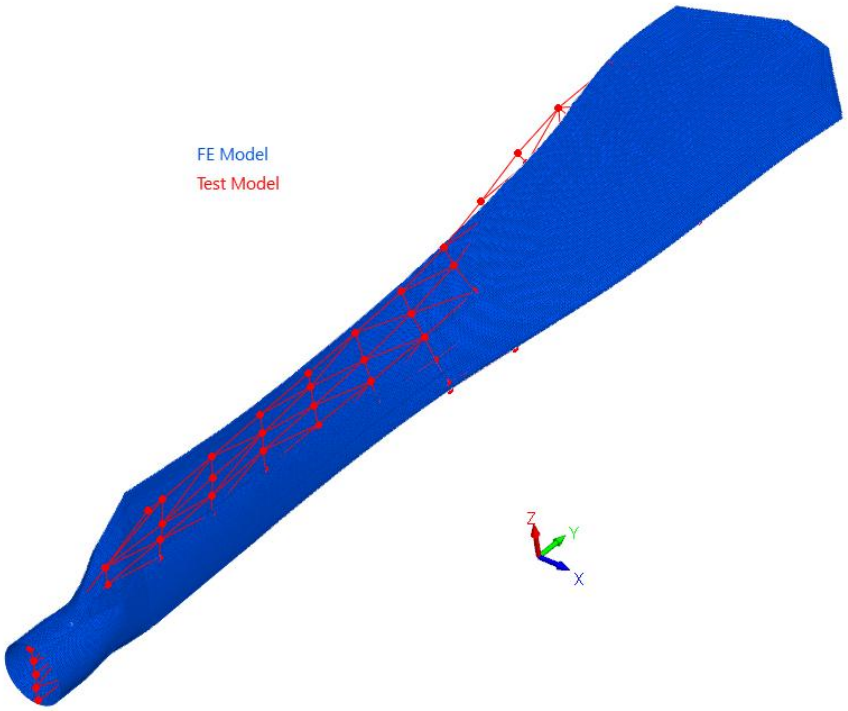

Figure C.5. 1st Torsion [59.50 Hz] - FEMTools Updated.